Tools for Estimating Dynamic Properties for the Purpose of Tuning Dynamic Vibration Absorbers

TOOLS FOR ESTIMATING DYNAMIC PROPERTIES FOR THE PURPOSE OF TUNING DYNAMIC VIBRATION ABSORBERS

BY

JULIA M. LEWIS, B.E.Sc.

A THESIS

SUBMITTED TO THE DEPARTMENT OF CIVIL ENGINEERING

AND THE SCHOOL OF GRADUATE STUDIES

OF MCMASTER UNIVERSITY

IN PARTIAL FULFILMENT OF THE REQUIREMENTS

FOR THE DEGREE OF

MASTER OF APPLIED SCIENCE

Master of Applied Science (2010) McMaster University

(Civil Engineering) Hamilton, Ontario, Canada

TITLE: Tools for Estimating Dynamic Properties for the Purpose of Tuning Dynamic Vibration Absorbers

AUTHOR: Julia M. Lewis

B.E.Sc.

University of Western Ontario, London, Canada

SUPERVISOR: Dr. Mike Tait

NUMBER OF PAGES: xxi, 113

Abstract

Tuned-liquid dampers (TLDs) can be used as vibration absorbers for tall buildings. The ability of TLDs to decrease a building's motions is highly dependent on them being tuned to the building's natural frequency. In the present study natural frequency and damping estimates are determined for a 187 m tall building equipped with TLDs. A properly tuned structure-TLD system acts as a coupled two-degree-of-freedom (2DOF) system. In this study several MATLAB (2009) programs were developed in order to determine the dynamic properties of both single-degree-of-freedom (SDOF) and 2DOF systems. These programs were based on the statistical maximum likelihood (ML) and least squares (LS) methods. The ML programs are based on earlier work by Montpellier (1997) and the LS programs were developed independently. All of the programs were verified using spectral and time-history data with known dynamic properties. The results of the programs were also compared to results generated by the well-known half-power bandwidth and random decrement methods. The ML and LS programs were found to produce results that were superior to the half-power bandwidth method and comparable to the random decrement program for SDOF systems. The ML and LS programs are superior to the half-power bandwidth and random decrement programs for analyzing coupled 2DOF systems as they are able to determine distinct property estimates for each mass. The natural frequency of the building studied for this project was found to be significantly higher than predicted at the time of its design. Thus the

TLDs were not optimally tuned to the building's actual natural frequency and as a result the studied building was behaving as a SDOF system. Therefore the dynamic properties estimated in this study are those of a SDOF system. However, the methods developed herein could be applied to a 2DOF system in the future.

For Brandon and Tammy

Acknowledgements

I would like to express my sincere thanks to my supervisor Dr. Mike Tait. His support, encouragement, and insight has been generously provided and indispensible throughout my graduate work.

I would also like to thank Dave Morrish from the Boundary Layer Wind Tunnel Laboratory at the University of Western Ontario for all his help with the full-scale monitoring data collection.

A special thanks to all of my collegues here at McMaster University. I would like to especially acknowlege Margaret Kirnbauer, Sandrina Rodrigues, Maggie Burke, Laura Toppozini, Sommer Abdel-Fattah, and Freesia Waxman for their friendship, stimulating conversation, and encouragement.

Thanks to my mother for all of her love, patience, and encouragement. Her limitless belief in my abilities is what encouraged me to reach my full potential and her example of hard work and determination has always been my motivation.

Finally, thanks to Brandon and Tammy. This thesis is dedicated to you because of your patience and unconditional love. You are what makes this all worthwhile.

Nomenclature

β	forced frequency ratio
$\ddot{q}$	amplitude of modal acceleration of the free surface in a TLD
$\ddot{q}_n$	amplitude of the modal acceleration of the free surface of a TLD
$\ddot{X}$	horizontal acceleration of a TLD tank
$\ddot{x}_a$	acceleration of secondary mass
$\ddot{x}_r$	acceleration of secondary mass relative to main mass
$\ddot{X}_s$	acceleration of main mass
δq_n	virtual displacements
Δt	sampling interval
δW_{nc}	virtual work done by non-conservative forces
δ	logarithmic decrement
Δ_n	integral portion of the nonlinear damping forces, Q_n
Δ_{FFT}	frequency resolution
$\dot{q}$	amplitude of modal velocity of the free surface in a TLD

$\dot{q}_n$ amplitude of modal velocity of the free surface in a TLD for the n^{th} mode

$\dot{X}$ horizontal velocity of the TLD tank

$\dot{x}_a$ velocity of secondary mass

$\dot{x}_r$ velocity of secondary mass relative to main mass

$\dot{X}_s$ velocity of main mass

ϵ error term

ϵ_b bias error

η free surface displacement of fluid particles in a TLD

Γ modal participation factor

γ^* excitation factor

γ_n^* excitation factor of the n^{th} mode

Γ_n modal participation factor for the n^{th} mode

$\hat{\Theta}$ estimated parameter

$\hat{\zeta}$ estimated damping ratio

$\hat{\zeta}_a$ estimated damping ratio of the absorber

$\hat{\zeta}_s$ estimated damping ratio of the structure

$\hat{a}$ peak acceleration

$\hat{a}_p$ peak acceleration based on predicted dynamic property values

$\hat{f}_0$ estimated natural frequency

$\hat{f}_a$ estimated natural frequency of the absorber

$\hat{f}_s$ estimated natural frequency of the structure

$\hat{S}(\omega_k)$ averaged spectra at ω_k

μ mass ratio

ν viscosity

Ω tuning ratio

ω forcing frequency

ω_1 natural frequency of the first mode

ω_a natural frequency of secondary mass

ω_n natural frequency for the n^{th} mode

ω_s natural frequency of main mass

Ω_{opt} optimal tuning ratio

ϕ velocity potential, true value of a parameter

ρ density of the fluid in a TLD

σ random error

σ^2 variance

σ_q root mean square of the free surface fluid amplitude in the first mode

σ_r root mean square of the equivalent response

Θ parameter(s)

$\tilde{S}(\omega_k)$ estimate of smoothed spectrum at frequencies ω_k

Ξ summation portion of the nonlinear damping forces, Q_n

ζ damping ratio

ζ_{eq}^* linearized generalized damping ratio

ζ_a damping ratio of secondary mass/absorber

ζ_s damping ratio of the structure

ζ_w damping ratio due to visous losses

ζ_{eff} effective damping ratio

ζ_{eff}^{opt} optimal effective damping ratio

ζ_{opt} optimal damping ratio of secondary mass

ζ_{total} total damping ratio

A solid portions of the screens in a TLD normal to the flow

A_r area under the peak of the frequency response function

A_{peak} area under the peak of the response spectrum

b width of TLD tank perpendicular to excitation, bias of an estimate

B_r half-power bandwidth

c_n^* generalized linear damping coefficient for the n^{th} mode

c_{eq}^* linearized generalized damping coefficient

c_a damping coefficient of secondary mass

C_d drag coefficient

C_l loss coefficient

c_s damping coefficient of main mass

c_{eq} equivalent damping coefficient

COV coefficient of variation

D_p peak value on decay curve

E expected value

F external force

f input displacement, force of liquid acting on TLD screens, forcing frequency

f_0 natural frequency

f_a natural frequency of the absorber

f_d force of liquid acting on TLD screens due to drag

f_i force of liquid acting on TLD screens due to inertia

f_j discrete frequency value

f_l lower frequency limit defining the resonance peak

f_p predicted natural frequency of the structure

f_s natural frequency of the structure

f_u upper frequency limit defining the resonance peak

f_{max} frequency value corresponding to the maximum value of the frequency response function

Hx dynamic magnification factor

Hx_r dynamic magnification factor for secondary mass

Hx_s dynamic magnification factor for the main mass

Hx_{max} maximum value of dynamic magnification factor

h fluid depth in a motionless TLD

j variable integer

K stiffness of main mass

k stiffness of secondary mass

k variable integer

k^* generalized stiffness

k_n^* generalized stiffness of the n^{th} mode

k_{eq} equivalent stiffness

L length of TLD tank in the direction of excitation, likelihood function

M mass of main mass

m mass of secondary mass, variable integer

M_s' mass of structure modified to account for non-participating component of the liquid

m^* generalized mass

m_n^* generalized mass of the n^{th} mode

m_{eq} equivalent mass

N number of values in a data block

n random variable, empirical constant, number of blocks into which a series of response measurements has been divided

ns number of screens

P_0 external load

PDF probability density function

q amplitude of modal displacement of the free surface in a TLD

Q_n nonlinear damping forces for the n^{th} mode

q_n amplitude of modal displacement of the free surface in a TLD for the n^{th} mode

Q_{2DOF} non-conservative forces for a two-degree-of-freedom system

R autocorrelation

r variable integer

R_r estimate of the autocorrelation function

S solidity of the screens in a TLD, frequency response function

s variable integer

$S(\omega)$ power spectral density

S_0 constant white noise spectral density

S_k series of spectral coefficients

S_R spectrum of response data

S_{Rnorm} normalized area under the response spectrum between two consecutive discrete frequencies

SC surface contamination factor

T velocity potential, total period of a block of data

T_{2DOF} velocity potential for a two-degree-of-freedom system

u horizontal velocity of fluid particles in a TLD

V gravitational potential

V_{2DOF} gravitational potential for a two-degree-of-freedom system

w vertical velocity of fluid particles in a TLD

x horizontal dimension of a TLD, measured independent variable

x_a displacement of secondary mass

x_r displacement of secondary mass relative to main mass, discrete response variable

X_s displacement of main mass

x_s series of discrete response variables

x_{st} static deflection

y measured dependent variable

z vertical dimension of a TLD, random variable

Contents

List of Tables

List of Figures

Chapter 1

Introduction

In recent years the trend in tall building design has been towards increasingly flexible, tall, and slender structures. These structures are sensitive to the dynamic forces generated by winds and, for serviceability reasons, it is important to limit building motions. In fact serviceability standards often dictate tall building design in terms of the required lateral stiffness. One method used to control building motions is to add supplementary damping devices such as tuned liquid dampers (TLDs). Building motions are dependent on several dynamic properties including the building's natural frequency and damping ratio. The natural frequency must be identified correctly if effective TLDs are to be added to the structure as they must be tuned to this frequency. The damping ratio is most important in controlling the magnitude of the building's motions. This is problematic as the building's damping ratio is difficult to predict and thus predicted dynamic motions can be quite inaccurate. Using current design techniques, designers estimate the damping ratio for a building prior to its construction. This estimate is based on experience. The estimated damping ratio is then used in subsequent design calculations. Once the building is designed, a scale model is constructed and tested in a wind tunnel. Observations obtained from this model are used to verify the original

damping estimate. However, this method of design has yet to be verified using full-scale data.

In the present work, damping and natural frequency values are determined for a residential tower that is equipped with ten tuned-liquid damping devices. There are two main purposes for determining the building's dynamic properties. Firstly the dynamic properties are compared to those predicted at the time of the building's design. These comparisons can be used in conjunction with results obtained from other monitoring projects in order to verify current tall building design methods (Kijewski-Correa *et al.*, 2006). Secondly the value of the identified natural frequency of the building will be used to adjust the TLDs in order to enhance their performance.

1.1 Thesis Overview

Chapter 2 discussed the equations used to express the dynamic properties of TLDs. This chapter begins by illustrating the development of an expression for the effective damping generated by a tuned-mass damper. In Section 2.2, the derivation of equations used to express TLDs as equivalent tuned-mass dampers in presented and the expression for the effective damping generated by the TLDs is derived.

Chapter 3 discusses the importance of full-scale monitoring. Current research on the monitoring of tall buildings and tall buildings equipped with TLDs is presented. Chapter 3 also discussed the importance of the building monitored in this study.

Chapter 4 reviews techniques that have traditionally been used in the identification of tall building dynamic properties. Forced vibration methods are discussed followed by a review of the statistical methods for estimating response spectra from ambient conditions. Finally the half-power bandwidth and random decrement methods are described.

Chapter 5 describes the maximum likelihood and least squares programs developed in this study. The chapter begins by summarizing the maximum likelihood method as presented by Montpellier (1997) and the least squares method. The development of MATLAB (2009) programs used to implement these methods is then presented. The MATLAB (2009) programs are also verified using data with known dynamic properties. This is done for both single-degree-of-freedom systems and two-degree-of-freedom systems.

Chapter 6 describes the full-scale data obtained from the studied building. The normalized dynamic properties of this building as determined by the maximum likelihood and least squares programs are presented and compared to those predicted at the time of the building's design. Finally, Chapter 7 concludes the present work and offers recommendations for future work.

Chapter 2

Theoretical Dynamic Vibration Absorber Equations

In this chapter the principle characteristics of dynamic vibration absorbers are explained and several key equations used to model the properties of these devices are presented. Section 2.1 describes tuned mass dampers (TMDs) which, like TLDs, are used to add supplemental damping to a structural system. The effective damping generated by a TMD, unlike that generated by a TLD, is independent of the device's response. Thus a structure-TMD system's response is linear and the effective damping can be determined in closed form. Section 2.1.1 begins by describing the general concept behind TMDs. The effect of a TMD on the structure-TMD's response to a harmonic load, as determined by Den Hartog (1956), is also illustrated. In Section 2.1.2 the importance of properly tuning the TMD is discussed and the optimal TMD parameters are found. Following this, the response of a structure-TMD system to white noise excitation is derived and the effective damping generated by the TMD is calculated in Section 2.1.3.

Section 2.2 expands on the equations provided in Section 2.1. Equations for a

structure-TLD system are derived by treating the system as an equivalent structure-TMD system.

2.1 Tuned Mass Dampers

2.1.1 Structure-TMD Response to Harmonic Load

The original concept for a tuned mass damper was developed in 1909 (Den Hartog, 1956). At that time, dynamic vibration absorbers were mainly being used for mechanical systems. Today, however, they are widely accepted as effective in reducing the dynamic response of tall buildings (Soong and Dargush, 1997). In its simplest representation, the TMD can be thought of as an auxiliary mass connected to the main mass (the mas of the structure) by a spring-dash-pot system. A schematic representation of the structure-TMD system is shown in Figure 2.1. The TMD works by absorbing

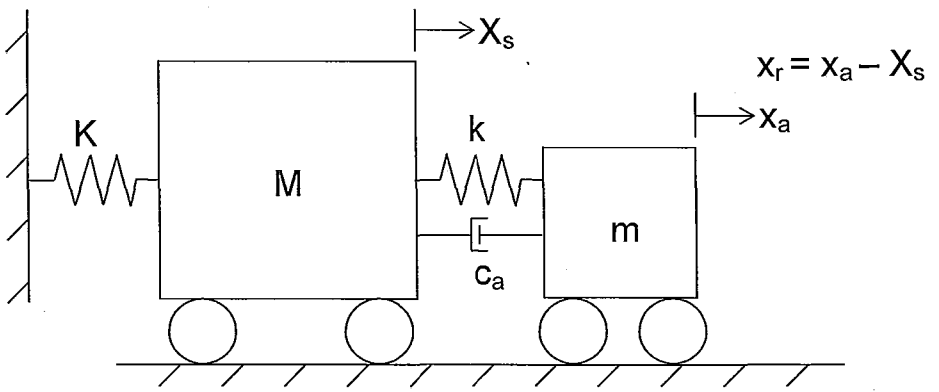

Figure 2.1: Schematic representation of a simple structure-TMD system (Tait, 2008)

the vibrational energy that is transferred to it via the structure. Den Hartog (1956) derived the equations of motion for both the structure and the TMD.

The efficacy of the TMD in reducing the structure's motions can be shown by examining the response of an undamped structure equipped with a TMD to a harmonic

load. This response is given in Equation 2.1

$$X_s = \frac{P_0[(k - m\omega^2) + i\omega c_a]}{(-M\omega^2 + K)(-m\omega^2) - m\omega^2 + k) - m\omega^2 k + i\omega c_a(-M\omega^2 + k - m\omega^2)} \tag{2.1}$$

where P_0 is the externally applied force, ω is the forcing frequency, c_a is the damping of the TMD, and k, m, K, and M are the mass and stiffness parameters shown in Figure 2.1. Equations 2.2 to 2.8 below define the mass ratio of the system (μ), the natural circular frequencies of the TMD (ω_a) and the structure (ω_s), the static deflection of the structure (x_{st}), the forced frequency ratio (β), the tuning ratio (Ω), and the damping ratio of the TMD (ζ_a). These equations are used to transform Equation 2.1 into the commonly used format and determine the dynamic magnification factor of the structure.

$$\mu = \frac{m}{M} \tag{2.2}$$

$$\omega_a^2 = \frac{k}{m} \tag{2.3}$$

$$\omega_s^2 = \frac{K}{M} \tag{2.4}$$

$$x_{st}^2 = \frac{P_0}{K} \tag{2.5}$$

$$\beta = \frac{\omega}{\omega_s} \tag{2.6}$$

$$\Omega = \frac{\omega_a}{\omega_s} \tag{2.7}$$

$$\zeta_a = \frac{c_a}{2m\omega_a}. \tag{2.8}$$

By substituting Equations 2.2 to 2.8 into Equation 2.1, the dynamic magnification factor (DMF) for the undamped structure-TMD system can be written as

$$Hx_s = \frac{X_s}{x_{st}} = \sqrt{\frac{(\Omega^2 - \beta^2)^2 + (2\zeta_a\Omega\beta)^2}{[(\Omega^2 - \beta^2)(1 - \beta^2) - \Omega^2\beta^2\mu]^2 + (2\zeta_a\Omega\beta)^2(1 - \beta^2 - \beta^2\mu)^2}} \tag{2.9}$$

Figure 2.2 shows the dynamic magnification factor for undamped structures equipped with TMDs having various TMD damping ratios. The magnitude of the dynamic magnification factor is based on both the tuning ratio, Ω, and TMD damping ratio, ζ_a. In Section 2.1.2 the optimal values for these parameters will be determined.

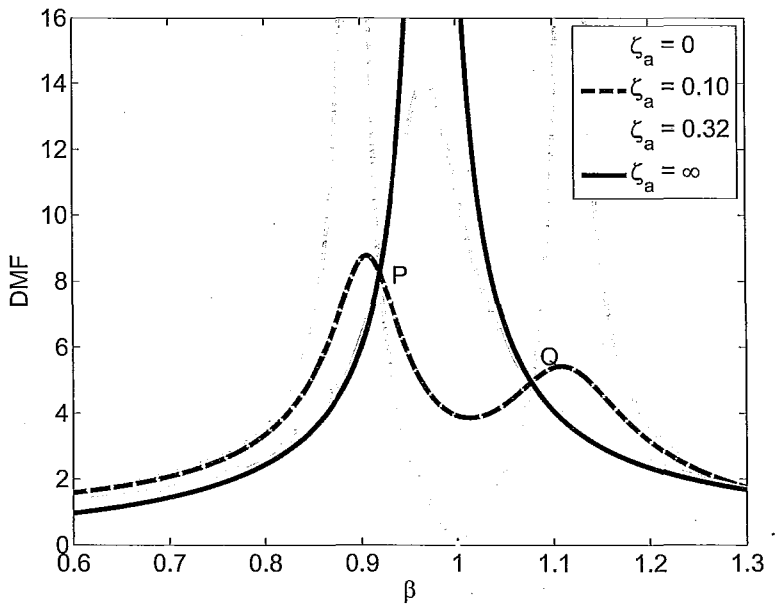

Figure 2.2: Dynamic Magnification Factor as a Function of β for Various ζ_a Values ($\mu = 0.05$, $\Omega = 1$)

2.1.2 Optimal TMD Parameters

In order to determine the optimal tuning ratio, Ω, and TMD damping ratio, ζ_a, we begin by examining Figure 2.2. From this figure it can be seen that if the TMD has zero damping both the TMD response and the structure response will theoretically be infinite (since the structure is assumed to have zero damping in this case). If the damping of the TMD is infinite, the structure and TMD behave as a single mass, $M + m$, and this single-degree-of-freedom response is, again, infinite (Den Hartog, 1956). Figure 2.2 also shows the response for a TMD with 10% damping and a TMD with 32% damping. From this figure it can be seen that there are two points (labeled as P and Q) at which the response is independent of the TMDs damping ratio. The minimum structure response can be obtained by adjusting Ω until these two points are at equal heights (Soong and Dargush, 1997). Using this technique, the Ω value which minimizes the response, Ω_{opt} is found as

$$\Omega_{opt} = \frac{1}{1+\mu} \tag{2.10}$$

(Soong and Dargush, 1997; Den Hartog, 1956). In the case shown in Figure 2.2 with $\mu = 0.05$, Ω_{opt} is found to be 0.95. Figure 2.3 shows this optimal response along with responses for several other Ω values. This figure illustrates the importance of properly tuning the dynamic vibration absorber.

Another important parameter in TMD design is the damping ratio of the TMD, ζ_a. The value of ζ_a that minimizes the response, ζ_{opt}, can be estimated by finding the average of the two ζ_a values that makes the slopes at points P and Q in Figure 2.2 equal to zero for the case of optimal tuning (Soong and Dargush, 1997; Den Hartog,

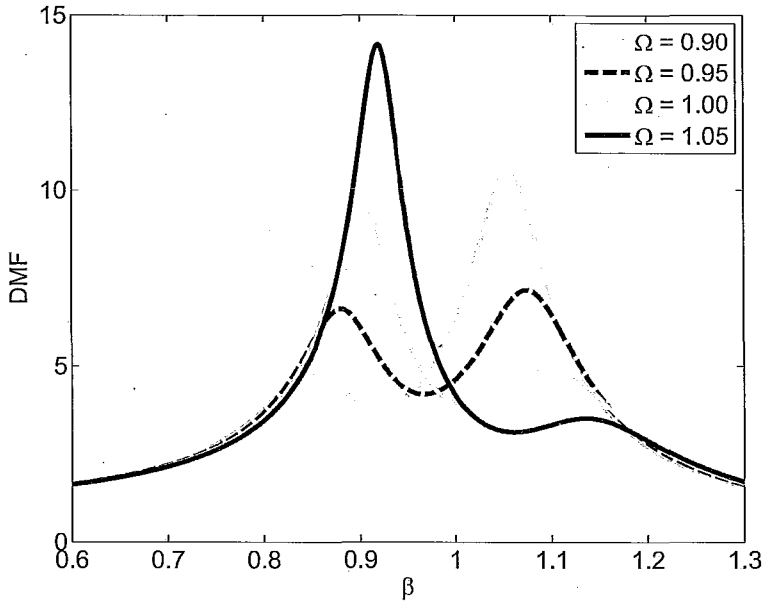

Figure 2.3: Dynamic Magnification Factor as a Function of β for Various Ω Values ($\mu = 0.05$, $\zeta_a = 0.1$)

1956). For the case of an undamped structure, ζ_{opt} is found as

$$\zeta_{opt} = \sqrt{\frac{3\mu}{8(1+\mu)}} \tag{2.11}$$

(Soong and Dargush, 1997; Den Hartog, 1956). For a structure-TMD system with $\mu = 0.05$ the ζ_{opt} value is found to be 13%. Figure 2.4 shows the response for this optimal TMD damping value along with several other values. This figure illustrates the importance of using an optimal absorber damping ratio.

2.1.3 Structure-TMD Response and Effective Damping for White Noise

In structural systems the excitation is caused by environmental loads such as winds which are not harmonic but instead have various frequencies and amplitudes. In order

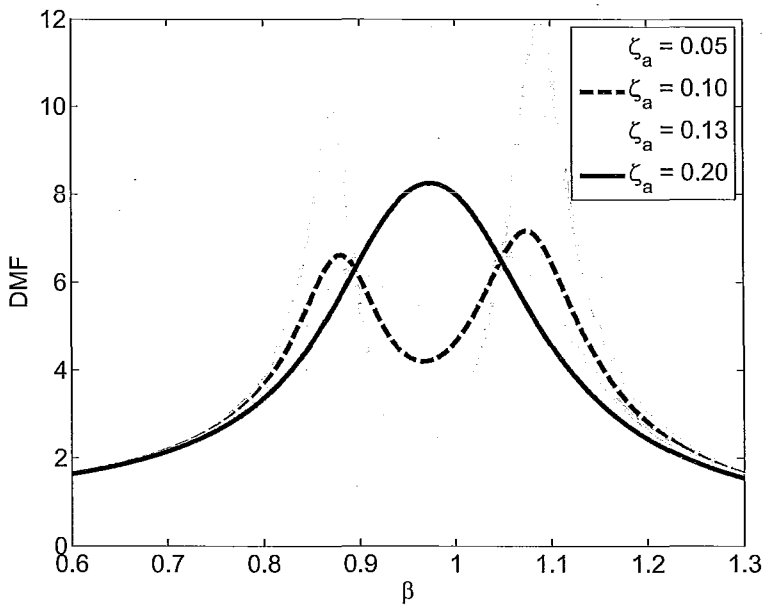

Figure 2.4: Dynamic Magnification Factor as a Function of β for ζ_a Values Close to ζ_{opt} ($\mu = 0.05$, $\Omega = 0.95$)

to model the response of a structure to wind loads the wind is assumed to act as white noise. This assumption is valid because the continuous excitation spectrum has a nearly uniform amplitude near the natural frequency of the response. In this case the responses of the structure and the TMD are best modeled using statistical probabilities. McNamara (1977) derived the mean square responses for a structure-TMD system and calculated the effective damping generated by the TMD. In the method presented by McNamara (1977), the dynamic magnification factors for both the structure and the TMD are determined due to a harmonic load. Statistical methods are then used to determine the mean square responses and effective damping due to white noise excitation. These derivations are presented below.

The structure-TMD system used in this derivation will be the same as that shown in Figure 2.1 and used to determine Equations 2.1 and 2.9 except that in this case both the TMD and the structure have damping. The damping of the structure will

be represented by c_s. The equations of motion for the structure and TMD are given respectively as

$$M\ddot{X}_s + c_s\dot{X}_s - c_a(\dot{x}_a - \dot{X}_s) + KX_s - k(x_a - X_s) = F(t) \tag{2.12}$$

and

$$m\ddot{x}_a + c_a(\dot{x}_a - \dot{X}_s) + k(x_a - X_s) = 0. \tag{2.13}$$

In order to simplify Equations 2.12 and 2.13 the absolute response of the TMD, x_a is replaced with the response of the TMD relative to the structure, x_r where

$$x_r = x_a - X_s \tag{2.14}$$

Inserting Equation 2.14 into Equations 2.12 and 2.13 gives

$$M\ddot{X}_s + c_s\dot{X}_s - c_a\dot{x}_r + KX_s - kx_r = F(t) \tag{2.15}$$

and

$$m(\ddot{X}_s + \ddot{x}_r) + c_a\dot{x}_r + kx_r = 0. \tag{2.16}$$

Now Equations 2.15 and 2.16 are divided by M and m respectively and the following relationship is used, along with Equations 2.2 to 2.4 and 2.8, to transform these equations

$$\zeta_s = \frac{c_s}{2M\omega_s} \tag{2.17}$$

where ζ_s is the damping ratio of the structure. Equations 2.15 and 2.16 can now be written as

$$\ddot{X}_s + 2\zeta_s\omega_s\dot{X}_s - 2\mu\zeta_a\dot{x}_r + \omega_a^2 X_s - \mu\omega_2^2 x_r = \frac{F(t)}{M} \tag{2.18}$$

and

$$\ddot{x}_r + \dot{X}_s + 2\zeta_a\omega_a\dot{x}_r + \omega_a^2 x_r = 0. \tag{2.19}$$

In order to calculate the dynamic magnification factors of the structure and TMD ($Hx_s(\omega)$ and $Hx_r(\omega)$ respectively) the input displacement

$$f(t) = e^{i\omega t} = \cos\omega t + i\sin\omega t \tag{2.20}$$

will be used. Now the input force $F(t)$ can be written as

$$F(t) = Kf(t). \tag{2.21}$$

This allow Equation 2.18 to be written as

$$\ddot{X}_s + 2\zeta_s\omega_s\dot{X}_s - 2\mu\zeta_a\dot{x}_r + \omega_a^2 X_s - \mu\omega_a^2 x_r = \omega_s^2 f(t). \tag{2.22}$$

Using the harmonic input described in Equation 2.20, the responses of the structure and TMD can be found by multiplying the input times the dynamic magnification factors $Hx_s(\omega)$ and $Hx_r(\omega)$. The equations for these dynamic magnification factors are currently unknown but will be solved for in the following calculations.

$$X_s(t) = Hx_s(\omega)e^{i\omega t} \tag{2.23}$$

and

$$x_r(t) = Hx_r(\omega)e^{i\omega t} \tag{2.24}$$

respectively. By taking the first and second derivatives of the displacement responses given in Equations 2.23 and 2.24 the velocities and accelerations of the structure and

TMD can be written as

$$\dot{X}_s = i\omega H x_s(\omega) e^{i\omega t}, \tag{2.25}$$

$$\dot{x}_r = i\omega H x_r(\omega) e^{i\omega t}, \tag{2.26}$$

$$\ddot{X}_s = -\omega^2 H x_s(\omega) e^{i\omega t}, \tag{2.27}$$

and

$$\ddot{x}_r = -\omega^2 H x_r(\omega) e^{i\omega t}. \tag{2.28}$$

Now Equations 2.23 to 2.28 can be substituted into Equations 2.22 and 2.19 to give the following relationship

$$\begin{bmatrix} \omega_s^2 - \omega^2 + 2\zeta_s\omega_s(i\omega) & -\mu(\omega_a^2 + 2\zeta_a\omega_a(i\omega)) \\ -\omega^2 & (\omega_a^2 - \omega^2 + 2\zeta_a\omega_a(i\omega)) \end{bmatrix} \begin{bmatrix} Hx_s(\omega) \\ Hx_r(\omega) \end{bmatrix} = \begin{bmatrix} \omega_s^2 \\ 0 \end{bmatrix}. \tag{2.29}$$

Finally, the equations for the dynamic magnification factors can be found by solving Equation 2.29 for $Hx_s(\omega)$ and $Hx_r(\omega)$. This gives

$$Hx_s(\omega) = \frac{-\omega_s^2\omega^2 + 2\zeta_a\omega_s^2\omega_a i\omega + \omega_s^2\omega_a^2}{\Delta\Omega} \tag{2.30}$$

and

$$Hx_r = \frac{\omega_a^2\omega^2}{\Delta\Omega} \tag{2.31}$$

where

$$\begin{aligned}\Delta\Omega = \omega^4 &- i\omega^3(2\zeta_a\omega_a + 2\zeta_s\omega_s + 2\mu\zeta_a\omega_a) \\ &- \omega^2(\omega_a^2 + 4\zeta_s\zeta_a\omega_s\omega_a + \omega_s^2 + \mu\omega_a^2) \\ &+ i\omega(2\zeta_s\omega_s\omega_a^2 + 2\zeta_a\omega_s^2\omega_a) + \omega_s^2\omega_a^2.\end{aligned} \tag{2.32}$$

The mean square responses of the structure and TMD will be determined below. But first several aspects of response to random vibration must be examined. The input displacement used in deriving the above equations was given in Equation 2.20 as $f(t) = e^{i\omega t}$. Here ω is a specific forcing frequency value and the input is given as a function of time. When examining randomly occurring natural processes the forcing frequency varies and it is not possible to determine the response at specific moments in time. For such processes, it is often useful to describe the process by its autocorrelation function which provides information about the frequencies present in the data (Newland, 2005). The autocorrelation function of the input force, $F(t)$ from Equation 2.21, is given as

$$R(\tau) = \lim_{T\to\infty} \frac{1}{T} \int_0^T F(t)F(t+\tau)dt. \tag{2.33}$$

Alternatively, the autocorrelation function can be described by the equation (Newland, 2005)

$$R(\tau) = E[F(t)F(t+\tau)] \tag{2.34}$$

where E defines the expected value of the input $F(t)F(t+\tau)$. The input can now be described in the frequency domain by taking the Fourier transform of the autocorrelation function which gives the power spectral density (Newland, 2005)

$$S(\omega) = \frac{1}{2\pi} \int_{-\infty}^{\infty} R(\tau)e^{-i\omega\tau}d\tau. \tag{2.35}$$

In the calculation of the power spectral density the autocorrelation function is integrated over all time step values from $-\infty$ to ∞, thus the power spectral density effectively describes the input force at any time as a function of the forcing frequency. The autocorrelation function can be retrieved from the power spectral density by taking the inverse Fourier function

$$R(\tau) = \int_{-\infty}^{\infty} S(\omega) e^{i\omega\tau} d\omega. \tag{2.36}$$

Wind force is assumed to be a stationary process which means that the probability distribution of $F(t+\tau)$ is identical to that of $F(t)$ independent of τ (Crandall *et al.*, 1958). That is, the statistical properties of the wind force should be the same no matter what value of τ is chosen. Since the the value of τ can be any real number, τ can be taken as zero, allowing Equation 2.34 to be written as

$$R(\tau = 0) = E[F^2]. \tag{2.37}$$

If the value of τ in Equation 2.36 is also taken to be equal to zero, then Equation 2.36 can be written as

$$R(\tau = 0) = \int_{-\infty}^{\infty} S(\omega) d\omega. \tag{2.38}$$

Combining the right sides of Equations 2.37 and 2.38 gives

$$E[F^2] = \int_{-\infty}^{\infty} S(\omega) d\omega \tag{2.39}$$

which is the mean square input force. The spectrum of the response can be found by multiplying the input force by the square of the dynamic magnification factor (Crandall *et al.*, 1958). Therefore the mean square responses of the structure and TMD can be

written as

$$E[X_s^2] = \int_{-\infty}^{\infty} S(\omega)|Hx_s(\omega)|^2 d\omega \tag{2.40}$$

and

$$E[x_r^2] = \int_{-\infty}^{\infty} S(\omega)|Hx_r(\omega)|^2 d\omega. \tag{2.41}$$

As mentioned at the beginning of Section 2.1.3, the input spectrum is often taken to be constant white noise as this assumption is valid in the region of the resonant response of the structure which is the region of interest. By taking $S(\omega)$ as constant, Equations 2.40 and 2.41 can be written as

$$E[X_s^2] = S_0 \int_{-\infty}^{\infty} |Hx_s(\omega)|^2 d\omega \tag{2.42}$$

and

$$E[x_r^2] = S_0 \int_{-\infty}^{\infty} |Hx_r(\omega)|^2 d\omega. \tag{2.43}$$

Now the integral solutions for $Hx_s(\omega)$ and $Hx_r(\omega)$ are needed. This is done using the integral solutions given by Crandall and Mark (1963). Using these solutions the integrated dynamic magnification factors can be written as

$$\int_{-\infty}^{\infty} |Hx_s(\omega)|^2 d\omega = \frac{\pi\left[\frac{B_0^2}{A_0}(A_2A_3 - A_1A_4) + A_3(B_1^2 - 2B_0B_2) + A_1B_2^2\right]}{A_1(A_2A_3 - A_1A_4) - A_0A_3^2} \tag{2.44}$$

and

$$\int_{-\infty}^{\infty} |Hx_r(\omega)|^2 d\omega = \frac{\pi(-A_1B_2^2)}{A_1(A_2A_3 - A_1A_4) - A_0A_3^2} \tag{2.45}$$

where

$$B_0 = \omega_s^2\omega_a^2 \tag{2.46}$$

$$B_1 = 2\zeta_a\omega_s^2\omega_a \tag{2.47}$$

$$B_2 = \omega_s^2 \tag{2.48}$$

$$A_0 = \omega_s^2 \omega_a^2 \tag{2.49}$$

$$A_1 = 2\zeta_s \omega_s \omega_a^2 + 2\zeta_a \omega_s^2 \omega_a \tag{2.50}$$

$$A_2 = 4\zeta_s \zeta_a \omega_s \omega_a + \omega_s^2 + \omega_a^2(1+\mu) \tag{2.51}$$

$$A_3 = 2\zeta_s \omega_s + 2\zeta_a \omega_a (1+\mu) \tag{2.52}$$

and

$$A_4 = 1. \tag{2.53}$$

Substituting Equations 2.44 and 2.45 into Equations 2.42 and 2.43 gives the mean square responses of the structure and TMD:

$$E[X_s^2] = \frac{S_0 \pi \left[\frac{B_0^2}{A_0}(A_2 A_3 - A_1 A_4) + A_3(B_1^2 - 2B_0 B_2) + A_1 B_2^2 \right]}{A_1(A_2 A_3 - A_1 A_4) - A_0 A_3^2} \tag{2.54}$$

and

$$E[x_r^2] = \frac{S_0 \pi (-A_1 B_2^2)}{A_1(A_2 A_3 - A_1 A_4) - A_0 A_3^2}. \tag{2.55}$$

The effective damping generated by the TMD, ζ_{eff}, can now be calculated by setting the mean square response of the structure equipped with the TMD (Equation 2.54) equal to the mean square response of a damped single-degree-of-freedom structure where the damping ratio is given as ζ_{eff}. The dynamic magnification factor for the damped single-degree-of-freedom structure is

$$Hx_s = \frac{\omega_s^2}{\omega_s - \omega^2 + i\omega 2\zeta_{eff}\omega_s}. \tag{2.56}$$

The integral solution for this dynamic magnification factor can again be found from

Crandall and Mark (1963) and is given as

$$\int_{-\infty}^{\infty} |Hx_s|^2 = \frac{\pi\omega_s}{2\zeta_{eff}}. \tag{2.57}$$

If this single-degree-of-freedom structure is also subjected to a white noise load spectrum, the mean square response can be can be calculated in the same way as the mean square responses of the structure-TMD system and will be given as

$$E[x_s^2] = \frac{S_0\pi\omega_s}{2\zeta_{eff}}. \tag{2.58}$$

Now by equating the left-hand sides of Equations 2.58 and 2.54, the effective damping generated by the TMD can be calculated as

$$\zeta_{eff} = \frac{\omega_s}{2}\left[\frac{A_1(A_2A_3 - A_1A_4) - A_0A_3^2}{\frac{B_0^2}{A_0}(A_2A_3 - A_1A_4) + A_3(B_1^2 - 2B_0B_2) + A_1B_2^2}\right]. \tag{2.59}$$

In theoretical computer calculations, McNamara (1977) found this effective damping value to be greater than 4% for a mass ratio value of 0.02. This value of effective damping was generated when $\Omega = 0.98$ and $\zeta_a = 7\%$.

In Section 2.1.2 the optimal tuning ratio and absorber damping ratio were calculated for a structure-TMD system subjected to harmonic excitation. For a structure-TMD system with zero structural damping subjected to white noise excitation these parameters are (Warburton, 1982)

$$\Omega_{opt} = \frac{\sqrt{1 + \frac{\mu}{2}}}{1 + \mu} \tag{2.60}$$

and

$$\zeta_{opt} = \sqrt{\frac{\mu + \frac{3\mu^2}{4}}{4 + 6\mu + 2\mu^2}}. \tag{2.61}$$

The optimal effective damping for such a system can also be calculated as (Warburton, 1982)

$$\zeta_{eff}^{opt} = \frac{1}{4}\sqrt{\frac{\mu + \mu^2}{1 + \frac{3\mu}{4}}}. \tag{2.62}$$

Equations 2.60, 2.61, and 2.62 are important in TMD design. For a given required effective damping the mass ratio, μ, can be determined from Equation 2.62. This mass ratio can then be used to find the optimal tuning ratio and absorber damping ratio from Equations 2.60 and 2.61 and these values are used in the design of the TMD.

2.2 Tuned Liquid Dampers

Tuned liquid dampers (TLDs) work using the same principles as TMDs (explained in Section 2.1) except that the damping provided by a TLD is due to the viscous action of the liquid itself. The calculations used in the design of a TLD are more complex than those used in the design of a TMD as the liquid sloshing must be correctly modelled in order to determine the dynamic properties of the TLD and because the structure-TLD response is non-linear. The task of correctly modelling the TLDs is further complicated by the fact that the energy dissipated by the boundary layer liquid sloshing is often far below that required for optimal damping (ζ_{opt}) (Warnitchai and Pinkaew, 1998). In practice, screens or poles are often fixed to the inside of the TLD tank in order to increase energy dissipation (Warnitchai and Pinkaew, 1998; Tait, 2008).

Warnitchai and Pinkaew (1998) developed a mathematical model to describe the liquid sloshing and determine the dynamic properties of the TLD. This model was developed specifically to incorporate the additional damping generated by the

presence of an energy dissipating device located at the centre of the TLD tank when the structure-TLD system is excited by a harmonic force. Tait (2008) expanded on this work by determining the equivalent damping generated by a TLD for a structure-TLD system excited by a random force. Tait (2008) also developed equations which allow the structure-TLD system to be expressed as an equivalent structure-TMD system. As the optimal properties given in Equations 2.60, 2.61, and 2.62 are based on a linear model, expressing the structure-TLD system as a structure-TMD system allows the designer to determine these optimal properties. To familiarize the reader with these equations their development is presented below. Section 2.2.1 follows the derivation of the generalized properties for a TLD in which the nonlinear non-conservative forces generated by the screens are ignored (Warnitchai and Pinkaew, 1998). Section 2.2.2 builds on the equations developed in Section 2.2.1 by developing an equation for the generalized damping coefficient generated by the screens (Tait, 2008). Finally, the generalized properties defined in Sections 2.2.1 and 2.2.2 are transformed into equivalent TMD properties in Section 2.2.3.

2.2.1 Generalized TLD Properties

For the development of the following equations, the variables identified in Figure 2.5 are used. The tank's horizontal motion is $X(t)$ and this motion is equivalent to that of the structure, $X_s(t)$, at the location of the TLD.

By assuming that the liquid is inviscid, incompressible, irrotational, and has negligible surface tension, and that the tank is rigid, the velocity of a liquid particle relative to the tank can be expressed as a gradient of the velocity potential, ϕ(x,z,t). Then we can state that the amount of liquid entering a given space must be equal to that exiting the space (that is the incompressible fluid has kinematic continuity), which

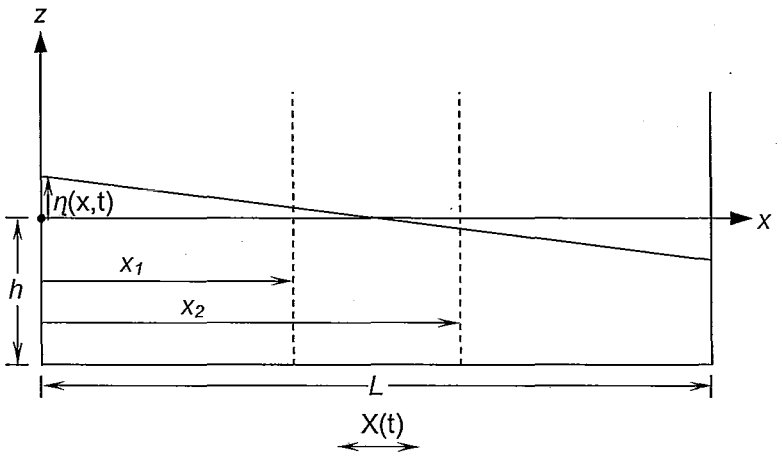

Figure 2.5: Definition Sketch for TLD Equation Development (Tait, 2008)

can be expressed as

$$\frac{\delta^2\phi}{\delta x^2} + \frac{\delta^2\phi}{\delta z^2} = 0. \tag{2.63}$$

The kinematic boundary conditions of the fluid are expressed as

$$u(x,z,t)|_{x=0,x=L} = \left.\frac{\delta\phi}{\delta x}\right|_{x=0,x=L} = 0 \tag{2.64}$$

and

$$w(x,z,t)|_{z=-h} = \left.\frac{\delta\phi}{\delta z}\right|_{z=-h} = 0. \tag{2.65}$$

The amplitude of the liquid sloshing is assumed to be small (i.e. $\eta << h$) allowing the linearized free surface condition to be applied. That is

$$\left.\frac{\delta\phi}{\delta z}\right|_{z=0} = \frac{\delta\eta}{\delta t}. \tag{2.66}$$

The solution satisfying the boundary conditions given by Equations 2.63, 2.64, and 2.65 is given in general form as the sum of infinite sloshing modes (Warnitchai and Pinkaew,

1998). That is

$$\phi(x,z,t) = \sum_{n=1}^{\infty} \dot{q}_n(t) \cos\left(\frac{n\pi x}{L}\right) \frac{\cosh\left[\frac{n\pi(z+h)}{L}\right]}{\left(\frac{n\pi}{L}\right)\sinh\left(\frac{n\pi h}{L}\right)}. \tag{2.67}$$

By substituting Equation 2.66 into Equation 2.67 the free surface can be expressed as

$$\eta(x,t) = \sum_{n=1}^{\infty} q_n(t) \cos\left(\frac{n\pi x}{L}\right) \tag{2.68}$$

where q_n is the free-surface sloshing amplitude of the n^{th} mode. The energy of the system can be expressed in terms of its gravitational potential and velocity potential, given respectively as

$$V = \frac{1}{2}\rho b g \int_0^L \eta^2(x,t)\mathrm{d}x \tag{2.69}$$

and

$$T = \frac{1}{2}\rho b \int_{-h}^{0}\int_0^L \left[\left(\dot{X} + \frac{\delta\phi}{\delta x}\right)^2 + \left(\frac{\delta\phi}{\delta z}\right)^2\right] \mathrm{d}x\mathrm{d}z \tag{2.70}$$

where ρ is the density of the fluid, b is the width of the tank perpendicular to its motion and $\dot{X}$ is the horizontal velocity of the tank (Lamb, 1945).

If this system is assumed to be conservative (that is we ignore the nonlinear non-conservative damping forces generated by the screen), it is defined by the following Lagrange equations (Tedesco *et al.*, 1999)

$$\frac{\mathrm{d}}{\mathrm{d}t}\left(\frac{\delta T}{\delta \dot{q}_n}\right) - \frac{\delta T}{\delta q_n} + \frac{\delta V}{\delta q_n} = 0. \tag{2.71}$$

If we substitute Equation 2.68 into Equation 2.69 and Equation 2.67 into Equation 2.70 then by application of the Lagrange equations given in Equation 2.71 the equation of

motion for the system can be written as

$$m_n^* \ddot{q}_n(t) + m_n^* \omega_n^2 q_n(t) = \gamma_n^* \ddot{X}(t) \tag{2.72}$$

where

$$m_n^* = \frac{1}{2} \frac{\rho b L^2}{n\pi \tanh\left(\frac{n\pi h}{L}\right)}, \tag{2.73}$$

$$\omega_n^2 = \frac{n\pi g}{L} \tanh\left(\frac{n\pi h}{L}\right), \tag{2.74}$$

and

$$\gamma_n^* = \rho b L^2 \frac{1 - cos(n\pi)}{(n\pi)^2} \tag{2.75}$$

are the generalized mass, squared natural frequency for the n^{th} sloshing mode, and excitation factor respectively. The generalized stiffness can be found from the product of Equations 2.73 and 2.74. That is

$$k_n^* = \frac{\rho b L g}{2}. \tag{2.76}$$

The modal participation factor is found by dividing the excitation factor (Equation 2.75) by the generalized stiffness (Equation 2.76). That is

$$\Gamma_n = \frac{\gamma_n^*}{m_n^*} = \frac{2}{n\pi}(1 - \cos(n\pi)) \tanh\left(\frac{n\pi h}{L}\right). \tag{2.77}$$

2.2.2 Generalized TLD Damping Coefficient

If the effect of the screens is considered, the nonlinear, non-conservative damping forces, Q_n, can be added to the Lagrange equations (Equation 2.71) to give

$$\frac{\mathrm{d}}{\mathrm{d}t}\left(\frac{\delta T}{\delta \dot{q}_n}\right) - \frac{\delta T}{\delta q_n} + \frac{\delta V}{\delta q_n} = Q_n \tag{2.78}$$

where the nonlinear damping force, Q_n, can be approximated by the product of the generalized linear damping coefficient, c_n^*, and the free-surface sloshing velocity $\dot{q}_n(t)$. That is

$$Q_n \approx c_n^* \dot{q}_n(\dot{t}). \tag{2.79}$$

The addition of the Q_n term to Equation 2.71 does not affect the derivations of m_n^*, ω_n^2, and γ_n^* given in Equations 2.73 to 2.75 so the only variable not yet defined is c_n^*. Tait (2008) determined this damping value generated by the use of screens. The derivation for this damping term follows.

For the screens shown at the discrete locations, x_j, in Figure 2.5, the solid portions of the screens normal to the flow is given as A. The solidity is then defined as (Tait *et al.*, 2005; Tait, 2008)

$$S = \frac{A}{bh}. \tag{2.80}$$

The drag coefficient, C_d, and loss coefficient, C_l, are related by the equation (Tait *et al.*, 2005; Tait, 2008)

$$C_l = SC_d. \tag{2.81}$$

The force of the liquid acting on the screens can be expressed as (Warnitchai and Pinkaew, 1998; Tait, 2008)

$$f(x,z,t) = f_i(x,z,t) + f_d(x,z,t) \tag{2.82}$$

where f_i is the inertia component of the force and f_d is the drag component of the force. The inertia component of the force does generate kinetic energy which should theoretically add a virtual mass to the generalized mass calculated in Equation 2.73. However, this virtual mass is small compared to the generalized mass and is often ignored for cases in which the h/L value of the TLD is less than 0.3 (Tait, 2008). In the TLDs monitored in this study the h/L value is 0.19 and the virtual mass was ignored in the design calculations; therefore, the derivation for the virtual mass will not be shown here. However, the drag component of the force given in Equation 2.82 is significant as it is used to calculate damping generated by the screens.

From fluid mechanics, the drag force can be expressed as

$$f_d(x_j, t) = \frac{1}{2}\rho u^2 A C_d. \tag{2.83}$$

Substituting Equations 2.67 and 2.81 into Equation 2.83 and taking the drag force at a specific height, z, and mode, n, gives

$$f_{d_n}(x_j, z, t) = \frac{1}{2}\rho b C_l \sin\left(\frac{n\pi x_j}{L}\right)^2 \left[\frac{\cosh\left[\frac{n\pi(z+h)}{L}\right]}{\sinh\left(\frac{n\pi h}{L}\right)}\right]^2 \times |\dot{q}_n(t)|\dot{q}_n(t). \tag{2.84}$$

A set of virtual horizontal displacements can be found by manipulating Equation 2.67 to find the horizontal displacements at x_j. That is

$$\delta q_n(x_j, z, t) = \frac{\cosh\left[\frac{n\pi(z+h)}{L}\right]}{\sinh\left(\frac{n\pi h}{L}\right)} \sin\left(\frac{n\pi x_j}{L}\right) \delta q_n(t). \tag{2.85}$$

The virtual work done by the non-conservative drag forces can be calculated by integrating the product of Equations 2.84 and 2.85 over the entire height of the fluid and

summing the forces generated by the number of screens, ns. The virtual work is given as

$$\delta W_{nc} = -\sum_{j=1}^{ns} \int_{-h}^{0} f_{d_n} \delta q_n \mathrm{d}z. \tag{2.86}$$

Substituting Equations 2.84 and 2.85 into Equation 2.86 produces

$$\delta W_{nc} = -\frac{1}{2}\rho b C_l \sum_{j=1}^{ns} \sin\left(\frac{n\pi x_j}{L}\right)^3 \times \int_{-h}^{0} \left[\frac{\cosh\left[\frac{n\pi(z+h)}{L}\right]}{\sinh\left(\frac{n\pi h}{L}\right)}\right]^3 \mathrm{d}z|\dot{q}_n|\dot{q}_n \delta q_n. \tag{2.87}$$

The virtual work expressed in Equation 2.87 can alternatively be expressed as the product of the non-conservative forces, Q_n, and the virtual displacement, δ_n. That is

$$\delta W_{nc} = \sum_{j=1}^{ns} Q_n \delta q_n. \tag{2.88}$$

Solving Equation 2.88 for Q_n allows the nonlinear damping forces to be expressed as

$$Q_n = -\frac{1}{2}\rho b C_l \sum_{j=1}^{ns} \sin\left(\frac{n\pi x_j}{L}\right)^3 \int_{-h}^{0} \left[\frac{\cosh\left[\frac{n\pi(z+h)}{L}\right]}{\sinh\left(\frac{n\pi h}{L}\right)}\right]^3 \mathrm{d}z|\dot{q}_n|\dot{q}_n. \tag{2.89}$$

Alternatively Q_n can be expressed as

$$Q_n = -\frac{\rho b L}{2n\pi} C_l \Delta_n \Xi_n |\dot{q}_n| \dot{q}_n \tag{2.90}$$

where

$$\Delta_n = \frac{1}{3} + \frac{1}{\sinh^2\left(\frac{n\pi h}{L}\right)} \tag{2.91}$$

and

$$\Xi_n = \sum_{j=1}^{ns} \sin\left(\frac{n\pi x_j}{L}\right)^3. \tag{2.92}$$

The equation for the damping coefficient generated by the inclusion of the screens can now be calculated from Equation 2.90. In Equation 2.79 above, the nonlinear damping forces are approximated based on a linear damping coefficient c_n^*. The equivalent linearized generalized damping coefficient, c_{eq}^*, will now be estimated by minimizing the error between the actual nonlinear damping force, Q, and the linearized generalized damping force, $c^*\dot{q}$. Since TLDs are typically designed to operate in their fundamental sloshing mode, this will be done for the first mode only. Thus the error term to be minimized is

$$\epsilon = Q_1 - c_1^*\dot{q} = C_l\frac{\rho bL}{2\pi}\Delta\Xi_1|\dot{q}|\dot{q} - c_{eq}^*\dot{q} \tag{2.93}$$

where c^* is now written as c_{eq}^* to indicate that this nonlinear generalized damping coefficient is equivalent to a linear generalized damping coefficient. The error is minimized by solving the derivative

$$\frac{\delta E(\epsilon^2)}{\delta c_{eq}^*} = 0 \tag{2.94}$$

where E indicates the expected value. This leads to

$$c_{eq}^* = C_l\frac{\rho bL}{2\pi}\Xi\Delta\frac{E(|\dot{q}|\dot{q}^2)}{E(\dot{q}^2)}. \tag{2.95}$$

Since c_{eq}^* is dependent on the excitation, q, the value of the damping coefficient can be determined for both harmonic and random excitation. For random excitation, the

damping coefficient is defined as (Tait, 2008)

$$c^*_{eq} = C_l \sqrt{\frac{2}{\pi}} \frac{\rho b L}{\pi} \Xi \Delta \sigma_q \omega_1 \tag{2.96}$$

where σ_q is the root mean square (RMS) of the free surface fluid amplitude in the first mode and ω_1 is the natural frequency of the first mode. The damping ratio can be found by dividing Equation 2.96 by the product of 2, ω, and, m^* given in Equation 2.73. That is

$$\zeta^*_{eq} = C_l \sqrt{\frac{2}{\pi}} \tanh\left(\frac{\pi h}{L}\right) \Xi \Delta \frac{\sigma_q}{L}. \tag{2.97}$$

The damping ratio given in Equation 2.97 represents the energy dissipation due to the screens. Additional energy is also dissipated due to the viscous shear created between the liquid and the tank. The damping ratio due to these boundary layer losses can be estimated as (Tait, 2004)

$$\zeta_w = \left(\frac{1}{2h}\right) \sqrt{\frac{\nu}{2\omega_n}} \left(1 + \frac{2h}{b} + SC\right) \tag{2.98}$$

where ν is the viscosity of the fluid in the TLD and SC is the surface contamination factor often taken as unity (Tait, 2008).

2.2.3 Equivalent Properties

In order to be able to calculate the optimal properties of a structure-TLD system, that system must be represented by an equivalent linear two-degree-of-freedom system such as a structure-TMD system. Once this is done, the generalized properties defined in Sectionss 2.2.1 and 2.2.2 can be expressed as equivalent properties. The equivalent properties can then be used to determine the optimal properties discussed in Section 2.1.2. The developement of these equivalent properties follows (Tait, 2008).

The equations of motion for the structure-TLD system can be determined by applying the Lagrange equations to an analogous structure-continuous-vibration-absorber system (Jacquot and Foster, 1977). Here the gravitational and velocity potentials are described for the entire system. That is

$$V_{2DOF} = \frac{1}{2}KX_s^2 + V \tag{2.99}$$

and

$$T_{2DOF} = \frac{1}{2}M\dot{X}_s^2 + T \tag{2.100}$$

where V is the gravitational potential for the TLD defined in Equation 2.69 and T is the velocity potential for the TLD defined in Equation 2.70. The non-conservative forces can be written as

$$Q_{2DOF} = F(t) - c_s\dot{X}_s - c_{eq}^*\dot{q} \tag{2.101}$$

where $F(t)$ is the external force and c_s is the damping coefficient of the structure. Application of the Lagrange equations to Equations 2.99 and 2.100 generates

$$\frac{\mathrm{d}}{\mathrm{d}t}\left(\frac{\delta T}{\delta \dot{X}_s}\right) = M\ddot{X}_s + \rho bhL\ddot{X}_s + \gamma^*\ddot{q}, \tag{2.102}$$

$$\frac{\delta V}{\delta X_s} = KX_s, \tag{2.103}$$

$$\frac{\mathrm{d}}{\mathrm{d}t}\left(\frac{\delta T}{\delta \dot{q}}\right) = \gamma^*\ddot{X}_s + m^*\ddot{q}, \tag{2.104}$$

and

$$\frac{\delta V}{\delta q} = k^*q. \tag{2.105}$$

Now the equations of motion for the structure-TLD system can be written by substi-

tuting Equations 2.101 to 2.105 into Equation 2.78. That is

$$\begin{bmatrix} (M+\rho bhL) & \gamma^* \\ \gamma^* & m^* \end{bmatrix} \begin{bmatrix} \ddot{X}_s \\ \ddot{q} \end{bmatrix} + \begin{bmatrix} c_s & 0 \\ 0 & c^*_{eq} \end{bmatrix} \begin{bmatrix} \dot{X}_s \\ \dot{q} \end{bmatrix} + \begin{bmatrix} K & 0 \\ 0 & k^* \end{bmatrix} \begin{bmatrix} X_s \\ q \end{bmatrix} = \begin{bmatrix} F(t) \\ 0 \end{bmatrix}. \tag{2.106}$$

In order to determine the equivalent properties of the structure-TLD system, Equation 2.106 must be written in a form equivalent to that of a structure-TMD system. The equations of motion for a structure-TMD system are given in Equations 2.15 and 2.19 and are written in matrix form as

$$\begin{bmatrix} (M+m) & m \\ m & m^* \end{bmatrix} \begin{bmatrix} \ddot{X}_s \\ \ddot{x}_r \end{bmatrix} + \begin{bmatrix} c_s & 0 \\ 0 & c_a \end{bmatrix} \begin{bmatrix} \dot{X}_s \\ \dot{x} \end{bmatrix} + \begin{bmatrix} K & 0 \\ 0 & k \end{bmatrix} \begin{bmatrix} X_s \\ x_r \end{bmatrix} = \begin{bmatrix} F(t) \\ 0 \end{bmatrix}. \tag{2.107}$$

In order to transform Equation 2.106 into the form shown in Equation 2.107, the fluid response, q, is related to the response, x_r, by the modal participation factor, Γ. That is (Tait, 2008)

$$q = \Gamma x_r \tag{2.108}$$

where x_r is equivalent to the displacement of the TMD in the structure-TMD system. The equivalent properties of the structure-TLD system are related to the generalized properties of the structure-TMD system by the square of the modal participation factor. That is

$$m_{eq} = \Gamma^2 m^*, \tag{2.109}$$

$$c_{eq} = \Gamma^2 c^*_{eq}, \tag{2.110}$$

and

$$k_{eq} = \Gamma^2 k^*. \tag{2.111}$$

Inserting Equations 2.108 to 2.111 into Equation 2.106 allows it to be written as

$$\begin{bmatrix} (M+\rho bhL) & m_{eq} \\ \gamma^* & \gamma^* \end{bmatrix} \begin{bmatrix} \ddot{X}_s \\ \ddot{x}_r \end{bmatrix} + \begin{bmatrix} c_s & 0 \\ 0 & c^*_{eq}\Gamma \end{bmatrix} \begin{bmatrix} \dot{X}_s \\ \dot{X}_r \end{bmatrix} + \begin{bmatrix} K & 0 \\ 0 & k^*\Gamma \end{bmatrix} \begin{bmatrix} X_s \\ X_r \end{bmatrix} = \begin{bmatrix} F(t) \\ 0 \end{bmatrix}. \tag{2.112}$$

Using the equation (Vandiver and Mitome, 1979)

$$M'_s = M + (\rho bhL - m_{eq}) \tag{2.113}$$

which modifies the mass of the structure to account for the non-participating component of the fluid and multiplying the second set of equations by Γ allows Equation 2.112 to be expressed as

$$\begin{bmatrix} (M'_s + m_{eq}) & m_{eq} \\ m_{eq} & m_{eq} \end{bmatrix} \begin{bmatrix} \ddot{X}_s \\ \ddot{x}_r \end{bmatrix} + \begin{bmatrix} c_s & 0 \\ 0 & c_{eq} \end{bmatrix} \begin{bmatrix} \dot{X}_s \\ \dot{X}_r \end{bmatrix} + \begin{bmatrix} K & 0 \\ 0 & k_{eq} \end{bmatrix} \begin{bmatrix} X_s \\ X_r \end{bmatrix} = \begin{bmatrix} F(t) \\ 0 \end{bmatrix}. \tag{2.114}$$

Equation 2.114 is in a form similar to Equation 2.107 and is expressed as an equivalent system.

The equivalent properties, m_{eq}, k_{eq}, and c_{eq}, are defined by the equations

$$m_{eq} = \frac{8\rho bL^2}{\pi^3} \tanh\left(\frac{\pi h}{L}\right), \tag{2.115}$$

$$k_{eq} = \frac{8\rho bLg}{\pi^2} \tanh^2\left(\frac{\pi h}{L}\right), \tag{2.116}$$

and

$$c_{eq} = C_l \frac{16\rho bL}{\pi^3} \sqrt{\frac{32}{\pi^3}} \tanh^3\left(\frac{\pi h}{L}\right) \Delta\Xi\omega_1\sigma_r \tag{2.117}$$

where σ_r is the RMS of the equivalent response. Finally the equivalent damping ratio, ζ_{eq}, is found by dividing c_{eq} by the product of 2, m_{eq}, and ω_1. That is

$$\zeta_{eq} = C_l \sqrt{\frac{32}{\pi^3}} \tanh^2\left(\frac{\pi h}{L}\right) \Delta\Xi\frac{\sigma_r}{L}. \tag{2.118}$$

Notice both the equivalent damping coefficient and equivalent damping ratio are dependent on the RMS of the amplitude, σ_r, thus these properties can be determined for a given amplitude. The total damping of the system is the sum of ζ_{eq} and ζ_w defined in Equation 2.98

$$\zeta_{total} = \zeta_{eq} + \zeta_w. \tag{2.119}$$

The effective damping for the system can now be calculated using Equation 2.59 with ζ_{total} being used in place of ζ_a.

Expressing the properties of the structure-TLD system in the equivalent form presented above allows the design equations used for a structure-TMD system to be used for the structure-TLD system. The preliminary design for the TLDs can be done using Equations 2.60, 2.61, and 2.62 which give the optimal damping ratio, absorber damping ratio, and effective damping for a structure-TMD system.

Chapter 3

Full-Scale Monitoring of Tall Buildings

3.1 Importance of Monitoring Tall Buildings

Monitoring the motion of existing tall buildings will allow designers to better predict the dynamic properties of new tall buildings during their design. This understanding is important considering that the current design of tall buildings relies solely on computer and scaled wind tunnel models. A complete database of dynamic properties obtained from full-scale monitoring would enable these current design methods to be verified. Unfortunately, such a database does not currently exist. In particular few estimates for buildings taller than 20 stories are available in the literature (Kareem and Gurley, 1996).

The scarcity of data available for tall buildings is problematic as these buildings are dominated by their resonant responses and thus can experience high accelerations when excited at their natural frequencies. In fact the need to limit the perceived motion of tall buildings is often a dominant design constraint. The level of discomfort

caused by building accelerations can range from perceiving the motion, to discomfort, nausea, or even effects on balance, task performance and motor functions. Occupants may also experience anxiety due to building motions as they often do not expect the building to move and may question the building's structural integrity if it does. Visual cues of movement such as swinging objects, moving sight lines, a swinging horizon, or changing light reflections can enhance occupants' perception of motion. Although building motion is undoubtedly an important design consideration, there is some debate over what criteria should be used for its evaluation. Debate encompasses both the choice of characteristic magnitude of acceleration and appropriate recurrence interval. The characteristic magnitude of acceleration could be chosen as the peak or RMS value, or some variation of these with the building period. In North America the recurrence interval is normally chosen as 10 years. Figure 3.1 shows commonly used acceleration criteria for tall buildings. (Isyumov, 1999, 1995).

The response of a tall building to dynamic loads is dependent on the building's damping ratio. This property depends on many different factors and is thus difficult to predict. The initial damping ratio estimate is normally obtained from tests conducted on existing buildings with similar material and structural systems. Using this method, the damping estimates are normally only within plus or minus 30% (Kareem and Gurley, 1996). Several tall buildings have recently been added to the full-scale monitoring literature. The damping estimates ascertained from these buildings will add vital tall-building data to the information used by researchers trying to develope empirical predictive tools for damping estimation such as those given in by Jeary (1986) and Satake *et al.* (2003).

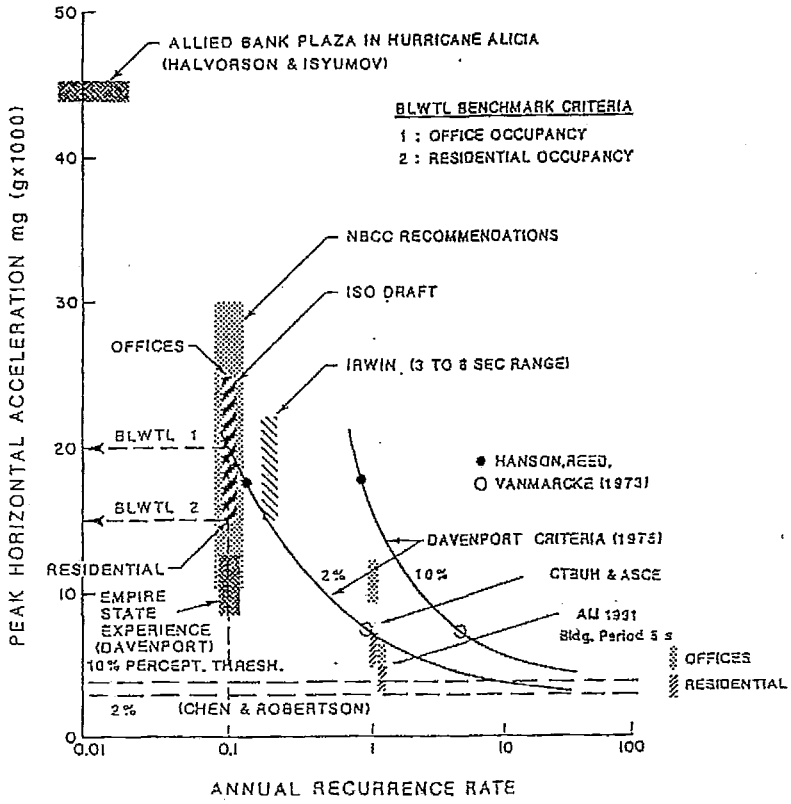

Figure 3.1: Commonly Used Acceleration Criteria for Tall Buildings (Isyumov, 1995)

3.2 Current Research on Tall Buildings

The tall buildings recently added to the full-scale monitoring literature include three buildings in Chicago (Kijewski-Correa *et al.*, 2006). As building owners are reluctant to permit access to researchers it was important that the anonymity of the buildings be maintained. Thus the buildings have been labeled as Building 1, Building 2, and Building 3. Building 1 resists lateral loads by the use of a steel tube system made up of exterior columns, spandrel ties, and additional stiffening elements. Building 2's lateral-load-resisting system is comprised of concrete shear walls located near the core. The core is tied to the outside columns via outrigger walls at two levels. Finally, Building 3 uses a steel moment-connected framed tubular system to resist lateral loads. In this

study both the spectral-based half-power bandwidth method and the random decrement technique were used to estimate the damping ratio from the full-scale response measurements. These parameter estimation techniques are discussed in detail in Chapter 4. Results presented by Kijewski-Correa *et al.* (2006) suggest that the in situ damping ratio values for Buildings 2 and 3 (the concrete and coupled steel buildings) were likely higher than the 1% value assumed for design. For Building 1 (the uncoupled steel building) the 1% value seemed accurate.

Two tall buildings in Hong Kong were also recently added to the full-scale literature. The shorter of the two is a 30-storey, 120 m tall composite structure. The taller is a 70-storey, 370 m tall building constructed of steel and concrete. The study of this building's response to wind loads is considered particularly important because its location makes it subject to very horizontal wind forces during typhoons (Li *et al.*, 1998).

The Di Wang Tower in Shenzhen City, China is another tall building with full-scale monitoring results in the literature (Li *et al.*, 2002, 2004). This building is a 79-storey, 324 m tall structure consisting of a concrete core tied to a steel perimeter frame at four levels via outrigger walls. The study of this building is important as it has a height-to-width ratio of 8.78 which exceeds the criteria given in China's design codes (Li *et al.*, 2002). In this study the damping ratios were again estimated using both the half-power bandwidth method and the random decrement technique. Special attention was paid to the amplitude-dependent characteristic of damping, originally identified by Jeary (1986). The amplitude-dependence of damping can be explained as follows. There are two principle means of energy dissipation; these are the rubbing of materials against each other at joints in the structure, and the lengthening of microcracks in the materials. As the amplitude of a building's motion increases, the number of joints and microcracks participating in the energy dissipation will increase. Thus more

energy will be dissipated through these mechanisms as the building's motion increases (Jeary, 1986). Jeary (1986) also found that there were upper and lower plateaus to damping as a lower threshold of building displacement must be overcome before the joints and microcracks can be mobilized and at an upper limit of building displacement the joints and microcracks will reach their maximum displacement and no more energy will be dissipated with increased building displacement. The measurements obtained in the study lead to damping estimates of 0.57% and 0.58% using the random decrement method (considered the more accurate damping estimation technique (Li *et al.*, 2004)). However, these estimates were obtained from measurements ascertained during moderate wind conditions. Thus a 1% damping ratio was considered appropriate for design to meet serviceability criteria as the damping ratio increases with increased acceleration.

3.3 Monitoring Structure-TLD Systems

Information gained from monitoring tall buildings equipped with TLDs can be used to tune the TLDs. In Chapter 2, Section 2.1.2 the importance of properly tuning TLDs to the structure's natural frequency is discussed. In order to properly tune a TLD the natural frequency of the building must be correctly identified. Through monitoring, a building's true natural frequency can be determined. This value can then be used to tune the TLDs (the natural frequency of a TLD can be adjusted simply by altering the height of the liquid in the tanks). Through further monitoring the effect of adjusting TLD parameters on the effective damping they generate can be determined. (The effective damping generated by a TLD is defined in Section 2.1.3, Equation 2.59).

3.4 Previous Structure-TLD Study

In 1995 Tamura studied four structures equipped with TLDs (Tamura *et al.*, 1995). These structures included the Nagasaki Airport Tower, a 42 m steel-framed tower; the Yokohama Marine Tower, a 101.3 m steel trussed structure; the Shin-Yokohama Prince Hotel, a 149 m tall cylindrical structure; and the Tokyo International Airport Tower, a 77.6 m tall tower. The TLDs in all four of these buildings differed from the ones located in the building currently being studied in this project in that they were shallow-water TLDs. Shallow-water TLDs use viscous action and wave breaking to dissipate energy, while deep-water ($h/L >> 0.1$) TLDs, like the ones in the building studied in this project, require the use of screens (discussed in Section 2.2.2) to dissipate energy (Kareem and Kijewski, 1999). The dynamic response and damping ratio of the buildings investigated by Tamura were found both before and after the TLDs were installed using the random decrement technique and forced-vibration. It was found that the TLDs reduced the acceleration response during strong wind events to 1/3 to 1/2 the response when the TLDs were not present.

3.5 Building-TLD Sytem in this Study

The building being monitored in this study is located in downtown Toronto, Canada. As mentioned in Section 3.2 it is important that monitored buildings remain anonymous. Thus the monitored building will be referred to as Building X in this report. Building X is 52 stories and 187 m tall. It resists lateral loads through the use of coupled concrete shear walls parallel to the building's short dimension. Building X is unique because it is very narrow in its East-West dimension. With an aspect ratio of 1:13, it is one of the most slender buildings in the world. Figures 3.2 and 3.3 show the accelerations of the building in the East-West and North-South directions, respectively. From these figures

it is clear that the East-West accelerations have a lower natural frequency and higher magnitude than the North-South accelerations.

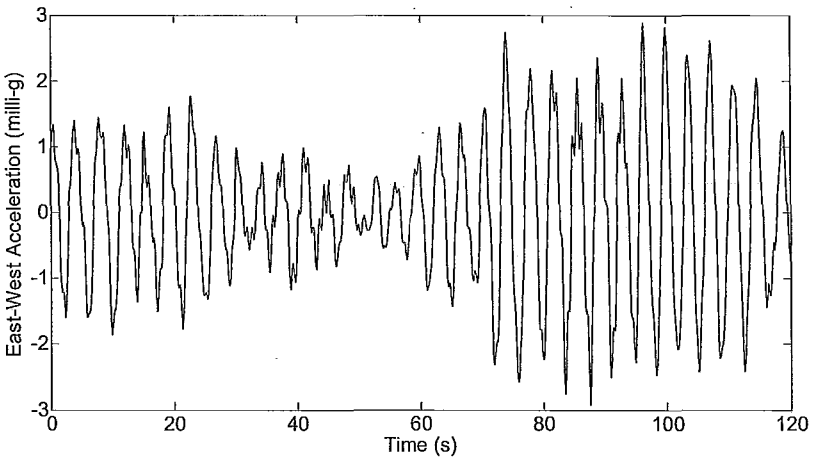

Figure 3.2: East-West Accelerations of a 187 m Building

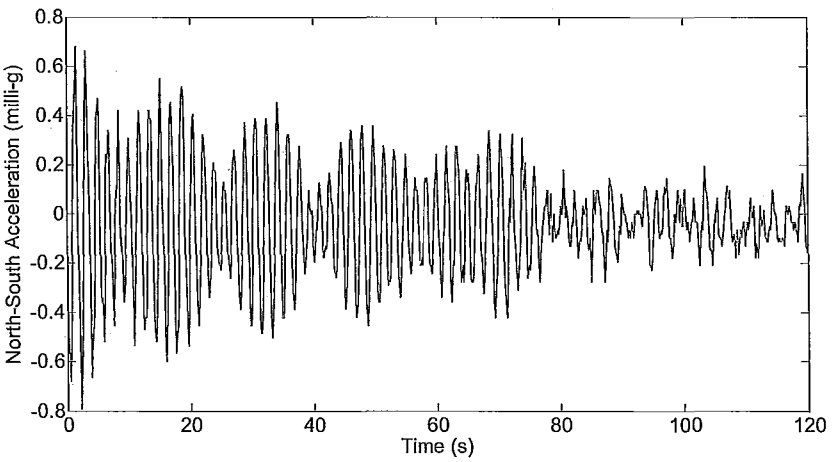

Figure 3.3: North-South Accelerations of a 187 m Building

As a result of Building X's slender aspect ratio, mandatory wind-tunnel tests were required to determine its predicted accelerations and dynamic properties. These tests were conducted at RWDI in Guelph, Ontario. As expected, the tests indicated that the East-West accelerations of the building would exceed acceptable limits. In

order to mitigate this problem a total of ten TLDs were added to the roof of the building during its construction.

Building X is an ideal structure for monitoring purposes. Since wind tunnel tests were performed on the building before its construction, the actual dynamic properties of the building can be compared to those predicted by scale-models. Also, since Building X is equipped with TLDs it is possible to use full-scale data in order to tune the TLDs as discussed in Section 3.3.

In this study, it was originally found that Building X's true natural frequency was higher than originally predicted. Since the TLDs in Building X were originally tuned to the predicted natural frequency, the TLDs were not operating optimally. Figure 3.4 shows the response spectrum for Building X's accelerations in the East-West direction. This figure shows that the structure is acting as a single-degree-of-freedom system.

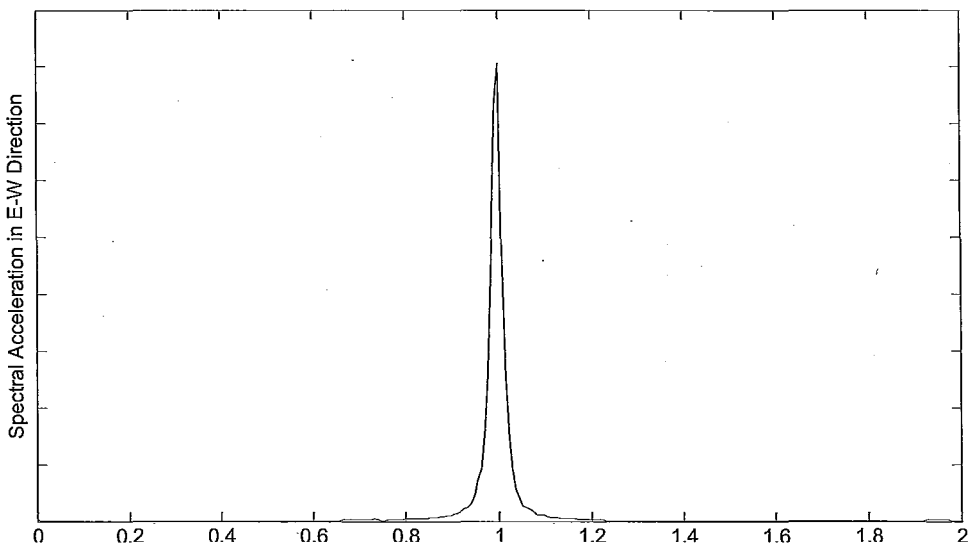

Figure 3.4: Response Spectrum Showing SDOF Behaviour

Although the TLDs were not performing optimally, the increase in peak acceleration is not significant. This is because the wind-induced motion of a structure decreases as its frequency increases (Isyumov *et al.*, 2010). The effect of this decrease in wind-

induced motion counteracts the effect of mistuning. The peak response acceleration, $\hat{a}$ can be estimated as

$$\hat{a} \propto \hat{a}_p \left(\frac{f_s}{f_p}\right)^{2-n} \left(\frac{\zeta_s}{\zeta_s + \zeta_{eff}}\right)^{1/2} \tag{3.1}$$

where $\hat{a}_p$ is the peak acceleration based on the predicted dynamic property values, f_s is the natural frequency of the structure, f_p is the predicted natural frequency of the structure, and n is an empirical constant that can take on different values (Isyumov *et al.*, 2010). Figure 3.5 shows the normalized peak hourly acceleration for a structure-TLD system optimized based on the originally predicted f_s values. The peak acceleration values are normalized by the predicted peak acceleration for a system with no TLDs and with $f_s = f_p$. In this figure the value of n is 2.45. The figure also shows the peak hourly acceleration for Building X if no TLDs were used.

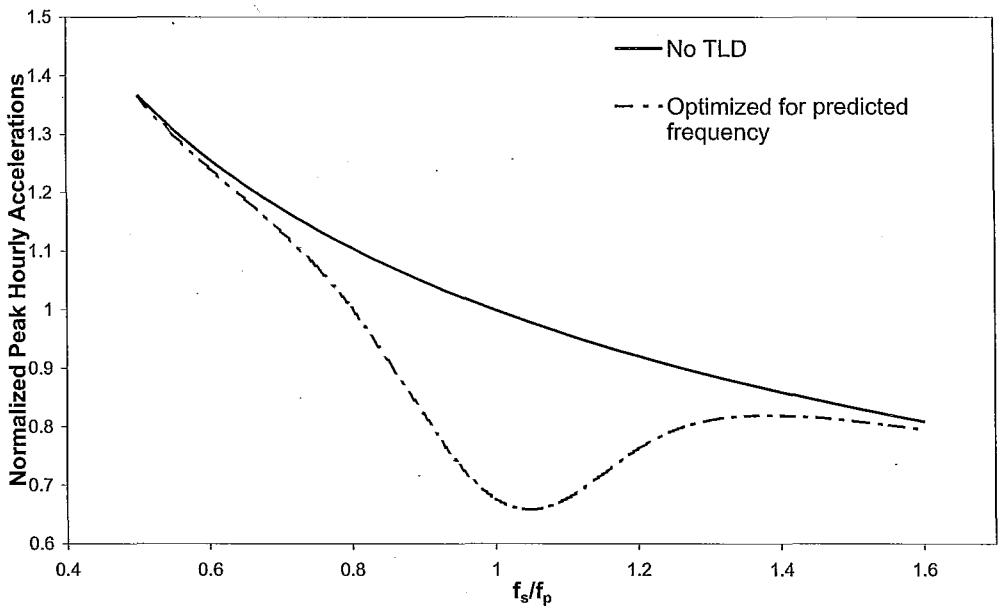

Figure 3.5: Influenc of f_s/f_p on Peak Acceleration

Chapter 4

Parameter Estimation Techniques

Currently, it is not possible for engineers to determine a structure's damping ratio using analytical methods based on first principles as this value is dependent on many different energy dissipating mechanisms. One of the most effective ways to gain insight into a structure's damping characteristics is through the use of full-scale monitoring. Once data is obtained from full-scale measurements, the dynamic characteristics of the structure can be determined using several different methods. These methods can be categorized as: frequency-domain, or spectral, methods and time-domain methods. The measurements themselves can be taken using either forced vibrations (including free vibration) or ambient vibrations (Littler, 1995).

In Section 4.1 forced vibration methods will be explained. Section 4.2 will describe statistical methods for determining spectral estimates from ambient conditions and the frequency-domain half-power bandwidth method used for estimating dynamic properties. Finally, Section 4.3 will describe the commonly used time-domain random decrement method and its limitations. The maximum likelihood method and least squares method, which are used for the analysis in this study, are described in detail in Chapter 5.

4.1 Forced Vibration Methods

Forced-vibration measurements can be obtained by using exciters to induce structural motion. These exciters usually consist of a set of contra-rotating masses that produce a sinusoidal force. There are two ways of determining response measurements from forced-vibration. The first is to generate a response spectrum and the second is to generate the decay signature through free vibration of the structure (Littler, 1995). These methods will be discussed in Sections 4.1.1 and 4.1.2, respectively. While forced vibration methods are the most accurate for obtaining dynamic property estimates, they are expensive and time-consuming (Littler, 1995) thus the ambient excitation methods discussed in Sections 4.2 and 4.3 and Chapter 5 are often more feasible.

4.1.1 Spectrum Generation through Forced Vibration

A structure's response spectrum can be generated by setting the exciters to a known frequency and recording the structure's accelerations via accelerometers once the structure's steady-state response motion is achieved. The frequency of the excitation is then incrementally increased and the response at each frequency is recorded. The response accelerations are converted to displacements and normalized by the applied force. The normalized displacements can then be plotted with respect to the applied excitations to generate the response spectrum (Littler, 1995). Finally, the dynamic properties can be determined from the response spectrum via the half-power bandwidth method described in Section 4.2.4.

The accuracy of this method depends on the accuracy and stability of the exciters and the accuracy of the accelerometers. It is also important that the incremental increases in the excitation frequency are small especially in the region of the resonant response. Small increases in the excitation frequency will ensure a high frequency res-

olution in the response spectrum. The importance of this is discussed in more detail in Section 4.2.1.

4.1.2 Decay Signature Generation through Forced Vibration

The decay signature of a structure can be determined by setting the exciters to the natural frequency of the structure which is determined from the response spectrum. The excitation is then ceased and the response of the structure is recorded via accelerometers (Littler, 1995). This response is the structure's damped free-vibration response or decay signature. The natural frequency of the structure can then be found as the inverse of the period between adjacent peaks. The damping ratio can be determined from the logarithmic decrement defined as

$$\delta = \ln \frac{D_p(n)}{D_p(n+1)} = \frac{2\pi\zeta}{\sqrt{1-\zeta^2}} \tag{4.1}$$

where $D_p(n)$ and $D_p(n+1)$ define the amplitudes of two consecutive peaks on the decay signature. For small values of ζ, ζ is thus approximated as

$$\zeta \approx \frac{\delta}{2\pi}. \tag{4.2}$$

The accuracy of this method depends only on the ability of the exciters to accurately produce specific frequencies and the ability of the accelerometers to accurately measure the accelerations. Thus this method is preferable to the one described in Section 4.1.1 when no information about the stability of the exciters is known (Littler, 1995).

4.2 Spectral Analysis

In Section 2.1.3 the spectral density is defined as the Fourier transform of the autocorrelation function. That is

$$S(\omega) = \frac{1}{2\pi} \int_{-\infty}^{\infty} R(\tau) e^{-i\omega\tau} d\tau. \tag{2.35}$$

When determining a spectrum based on measured response values, the continuous response, $x(t)$, is approximated by the discrete response values x_s at times s. The finite series of response measurements is divided into n data blocks of equal length. The autocorrelation function can be estimated as

$$R_r = \frac{1}{N} \sum_{s=0}^{N-1} x_s x_{s+r} \tag{4.3}$$

where

$$N = \frac{T}{\Delta t} \tag{4.4}$$

is the number of points per block, T is the total period of the block, and Δt is the sampling interval. In a manner similar to that shown in Equation 2.35 the discrete Fourier transform of the estimated autocorrelation function can be taken as

$$S_k = \frac{1}{N} \sum_{r=0}^{N-1} R_r e^{-i(2\pi kr/N)} \tag{4.5}$$

where S_k are a series of spectral coefficients. In practice the Fourier transform is normally obtained using the Fast Fourier transform algorithm. The smoothed spectrum can be estimated at frequencies $\omega_k = 2\pi k/T$ as

$$\tilde{S}(\omega_k) \simeq \frac{T}{2\pi} S_k. \tag{4.6}$$

Finally, the values of the averaged spectra at ω_k can be found as

$$\hat{S}(\omega_k) = \frac{1}{2n+1} \sum_{m=-n}^{n} \tilde{S}(\omega_{k+m}) \tag{4.7}$$

where n is the number of blocks into which the response measurements have been divided (Newland, 2005).

Damping and natural frequency estimates can then be found from a frequency-domain method. The commonly used half-power bandwidth method is described in Section 4.2.4 and the maximum likelihood method and least squares method, which are the frequency domain techniques used in this study, are described in Chapter 5. The accuracy of any dynamic property estimate obtained from a frequency-domain method can be eroded by the presence of bias and variance errors. Descriptions of these errors follow in Sections 4.2.1 and 4.2.2 respectively.

4.2.1 Bias Error

In statistical terms, a bias exists when the mean value of many estimated parameter values is consistently different from the actual parameter value. An example of a bias error is illustrated in Figure 4.1. The bias of an estimated parameter is given as

$$b[\hat{\Theta}] = E[\hat{\Theta}] - \Theta \tag{4.8}$$

where Θ is the true value of the parameter being estimated, $\hat{\Theta}$ is the estimate, and E denotes the expected value. It is often convenient to express the bias as a percentage of that parameter. This results in the normalized bias error defined as

$$\epsilon_b = \frac{E[\hat{\Theta}]}{\Theta} - 1. \tag{4.9}$$

Spectral estimates are prone to bias as illustrated in Figure 4.2. Since, for real measurements, the number of points per block, N, cannot be infinite, the rapid variation in the amplitude of the spectrum near resonance will not be accurately represented by the points. Thus the magnitude of the spectrum near resonance will always be underestimated. As N increases, the bias error will decrease.

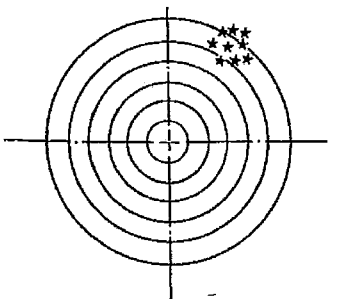

Figure 4.1: Bias Error in Gun Shots at a Target (Bendat and Piersol, 2000)

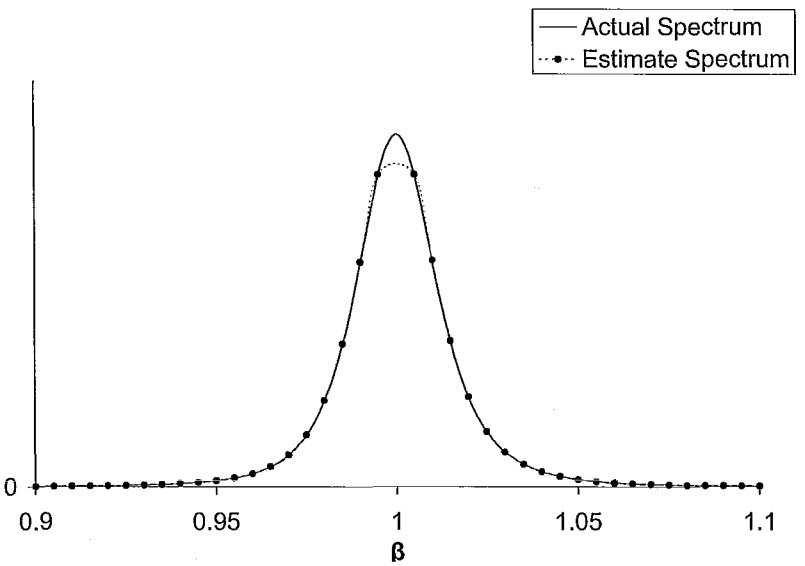

Figure 4.2: Spectral Estimate Showing Bias

Bendat and Piersol (2000) have shown that for a spectral estimate of a stationary

ergodic random process filtered using a rectangular window, the normalized bias error is given as

$$\epsilon_b = -\frac{1}{3}\left(\frac{\Delta_{FFT}}{B_r}\right)^2 \tag{4.10}$$

where

$$\Delta_{FFT} = \frac{1}{T} = \frac{1}{N\Delta t} \tag{4.11}$$

is the frequency resolution of the Fourier transform for a block of length N and

$$B_r \approx 2\zeta f_0 \tag{4.12}$$

approximates the half-power bandwidth of the spectrum with damping ratio, ζ, and natural frequency, f_0 (Bendat and Piersol, 2000). For a stationary ergodic random process filtered using a continuous window, such as the Hamming window used in this study, the bias error will be less than that given in Equation 4.10 provided that (Schmidt, 1985)

$$\frac{B_r}{\Delta_{FFT}} \gtrsim 4. \tag{4.13}$$

Bendat and Piersol (2000) recommend that Equation 4.13 be adhered to even for data filtered using a rectangular window, in order to limit the bias error to 2%. Thus in order to decrease the bias error, it is necessary to increase the block lenghth, N. However for a given record length, increasing the block length will necessitate decreasing the number of blocks, n. This will increase the variance error as illustrated in the following section.

4.2.2 Variance Error

The variance error, or random error, describes the error that can occur in any direction and have any magnitude. An example of a variance error is illustrated in Figure 4.3.

The variance of an estimated parameter, $\hat{\Theta}$, is given as

$$\sigma^2[\hat{\Theta}] = E[(\hat{\Theta} - E[\hat{\Theta}])^2]. \tag{4.14}$$

In order to express the variance in the same units as the parameter Θ it is often reported as the random error defined as

$$\sigma[\hat{\Theta}] = \sqrt{E[(\hat{\Theta} - E[\hat{\Theta}])^2]}. \tag{4.15}$$

The random error expressed as a percentage of the true parameter value Θ defines the normalized random error or coefficient of variation

$$COV = \frac{\sqrt{E[(\hat{\Theta} - E[\hat{\Theta}])^2]}}{\Theta}. \tag{4.16}$$

Bendat and Piersol (2000) have shown that for a spectral estimate generated from n different subrecords, the coefficient of variation is given as

$$COV = \frac{1}{\sqrt{n}} \tag{4.17}$$

where n is the number of blocks averaged to create $\hat{S}(\omega_k)$. Increasing the number of blocks decreases the variance. This makes intuitive sense since increasing the number of blocks increases the likelihood that the sampled spectra accurately represent the actual response spectrum.

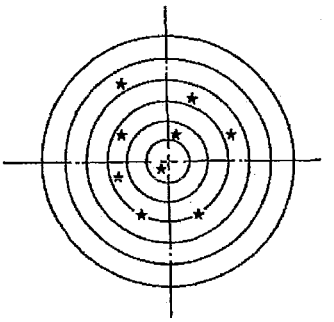

Figure 4.3: Variance Error in Gun Shots at a Target (Bendat and Piersol, 2000)

4.2.3 Selective Ensemble Averaging

A random process is said to be stationary if the statistical characteristics of that process are independent of the origin time at which the recording of the process begins. An averaged response spectrum can only be an accurate representation of the true response if the process being averaged is stationary. This means that Equation 4.3 must be independent of s. In order to collect enough stationary data, so that an averaged response spectrum of sufficient length can be generated, selective ensemble averaging is often used. This is done by stringing together many records which were obtained under similar wind conditions. The stringing together of many records creates one continuous record. Littler (1995) recommends that the difference in response between the records used to create the continuous record be less than that due to variance error. That is

$$\Delta\sigma^2 \leq \frac{1}{\sqrt{n}}. \tag{4.18}$$

This method of ensemble averaging was used in the current study.

4.2.4 Half Power Bandwidth

The dynamic properties of a single-degree-of-freedom system are commonly estimated using the half power bandwidth (HPBW) technique. This technique essentially fits the

response spectrum to the dynamic magnification function (DMF) at two points. The dynamic magnification function for a single-degree-of-freedom system is given as

$$Hx = \frac{1}{\sqrt{(1-\beta^2)^2 + (2\zeta\beta)^2}}. \tag{4.19}$$

The maximum value of DMF is defined as

$$Hx_{max} = \frac{1}{2\zeta\sqrt{1-\zeta^2}}. \tag{4.20}$$

The frequencies at which the response is reduced to $1/\sqrt{2}$ of the peak response can be determined using the following derivation

$$\frac{1}{\sqrt{(1-\beta^2)^2 + (2\zeta\beta)^2}} = \frac{1}{\sqrt{2}}\left(\frac{1}{2\zeta\sqrt{1-\zeta^2}}\right). \tag{4.21}$$

Solving Equation 4.21 for β^2 yields the two roots

$$\beta_{1,2}^2 = 1 - 2\zeta^2 \pm 2\zeta\sqrt{1-\zeta^2}. \tag{4.22}$$

The difference between β_1 and β_2 is

$$\beta_1 - \beta_2 = 2\zeta\sqrt{1-\zeta^2} \approx 2\zeta \tag{4.23}$$

for small ζ. Now ζ can be estimated by dividing Equation 4.23 by 2

$$\zeta \approx \frac{\beta_1 - \beta_2}{2}. \tag{4.24}$$

The natural frequency can simply be estimated as the frequency value corresponding to the maximum value of DMF. (Tedesco *et al.*, 1999; Chopra, 2007).

4.3 Random Decrement Technique

The random decrement technique (RDT) is a time-history method for determining the dynamic properties of a structure. It was first developed in 1973 to be used for on-line detection of cracks in aerospace structures (Cole, 1973). The principle behind the random decrement technique is that the response of a structure can be represented by the superposition of a random component and a homogeneous component. The random component is due to the forced vibration and is dependent upon the random externally applied force. The homogeneous component represents the damped free vibration response of the structure. This component is dependent on the dynamic properties of the structure and the initial displacement and velocity of the structure.

The random decrement method sequentially scans a time-history record for given displacement and velocity values. These values are known as the trigger values, X_0 for displacement and $\dot{X}_0$ for velocity. The merits of various trigger conditions are discussed in detail by Kijewski-Correa (2003). Segments from the time-history having a prescribed length and the given trigger values are collected and averaged together. The result is that random components of the time-histories will cancel out and the homogeneous components will all be representative of the same free vibration response and will thus average to this response. The process is illustrated in Figure 4.4 where X_F is the random component. The response curve obtained in the bottom left of Figure 4.4 represents the damped free vibration response for a single-degree-of-freedom system. The natural frequency of the system can be found as the inverse of the period between consecutive peaks of the response curve and the damping ratio can be found from the logarithmic decrement defined in Equations 4.1 and 4.2. The drawback of this technique is that it cannot be used to model coupled two-degree-of-freedom systems such as structure-TLD systems. In the present study, the random decrement technique is used to verify the maximum likelihood and least squares programs for single-degree-

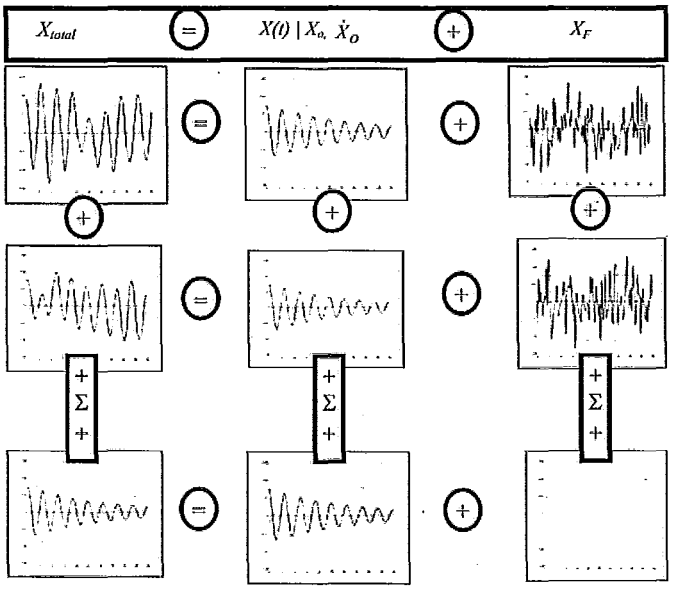

Figure 4.4: Illustration of the Random Decrement Technique (Kijewski-Correa, 2003)

of-freedom systems described in Chapter 5. The RDT is not designed to be used for multi-degree-of-freedom systems. A comparison of the results generated by the maximum likelihood method, least squares method, and RDT for 2DOF data is provided in Chapter 5.

Chapter 5

Maximum Likelihood Method and Least Squares Method Descriptions and Validations

In this study two novel computer programs were developed based on two different parameter estimation methods. These programs can be used to estimate the dynamic properties of both single-degree-of-freedom (SDOF) and two-degree-of-freedom (2DOF) structures. The parameter estimation methods used to develop the programs are the maximum likelihood (ML) method and the least squares (LS) method. The programs used to implement these methods were written using MATLAB (2009). The ML method used in this study is based on the procedure introduced by Montpellier (1997) and the LS method was developed independently. Initially programs used to implement these methods for a single-degree-of-freedom (SDOF) structure were developed and these programs are described in Section 5.1. The programs used to implement ML and LS methods for coupled 2DOF structures are described in Section 5.2. Section 5.3 describes how these MATLAB programs were verified. Finally, Section 5.4 investigates

the performance of both the ML and LS programs.

5.1 Methods Using SDOF Models

The ML and LS parameter estimation methods operate using the same principles. In both cases, a sample of random data is obtained and a curve with unknown parameters, Θ, is fit to this data. In signal analysis, the time-history data obtained from measurement is first transformed into the frequency domain using the methods discussed in Section 4.2 and it is the frequency response spectrum to which a curve is fit. For SDOF systems, the curve fit to the sample acceleration spectral data is the equation of the frequency response function for a SDOF. That is

$$|S(f)|^2 = \frac{\left(\frac{f}{f_0}\right)^4}{\left[1-\left(\frac{f}{f_0}\right)^2\right]^2 + \left[2\zeta\left(\frac{f}{f_0}\right)\right]^2} \tag{5.1}$$

where $S(f)$ is the frequency response function for the SDOF system, f is the forcing frequency, f_0 is the system's natural frequency, and ζ is the damping ratio of the system. In the curve described by Equation 5.1 the unknown parameters, Θ, are f_0 and ζ. These parameters are adjusted in order to best fit the sample data and the parameters corresponding to the best fit are the estimates of the true f_0 and ζ values for the system. The estimated parameters are given the notation $\hat{\Theta}$ or $\hat{f_0}$ and $\hat{\zeta}$. The difference between the ML and LS methods is the way in which the curve fitting is performed.

5.1.1 ML Method Description

The maximum likelihood method is a commonly used statistical technique for obtaining parameter estimates. This method can be described in generic form as follows. Assume a set of independent random variables is given as $x_1, ..., x_n$ and this data is known to have the probability density function $PDF(x, \Theta)$ which depends on the random variables, x, and the unknown parameter(s), Θ. Then the likelihood function for this data is given as

$$L(x_1, ...x_n) = PDF(x_1, \Theta) \times PDF(x_2, \Theta) \times ...PDF(x_n, \Theta). \tag{5.2}$$

The likelihood function describes the probability that the n sampled values would have occurred for a given Θ. It is often more convenient to write Equation 5.2 in the following form

$$\ln L(x_1, ..., x_n, \Theta) = \sum_{i=1}^{n} \ln PDF(x_i, \Theta). \tag{5.3}$$

For a given fixed set of sample data, $x_1, ...x_n$, L is dependent on Θ only. The values of Θ that make L a maximum are the estimates, $\hat{\Theta}$, of the true values of the unknown parameters. This makes intuitive sense, as the maximum value of the likelihood function occurs when the values of the parameters, Θ, are such that it is most likely that the sampled values would be observed. Traditionally the estimated parameters, $\hat{\Theta}$, would be found by taking the derivative or partial derivatives of L with respect to Θ, setting these derivative equations equal to zero and solving for Θ (Montpellier, 1997; Hayter, 2002). However, using MATLAB (2009) tools, it is not necessary to take derivatives of the likelihood function, rather, the values of Θ that maximize L can be found directly. It is beneficial to use the tools available in MATLAB (2009) for finding the maximum of the L function as opposed to taking its derivatives because the L function changes rapidly with respect to the forcing frequency in the region of the resonant peak. Due

to this rapid variation, the partial derivative of the likelihood function with respect to f may have a discontinuity at $f = f_0$ making it impossible to find a solution that will set all partial derivatives equal to zero. The method employed by the MATLAB (2009) tools to find the maximum value of L is discussed in Section 5.1.3.

Montpellier (1997) proposed a method for using the ML method to determine the dynamic properties, f_0 and ζ, of a SDOF system by allowing the normalized mechanical admittance function to replace the probability density function in the likelihood equation. The parameters, Θ, that are adjusted in order to maximize the likelihood function are then f_0 and ζ. The PDF function used in Equation 5.3 is thus

$$PDF(f, f_0, \zeta) = \left(\frac{|S(f)|^2}{A_r}\right)^{\frac{S_R(f)}{A_{peak}}} \tag{5.4}$$

where $S(f)$ is the frequency response function for a SDOF system defined in Equation 5.1, A_r is the area under the resonant peak of the frequency response function, S_R is the spectrum of the response data, and A_{peak} is the area under the resonant peak of the response spectrum. The criteria for defining the limits of the resonant peaks are described in Section 5.1.3. The exponent $S_R(f)/A_{peak}$ is a weighting value. By taking the logarithm of Equation 5.4 and writing this equation such that it can be applied to discrete values, the function to be maximized is

$$\ln PDF(f_j, f_0, \zeta) = \sum_j \left(\frac{S_R(f_j)}{A_{peak}}\right) \ln\left(\frac{|S(f_j)|^2}{A_r}\right) \tag{5.5}$$

where f_j are frequency values ranging from the lower frequency limit f_l to the upper frequency limit f_u. These frequency limits are defined such that the resonant peak is isolated and the methods for finding them are given in Section 5.1.3. The areas A_{peak} and A_r are also calculated over the range of f_l to f_u and these calculations are also

discussed in Section 5.1.3.

5.1.2 LS Method Description

The least squares method, like the maximum likelihood method, is a commonly used method for estimating parameters. This method minimizes the vertical distance between the data points $(x_1, y_1), ...(x_n, y_n)$ and the model to which they are being fit. The equation to be minimized is thus

$$Q = \sum_{i=1}^{n} (y_i - y(x_i, \Theta))^2 \tag{5.6}$$

where y_i is the measured data point at i and $y(x_i, \Theta)$ is the model which depends on both x_i and the unknown parameter(s) Θ. Like the ML method, the unknown parameters, Θ, that minimize Equation 5.6 can be found by taking the partial derivatives of that equation with respect to Θ. The derivative equations can then be set to zero and solved for Θ. Also like the ML method, for application in the current study it was found to be more effective to find the values of the Θ that minimize Equation 5.6 using the built-in minimization function in MATLAB (2009). The method employed by MATLAB is discussed in Section 5.1.3.

In this study the value being minimized is the area between the normalized response spectrum, obtained from the full-scale data, and the normalized frequency response function. Thus the LS method attempts to match the variances of the two response spectra. The difference in area is weighted by the area under the normalized response spectrum curve at each increment. This allows more importance to be placed on the values at resonance. The function to be minimized is thus

$$\sum_j S_{Rnorm}(f_{j,j+1}) \times \left[|S(f_{j,j+1})|^2_{norm} - S_{Rnorm}(f_{j,j+1}) \right]^2 \tag{5.7}$$

where $S_{Rnorm}(f_{j,j+1})$ is the area under the S_R curve between f_j and f_{j+1} normalized by the area under S_R, A_{peak} and $|S(f_{j,j+1})|^2_{norm}$ is the area under the $|S(f)|^2$ curve between f_j and f_{j+1} normalized by the area A_r. As in the ML method the values of f_j range from f_l and f_u, and the areas A_{peak} and A_r are also calculated over this range. The technique for determining these limits for the LS method is described in Section 5.1.4.

5.1.3 ML MATLAB Program

As discussed in Section 5.1.1, the maximum likelihood method attempts to maximize the function

$$\ln PDF(f_j, f_0, \zeta) = \sum_j \left(\frac{S_R(f_j)}{A_{peak}}\right) \ln\left(\frac{|S(f_j)|^2}{A_r}\right). \tag{5.5}$$

For this project a MATLAB (2009) program to optimize this function was developed. The MATLAB (2009) program transforms the time-history data into the response spectrum $S_R(f_j)$ using a Hamming window where the difference between adjacent discrete frequencies is given by

$$f_j = j\Delta FFT. \tag{5.8}$$

The frequency response function to be fit to the response spectrum is given by Equation 5.1. The resonant peak is isolated by assuming that is begins exactly when $|S(f_j, f_0, \zeta)|^2 > 1$. This value was chosen based on the method outlined by Montpellier (1997). Thus f_l can be calculated as

$$f_l = f_j \text{ exactly when } |S(f, f_0, \zeta)|^2 > 1 \tag{5.9}$$

where f_l is the minimum frequency value, f_j used in Equation 5.5. The frequency response function is assumed to be symmetric about its maximum value. Thus f_u can

be calculated as

$$f_u = f_l + 2(f_{max} - f_l) \tag{5.10}$$

where f_u is the maximum frequency value, f_j, used in Equation 5.5 and f_{max} is the value of f that corresponds to the maximum value of $|S(f_j, f_0, \zeta)|^2$. The area, A_r, under the frequency response function and the area under the response spectrum, A_{peak}, are estimated using the trapezoidal method. The values $S(f, f_0, \zeta)$ and A_r are calculated based on the unknown parameters f_0 and ζ. MATLAB (2009) iterates through different values of these unknown parameters, for a maximum of n iterations, until the maximum value of $\ln(PDF(f_j, f_0, \zeta))$ is found. The program uses the interior-point algorithm to solve the minimization problem

$$\min(-\ln((PDF(f_j, f_0, \zeta))) \tag{5.11}$$

which is equivalent to the maximization problem

$$\max(\ln(PDF(f_j, f_0, \zeta))). \tag{5.12}$$

The interior-point algorithm was originally developed by Karmarkar in 1984. It is an advantageous linear optimization method since the number of iterations necessary grows more slowly than the dimension grows. The interior-point algorithm works by moving along the central path of a problem towards the solution so that the distance between the estimated solution and the optimal solution is decreased with each iteration. This is done by solving a series of equality constrained problems which estimate the inequality constrained problem. (Ignizio and Cavalier, 1994; Roos *et al.*, 2006; Ye, 1997). In the current study the minization problem defined by Equation 5.11, and is subject to the

bounds

$$0.1 \leq f_0 \leq 0.5 \tag{5.13}$$

and

$$0.010 \leq \zeta \leq 0.10. \tag{5.14}$$

These constraints were chosen to encapsulate all expected values of f_0 and ζ. The termination tolerance was set to be 10^{-9}. This value was found to be sufficient to allow MATLAB (2009) to converge to the optimal solution in all cases tested. The maximum number of iterations for the interior-point algorithm was chosen to be $n = 40$. This number allowed the program to converge for all tested situations (the tests are described in Section 5.3).

The interior-point algorithm requires initial estimates for the values of the unknown parameters. The ML program was written such that initial guess for f_0 and ζ are generated using the half-power bandwidth method described in Section 4.2.4. This was done because the ML program will only converge to the values of f_0 and ζ that generate a global maximum of the likelihood function if the initial estimate f_0 is close to the true f_0 value (within $\pm$ 10%). The reason for this is discussed in more detail in Section 5.3.1. Actual estimates generated by the ML program are given in Section 5.3. The ML program was not found to be sensitive to the initial ζ estimate; however, the HPBW method is a convenient method for generating this initial estimate. The program also generates a plot of both the response spectrum, S_R, and the frequency response function as a function of $\hat{f}_0$ and $\hat{\zeta}$, $S(f, \hat{f}_0, \hat{\zeta})$. This plot will allow the user to see if the fit generated by the program is suitable.

5.1.4 LS MATLAB Program

The least squares MATLAB (2009) program works using the same principles as the maximum likelihood program. In the LS program, MATLAB (2009) is programmed to minimize the weighted least-squares function defined in Equation 5.7. Again, the MATLAB (2009) program transforms the time-history data into the response spectrum $S_R(f_j)$ and the frequency response function to be fit to the response spectra is given by Equation 5.1. The lower and upper frequency limits are defined in Equations 5.9 and 5.10 respectively. The areas, A_r and A_{peak}, are calculated in the same manner as for the ML program and the difference between the two curves, $[|S(f_{j,j+1})|^2_{norm} - S_{Rnorm}(f_{j,j+1})]^2$, is estimated using the trapezoidal method. MATLAB (2009) iterates through different values of f_0 and ζ in order to find the minimum value of Equation 5.7. This is done using the interior-point algorithm and the termination tolerance is set to 10^{-9} while the maximum number of iterations is set to 40. These values are the same as those chosen for the ML method and the justification for these values is described in Section 5.1.3. Again the initial guesses for f_0 and ζ are found using the half-power bandwidth method. The values of $\hat{f}_0$ and $\hat{\zeta}$ which correspond to the minimum value of Equation 5.7 are the estimates of the true f_0 and ζ values for the response spectrum.

Using the above method, this program was not always able to find the optimal solution. When the interior-point algorithm began to converge towards an incorrect solution, the LS program would attempt to minimize the distance between f_l and f_u in order to minimize the value of the weighted least-squares function given in Equation 5.7. In order to prevent this error from leading to incorrect f_0 and ζ estimates, the program is now designed to redefine f_l and f_u when the value of the weighted least-squares function is found to be greater than 10^4. This criteria was chosen because in all trials in which the LS program converged to an incorrect solution the value of the weighted least-squares function was found to be greater than 10^4. In cases where the weighted

least-squares function exceeds 10^4 the value of f_l is defined as

$$f_l = f_j \text{ exactly when } S_R(f_j)^2 > \sigma^2 \tag{5.15}$$

where σ^2 is the variance of the response spectrum. The upper frequency limit, f_u is still defined according to Equation 5.10 except that now the value of f_l used in that equation is found using Equation 5.15. Using this alternative definition for f_l and f_u in cases where the primary definitions of f_l and f_u would lead to incorrect property estimates, allows the LS program to converge towards the optimal solution. The definition of f_l given in Equation 5.15 is not used as the primary definition because estimates obtained using Equations 5.9 are otherwise more accurate that those obtained using Equation 5.15. Like the ML program, the LS program produces a plot of both the response spectrum and the fitted frequency response function so that the user can determine if the estimated parameters are suitable.

5.2 Methods Using 2DOF Models

The ML and LS methods were selected as these methods allow the response spectrum to be fit to coupled multi-degree-of-freedom systems. For a function to be employed by the ML method, it must satisfy the following criteria

$$PDF(x, \Theta) \geq 0 \tag{5.16}$$

and

$$\int_{f_l}^{f_u} PDF(x, \Theta) dx = 1. \tag{5.17}$$

For the LS method any model that is differentiable with respect to the unknown parameters can be used. Therefore these methods are well suited for modeling the coupled

two-degree-of-freedom behaviour exhibited by properly tuned structure-TLD systems.

The equation for the dynamic magnification factor for a coupled two-degree-of-freedom system is given in Equation 2.30 as

$$Hx_s(\omega) = \frac{-\omega_s^2\omega^2 + 2\zeta_a\omega_s^2\omega_a i\omega + \omega_s^2\omega_a^2}{\Delta\Omega}. \tag{2.30}$$

This equation can be expressed in the following form

$$H(f, f_s, f_a, \zeta_s, \zeta_a)^2 = \frac{[(\Omega^2 - \beta^2)^2 + (2\zeta_a\beta\Omega)^2]}{\Delta\Lambda}. \tag{5.18}$$

where

$$\begin{aligned}\Delta\Lambda = &\left[\Omega^2(1-\beta^2) - \mu\Omega^2\beta^2 - \beta^2(1-\beta^2) - 4\zeta_a\zeta_s\Omega\beta^2\right]^2 \\ &+ \left[2\zeta_a\beta\Omega(1-\beta^2-\mu\beta^2) + 2\zeta_s\beta(\Omega^2-\beta^2)\right]^2.\end{aligned} \tag{5.19}$$

Multiplying Equation 5.18 by β^4 produces the frequency response function for the acceleration of a coupled 2DOF system. That is

$$H(f, f_s, f_a, \zeta_s, \zeta_a)^2 = \beta^4\frac{[(\Omega^2 - \beta^2)^2 + (2\zeta_2\beta\Omega)^2]}{\Delta\Lambda} \tag{5.20}$$

where β, Ω, and μ are the forced frequency ratio, frequency ratio, and mass ratio respectively and were defined in Chapter 2 as

$$\mu = \frac{m}{M}, \tag{2.2}$$

$$\beta = \frac{\omega}{\omega_s}, \tag{2.6}$$

and

$$\Omega = \frac{\omega_a}{\omega_s}. \tag{2.7}$$

Equation 5.20 is the model function used in the ML and LS methods. The unknown parameters are the natural frequencies and damping ratios of the structure and the absorber, f_s, f_a, ζ_s, and ζ_a. The variables f and the masses of the structure, M, and the absorber, m are fixed and given.

5.2.1 Description of 2DOF Programs

The programs to implement the ML and LS methods for the 2DOF model operate similarly to the programs for the SDOF model except that in this case the spectral response data is fit to Equation 5.20 instead of Equation 5.1. The variables M and m also need to be input to the MATLAB (2009) program. These variables can be defined for either a structure-TMD system or a structure-TLD system depending on the data being analyzed by the programs. For a structure-TLD system these variables were given in Equations 2.113 and 2.115 respectively. The frequency limits surrounding the coupled resonant peaks must be carefully defined in these programs. Since the frequency response function for a coupled 2DOF system has two resonant peaks, the upper frequency limit cannot be defined by assuming a symmetric distribution of the frequency response function about its maximum value. Therefore, the frequency limits must be defined according to different criteria. In this study, the lower frequency limit, f_l, was set such that 0.5% of the area under the response spectrum would be contained between $f = 0$ and $f = f_l$. The upper frequency limit, f_u, was set such that 80% of the area under the response spectrum would be contained between $f = 0$ and $f = f_u$. These values were chosen to encapsulate all expected values of the resonant frequencies. The optimization problems used in both the ML and LS methods are subject to the following inequality constraints

$$0.1 \leq f_s \leq 0.5, \tag{5.21}$$

$$0.1 \leq f_a \leq 0.5, \tag{5.22}$$

$$0.01 \leq \zeta_s \leq 0.20. \tag{5.23}$$

and

$$0.01 \leq \zeta_a \leq 0.20. \tag{5.24}$$

These values were chosen to encapsulate all expected values of f_s, f_a, ζ_s, and ζ_a for the monitored structure-TLD system in this study. They can be adjusted as required for studies on additional systems.

5.3 Validation of MATLAB Programs

The ML and LS programs developed in this study were validated using data with known properties before they were used to determine the properties of the data obtained from full-scale measurements. Several methods were used to validate the programs. First, response spectrum data, with no noise, was input into the programs. This was carried out to ensure the fit of the programs. In this case the programs did not need to transform time-history data into the frequency domain. The programs were only used to fit the spectral data to the spectral model. The results from these tests are given in Section 5.3.1. Secondly, the programs were tested on time-history data with no noise. This was to ensure that for data without noise, the programs would converge to the correct solution.

One of the main purposes of developing the programs used in this study is to correctly estimate the dynamic properties of a coupled 2DOF structure-absorber system so that adjustments to the absorber(s) can be made in order to optimize performance. The results presented in this section show that they are well suited for this purpose.

5.3.1 Description of Validation Tests for Spectral Input

In order to test the SDOF programs, a response spectrum with known dynamic property values was created using Equation 5.1. As discussed in Section 5.1.3 and 5.1.4, the initial guesses for the dynamic properties are generated via the HPBW method internally in the MATLAB (2009) programs for both the ML and LS methods. Therefore, the only input value that can be altered in these programs is the frequency resolution ΔFFT. Although this set of tests does not require the input data to be transformed from the time domain to the frequency domain, the frequency resolution is important since Equation 5.1 is fit to the input data at the discrete frequencies f_j defined as

$$f_j = j\Delta FFT. \tag{5.8}$$

Using more discrete frequencies increases the likelihood that the MATLAB (2009) programs will converge to the exact property values. This result is illustrated below.

In this test several representative dynamic property values were used. The f_0 values used in the test vary between 0.2 Hz and 0.3 Hz. These values were chosen because initial analysis of the data obtained from Building X suggested that that building's natural frequency is within this range. The true ζ values used in the test vary between 1.00% and 3.00%. Several variations of these parameters were tested. The ΔFFT values used in the test were 4.0690 x 10^{-3} Hz, 2.0345 x 10^{-3} Hz, and 1.0173 x 10^{-3} Hz. These values are calculated based on the sampling frequency, 8.3333 Hz, that was used for collecting the full-scale data, and block sizes, N, of 2048, 4096, and 8192 respectively. The results generated by the ML program are given in Figures 5.1 and 5.2. The figures show the results for various f_0 values with a constant ζ value on the left and various ζ values with a constant f_0 value on the right. Figure 5.1 shows the errors in the f_0 estimates for the tested true dynamic property values and the three

block sizes. Figure 5.2 shows the percent errors in the ζ estimates for the tested true dynamic property values and the three block sizes.

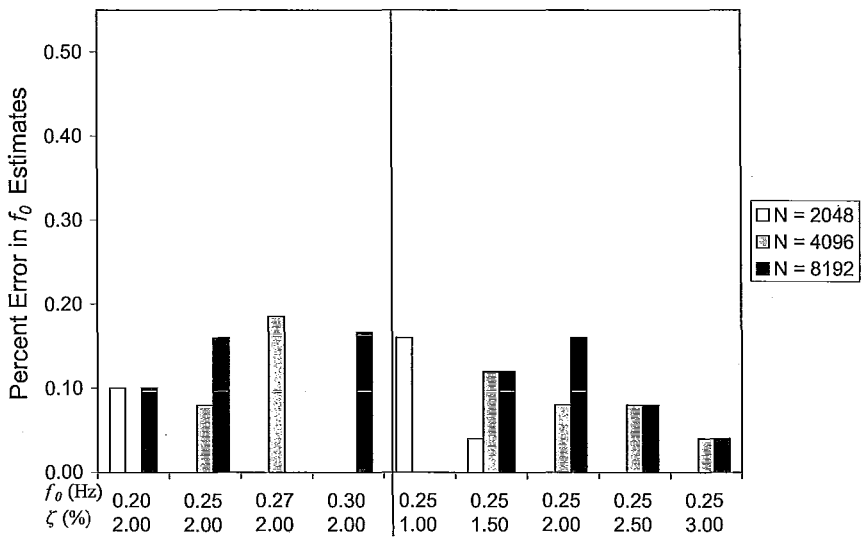

Figure 5.1: Percent Error in f_0 Estimates Generated by the ML Program using Spectral Input

The results generated by the ML program show that the errors in the f_0 estimates are small (all less than 0.20%). In some cases the errors increase as N increases. This is due to the effect that the limits f_l and f_u have on the likelihood function. These limits are calculated according to Equations 5.9 and 5.10 and are dependent on the resolution. However, since the errors in the f_0 estimates are all less than 0.20%, the tendancy for the errors to sometimes increase with increased N was considered trivial. The application of the estimates generated by the ML program is discussed below.

Figure 5.2 shows a tendancy for the $\hat{\zeta}$ errors to increase with decreased damping. Here it is observed that, for N is equal to 2048, the errors are larger when the true ζ value is equal to 1.00 %, 1.50%, and 2.00% than when it is equal to 2.50 % and 3.00 %. This result is expected as the narrow resonant peak associated with a low damping ratio is difficult to fit to a model using a discrete number of points. When N is equal

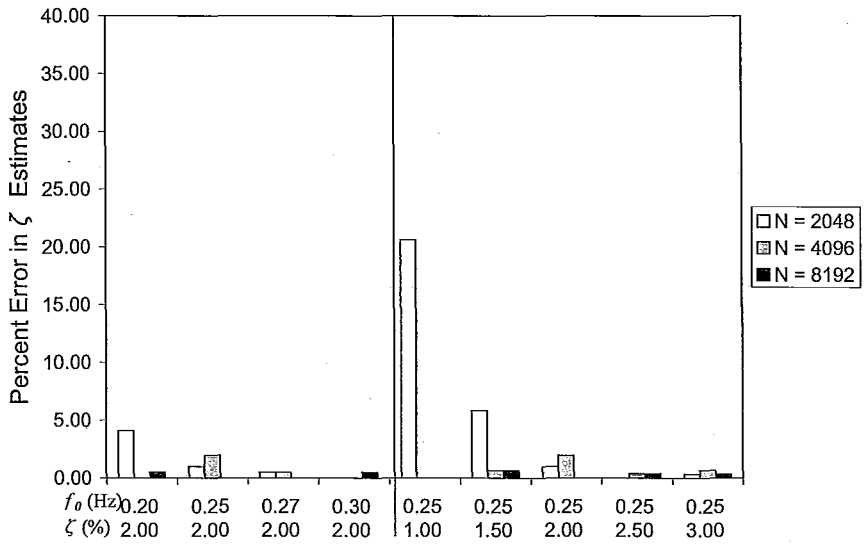

Figure 5.2: Percent Error in ζ Estimates Generated by the ML Program using Spectral Input

to 4096 and 8192, the tendancy for the $\hat{\zeta}$ errors to increase with decreased damping is not shown because these larger values of N allow for the narrow resonant peak to be resolved by the discrete points.

There are several cases in which the $\hat{\zeta}$ error increases as N increases. This result is not expected since the larger values of N provide more discrete points at which to fit the response spectrum to the frequency response function. However, in all the cases in which the $\hat{\zeta}$ error increases with increased N, the relative percent $\hat{\zeta}$ errors are less than 2.00%. These percent errors in the estimates for these cases are shown on a smaller scale in Figure 5.3. This represents an absolute difference of only 0.04% between the true and estimated ζ values. Since damping ratios are typically only reported to the first decimal place, these differences are considered trivial. The differences arise from the flat shape of the likelihood function with respect to the damping estimate and the distortion of the resonant peak due to the continuous response function being represented by a discrete number of points. The shape of the likelihood function is shown in Figure 5.4. The

issue of the distortion of the resonant peak is discussed further in Section 5.3.2.

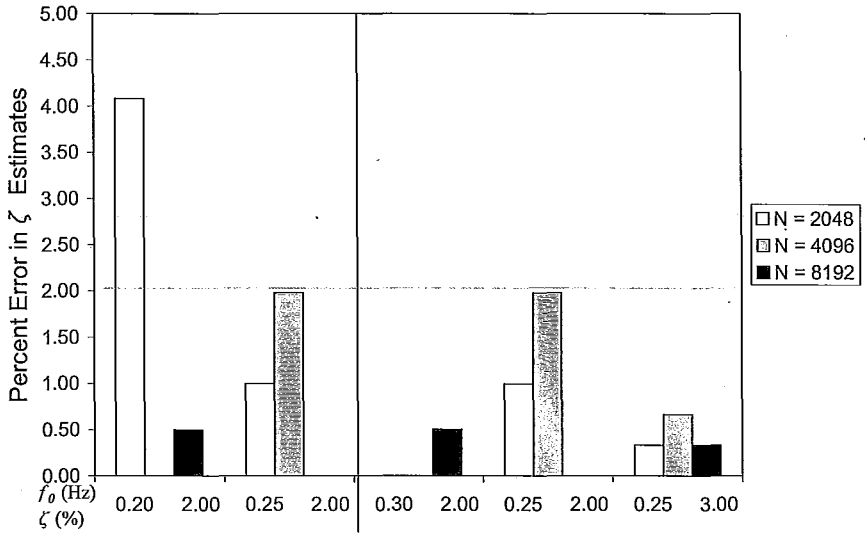

Figure 5.3: Percent Error in ζ Estimates where Error Increases with Increased N

The results show that the errors in the natural frequency estimates are much smaller than the errors in the damping ratio estimates (the maximum error in the damping estimates is 20.63% compared to a maximum error of 0.19% for the natural frequency estimates). The is due to the shape of the likelihood function with respect to each of these parameters. Figure 5.4 shows the shape of the likelihood function for true f_0 and ζ values of 0.25 Hz and 2.00% and various estimated f_0 and ζ values. This figure shows that the rate of change in the likelihood function is much greater with respect to the estimated f_0 value than it is with respect to the estimated ζ value. In this case the value of the likelihood function is 1507 when the estimated ζ value is equal to the true ζ value. The value of the likelihood function is also equal to 1507 when ζ is equal to 2.04% (this is the case which resulted in the 1.98% error discussed above). This is shown in the contour plot given in Figure 5.5. Since the likelihood function is flat over a range of $\hat{\zeta}$ values, the value of $\hat{\zeta}$ returned by the ML method will be dependent on the initial estimates and decreasing the error tolerance will not increase the accuracy

of the ζ estimate.

From Figure 5.4, it is evident that there are more local maxima with respect to the natural frequency estimate than there are with respect to the damping ratio estimate. This fact explains why the accuracy of the estimates generated by the ML program is highly dependent on the initial natural frequency estimate.

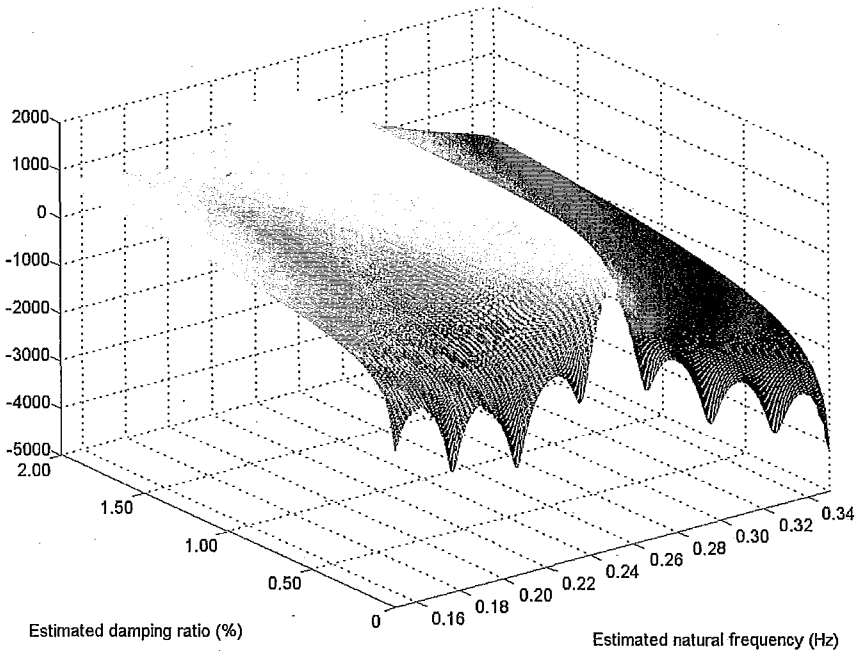

Figure 5.4: Surface Plot of Likelihood Function for True f_0 and ζ values of 0.25 Hz and 2.00% and Various f_0 and ζ Estimates

The ML method generated a maximum $\hat{f}_0$ error of 0.19% and a maximum $\hat{\zeta}$ error of 20.63%. The maximum $\hat{\zeta}$ error is limited to 1.98% for all cases in which N is greater than or equal to 4096. If the same data is tested using the HPBW method, the maximum $\hat{f}_0$ error is 0.72% and the maximum $\hat{\zeta}$ error is 57.14% (6.76% for cases in which N is greater than or equal to 4096). Thus the ML method is more accurate than the HPBW method in the tested cases.

One of the main purposes of developing the ML program used in this study

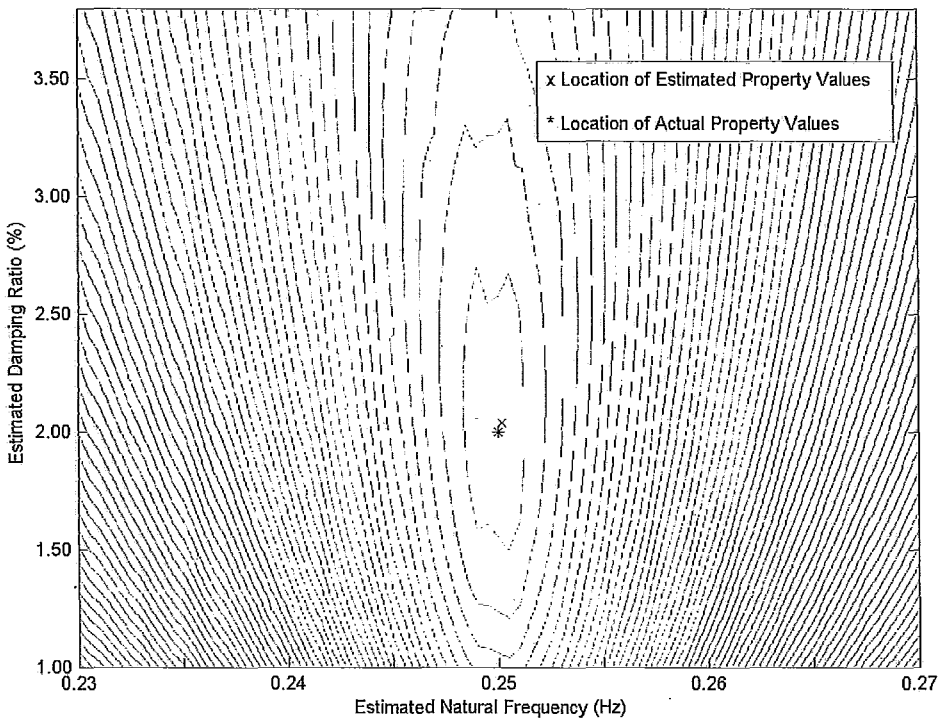

Figure 5.5: Contour Plot of Likelihood Function for True f_0 and ζ values of 0.25 Hz and 2.00% and Various f_0 and ζ Estimates

is to correctly estimate the dynamic properties of a coupled 2DOF structure-absorber system so that adjustments to the absorber(s) can be made in order to optimize performance. In absorber design, a target mean square response value is chosen and the effective damping required to meet that response is calculated from Equation 2.58. The structural damping is often assumed to be zero or a small value at this stage to be conservative. The mass ratio can then be calculated from Equation 2.62. Using the mass ratio generated from Equation 2.62, the optimal tuning ratio and absorber damping ratio can be calculated from Equations 2.60 and 2.61. Equations 2.60, 2.61, and 2.62 assume zero structural damping. If the natural frequency of the structure changes or is found to be different from the value assumed during design, the natural

frequency of the absorber(s) can be adjusted to tune the system. Section 3.3 discusses how structure-TLD systems are adjusted. The accuracy of the estimates generated by the ML program show that it is well suited for the purpose of adjusting absorber(s) to enhance performance.

The ability of the ML program to deliver information that can be used to tune the absorber(s) was evaluated in the following way. The true dynamic property values of a structure-TLD system were assumed to be those given in Table 5.1. These are the values of an optimally tuned structure-TLD system. If the natural frequency of the structure was incorrectly estimated by 0.19% (the maximum error in the f_0 estimates generated by the ML program in the cases tested above) and this incorrect f_0 estimate was used to tune the TLDs, the relative decrease in the effective damping would be 0.01% of the optimal effective damping value for a given mass ratio. The value of the estimated damping ratios are not used to adjust the TLD properties so inaccuracies in their estimates would not affect the effective damping generated by the TLDs.

The LS program was tested using the same true dynamic property values that were used to test the ML program. The LS program converged to the exact dynamic property values with zero error in all tested cases.

The 2DOF programs were also tested using spectral input. The spectral input was written using Equation 5.20. The true dynamic property values used in Equation 5.20 are given in Table 5.1. For these programs the initial estimates of the dynamic properties cannot be generated using the HPBW method, thus the user must input the initial estimates. This means that the 2DOF programs have four additional input values compared to the SDOF programs, as the four initial estimates, $\hat{f}_s$, $\hat{f}_a$, $\hat{\zeta}_s$, and $\hat{\zeta}_a$ as well as the block size, N, can all take on various values. The user is assisted in selecting the $\hat{f}_s$ and $\hat{f}_a$ values. Before the user is prompted to enter these initial estimates both programs generate a plot of the response spectrum. From the plot the user can see the

locations of the resonant peaks and use these values as initial frequency estimates.

Table 5.1: True Dynamic Property Values for 2DOF Tests

Property	Value
M_s (kg)	12080590
f_s (Hz)	0.2720
ζ_s(%)	1.86
m_a (kg)	308359
f_a (Hz)	0.2703
ζ_a (%)	9.14

Since the initial property estimates are not automatically generated within the programs, the ability of the programs to correctly estimate the dynamic property values was evaluated for several initial estimate values. Figure 5.6 shows the accuracy of the dynamic property estimates generated by the ML program with respect to the accuracy of the initial estimates. In Figure 5.6(a) the initial f_a, ζ_s, and ζ_a estimates are kept constant at the true dynamic property values, while the value of the initial f_s estimate is varied from -20% to 20% of the true f_s value. In Figure 5.6(b) the values of f_s, ζ_a, and ζ_s are kept constant while the value of f_a is varied. Figure 5.7 shows equivalent plots generated by the LS method. Plots generated by varying the inital damping ratios were also generated. However when either of the initial damping ratios was varied between -20% and 20% of its true value, both programs converged to the true dynamic property values with percent errors equal to zero. Thus plots generated by altering the damping ratios have been omitted. For the illustrated tests the block size is kept constant at 4096. The effect of altering the block size was examined and, as expected, the accuracy of the results increased with increased block size. The plots generated using other block sizes are omitted for beverity.

Figure 5.6 shows that the ML method will converge to estimates within $\pm$ 1% of the true values when the initial f_s estimate is within $\pm$ 10 % of its true value and when the initial f_a estimate is within -16% to 18% of its true value. Figure 5.7

shows that the LS method will converge to estimates with 0% error when the initial f_s estimate is within -9% to 8% of its true value and when the initial f_a estimate is within $\pm$ 7% of its true value. These results show that the 2DOF programs are useful for practical applications. In all cases studied, the user would be able to determine the initial estiamtes for the natural frequencies from the generated plot of the response spectrum with enough accuracy to allow the programs to converge to within $\pm$ 1% of the correct solutions. The user is not aided in determining initial estimates for the damping ratios; however, the results show that the accuracy of the programs is not dependent on the initial damping ratio estimates. If the estimated dynamic properties were used to adjust the TLDs in this study (with true dynamic property values given in Table 5.1) in order to enhance their performance, an error of 1% in the structure's natural frequency estimate would result in a relative decrease of 0.28% in the effective damping compared to the optimal effective damping.

The ML and LS programs are advantageous because they can be used to estimate the dynamic properties of a 2DOF system. The data used in this test was also analyzed using the HPBW method in order to illustrate the advantage of using the ML and LS methods compared to the HPBW method. The HPBW method is not designed to be used with 2DOF data, thus it only produces one frequency estimate and one damping estimate and a direct comparison between the ML and LS methods and the HPBW method is not possible for 2DOF systems. However, the estimates generated by the HPBW method are preseneted below in order to illustrate the advantage of the ML and LS methods for estimating the dynamic properties of 2DOF systems. The f_0 estimate generated by the HPBW method is an estimate of the resonant frequency associated with the higher resonant peak (in this case f_a). The ζ estimate generated by the HPBW method is, in this case, higher than both damping values and the effective damping value because both resonant peaks are included in the estimate. The f_0 and ζ estimates

generated by the HPBW method are 0.2543 Hz and 1.24% respectively. The estimated f_0 value is 6.10% lower than the true f_a value. The estimated ζ value is 76.64% higher than the effective damping value. Since the ML and LS programs are able to accurately estimate the dynamic property values for both masses of the 2DOF system within $\pm$ 1% of their true values over the ranges listed above, they are clearly superior to the HPBW method for estimating the dynamic properties of a 2DOF system.

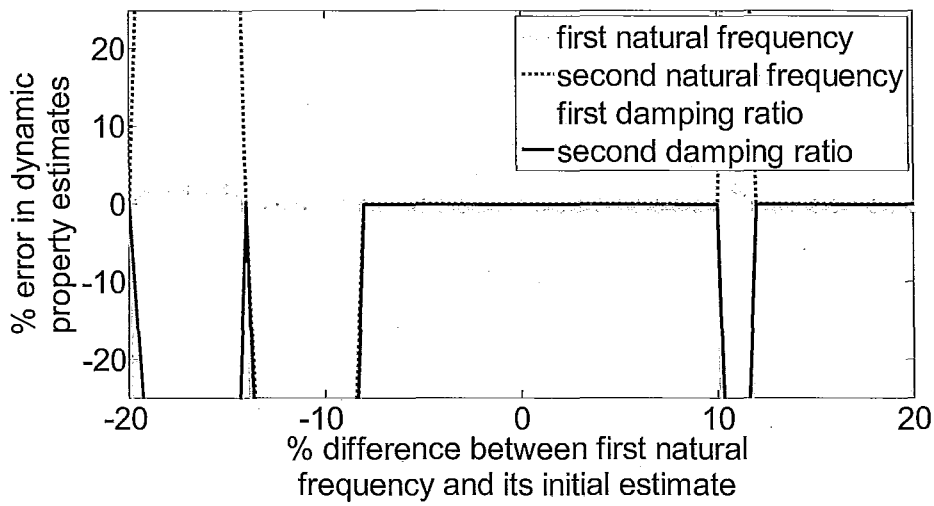

(a) Various Initial $\hat{f}_s$

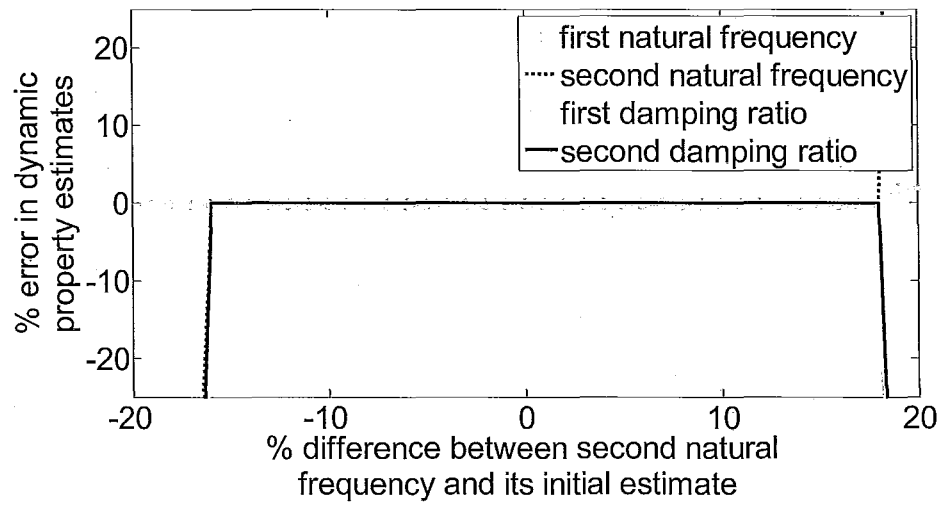

(b) Various Initial $\hat{f}_a$

Figure 5.6: Accuracy of Dynamic Property Estimates for Various Initial Frequency Estimates Generated by the ML Method

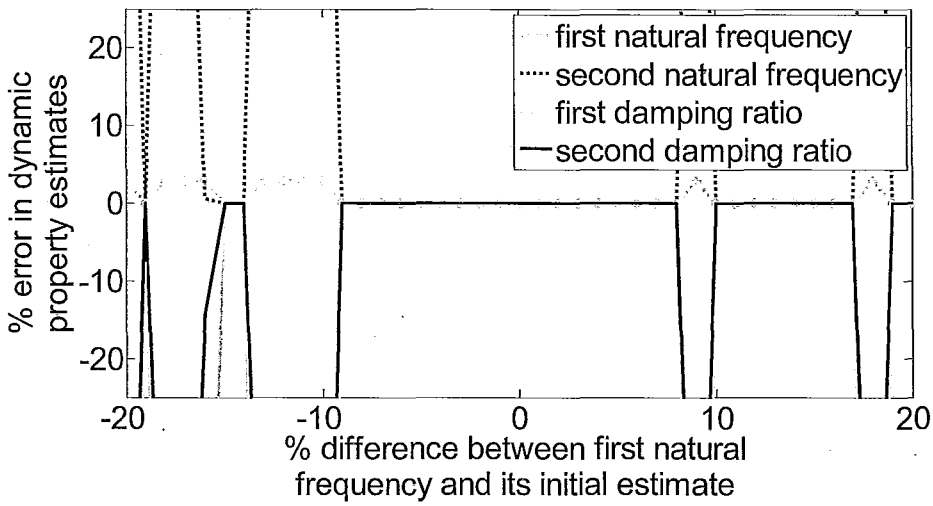

(a) Various Initial $\hat{f}_s$

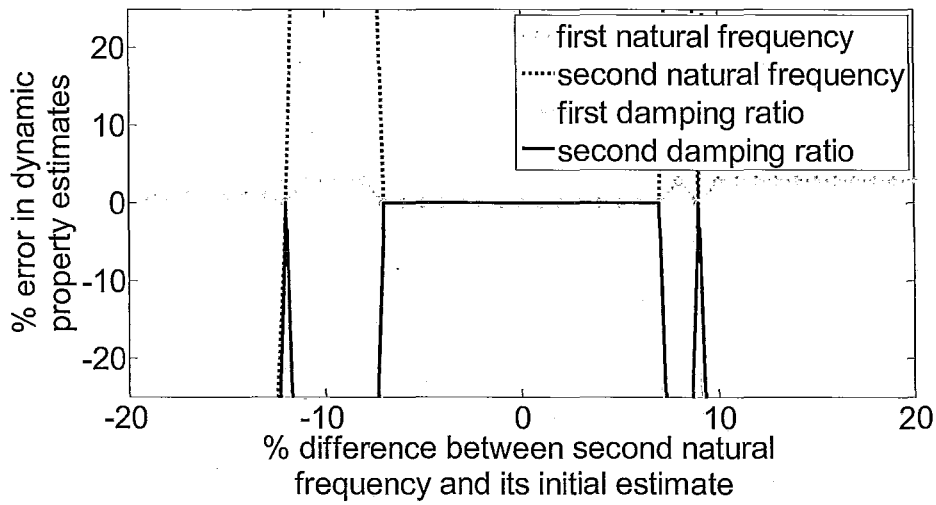

(b) Various Initial $\hat{f}_a$

Figure 5.7: Accuracy of Dynamic Property Estimates for Various Initial Frequency Estimates Generated by the LS Method

5.3.2 Description of Validation Tests for Time Domain Input

The SDOF ML and LS programs developed in this study were tested on time history data with known dynamic property values. Newmark's method was used in order to create this time history data. Newmark's method is a classic numerical method that uses a time-step method to evaluate the equation of motion based on a known applied force, $p(t)$. The initial velocity and displacement of the structure being evaluated must also be known along with its dynamic properties damping, stiffness, and mass. A time step value must also be chosen. Chopra recommends that this time step value be less than or equal to 0.551 times the structure's natural period (Chopra, 2007). The data in the current study was generated using the linear acceleration method which assumes that the change in acceleration between time steps in linear.

The time history data for this study was written using a MATLAB program (MATLAB, 2009) and the method outlined by Chopra (2007). For this program, the dynamic property f_0 was varied between 0.20 Hz and 0.30 Hz and ζ was varied between 1.00% and 3.00%. These values are the same as those used in the evaluation of the SDOF programs using input spectral data and are based on the initial analysis of Building X. The time step value used was 0.12 s which is the same as the sampling rate used to collect the full-scale data and is well below the maximum time step value recommend by Chopra (1.84 s for a building with a natural frequency of 0.30 Hz). The input force, $p(t)$ is a time history of white noise. A sample of the forcing data is shown in Figure 5.8. Figure 5.9 shows a sample of the response of the building generated using Newmark's method. As in the test for the input spectral data, the block size N was varied for this test between 2048, 4096, and 8192. The number of blocks was kept constant at 100.

The results generated by the ML program are given in Figures 5.10 and 5.11. Figure 5.10 shows the percent errors in the f_0 estimates for the tested true dynamic property values and the three block sizes. Figure 5.11 shows the percent errors in

the ζ estimates for the tested true dynamic property values and the three block sizes. Equivalent plots for the results generated by the LS program are given in Figures 5.12 and 5.13.

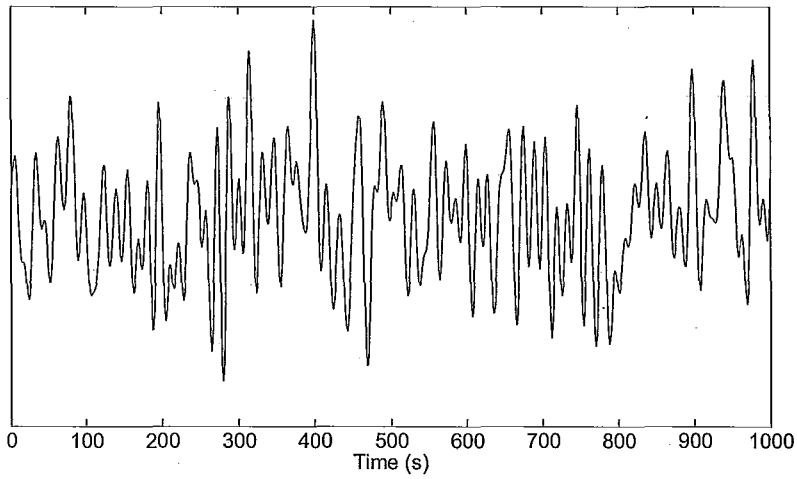

Figure 5.8: Input Force for Generation of Time History Response

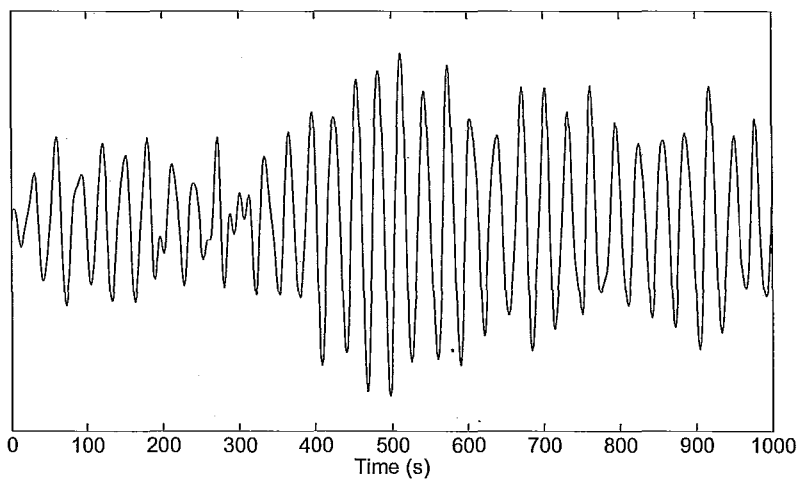

Figure 5.9: Response Time History Generated Using Newmark's Method

The results generated by the ML program show that, in general, the accuracy of the estimated ζ value increases as N increases. This is the expected result and this trend

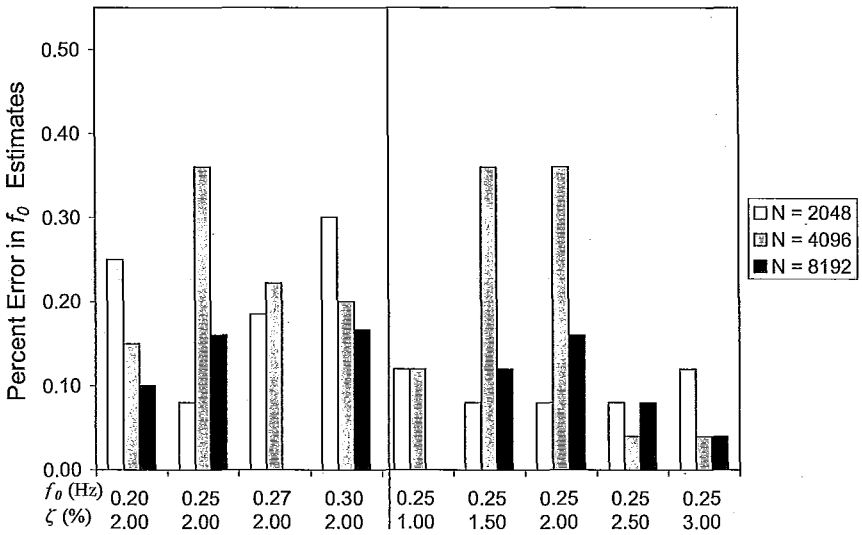

Figure 5.10: Percent Error in f_0 Estimates Generated by the ML Program using Time-History Input

was also illustrated by the ML program tested on spectral input data. There are two cases in which this pattern is not evident; these are when f_0 is equal to 0.25 Hz and ζ is equal to 2.50 % and 3.00 %. These cases are anomolies and do not follow the expected pattern because of the distortion of the peak that occurs when the continuous reponse spectrum is represented by a discrete number of points. Figure 5.14 shows the response spectrum for a time history with f_0 equal to 0.25 Hz, ζ equal to 2.50%, and N equal to 2048. In this figure, the response spectrum is fit to a frequency response function with f_0 and ζ also equal to 0.25 Hz and 2.50%. Figure 5.15 shows the same frequency response spectrum fit to a frequency response function with f_0 and ζ values equal to the estimates generated by the ML program, 0.2498 Hz and 2.65%. From Figure 5.14 is is clear that the frequency response function has a higher peak value than the response spectrum. Thus in order to produce a good fit the ML program overestimates the damping in the frequency response function to lower its peak. Figures 5.16 and 5.17 show plots similar to those given in Figures 5.14 and 5.15 except in these plots the block

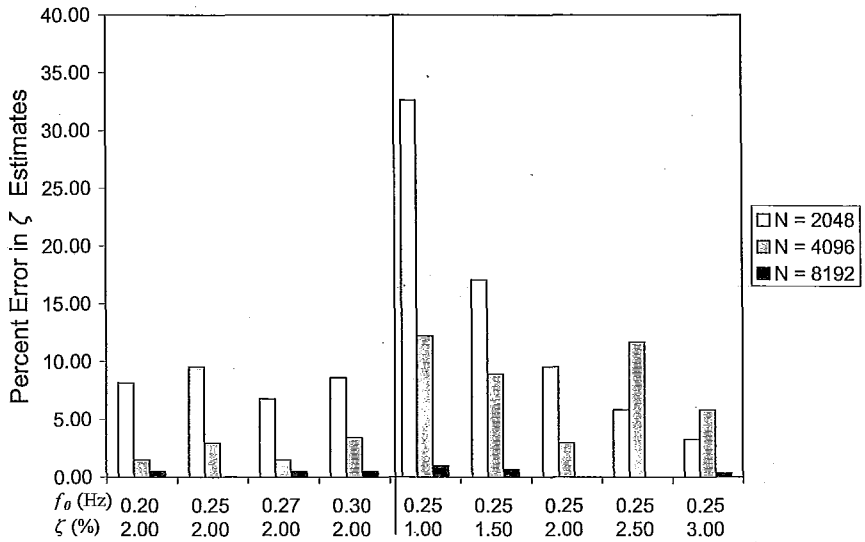

Figure 5.11: Percent Error in ζ Estimates Generated by the ML Program using Time-History Input

size is 4096. From Figure 5.16 it is evident that the peak of the frequency response function with f_0 and ζ equal to 0.25 Hz and 2.50%, respectively, is higher than the response spectrum. Again the ML program overestimates the damping in order to decrease the amplitude of the response function's peak. The damping for the case where the block size is equal to 4096 is overestimated more than that when the block size is equal to 2048 because of the way in which the function is resolved by the discrete number of points. From Figure 5.14 it is evident that the peak is essentially cut off by the poor resolution when N is equal to 2048; thus, the amplitude of the peak of the frequency response function is lower for this case than for N is equal to 4096 and the damping does not need to be as large to fit the function to the response spectrum.

The results show that the accuracy of the estimated ζ value decreases with decreasing damping. This result is expected due to the narrow peak associated with low damping. This result was also illustrated by the ML program tested on spectral input data and is discussed in Section 5.3.1. The numerical method used in this study

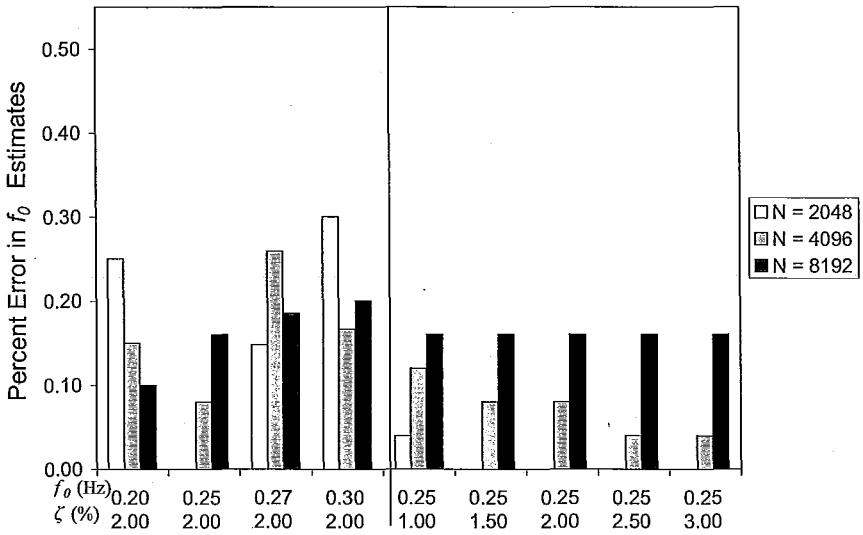

Figure 5.12: Percent Error in f_0 Estimates Generated by the LS Program using Time-History Input

does not produce amplitude decay which would be manifested as additional damping. The f_0 estimates are all lower than the true f_0 values. This is an expected result as the numerical method required to produce the time history data introduces a period elongation error into the data. Using the linear acceleration method with natural frequencies between 0.2 and 0.3 Hz the period elongation is expected to be less than 0.75%. The percentage error in the f_0 estimates corresponds to errors in the third decimal place of the f_0 estimate and thus the discrepencies between f_0 estimates are not considered. The accuracy of the estimates generated using the time domain data is lower than that generated using the spectral data. This result is expected due both to numerical errors mentioned above and errors introduced by the transformation of the data from the time domain to the frequency domain.

The results generated by the LS program are very similar to those generated by the ML program. Unlike the spectral input case, the LS program does not generate zero error when the input is in the time domain. The error in the damping estimates

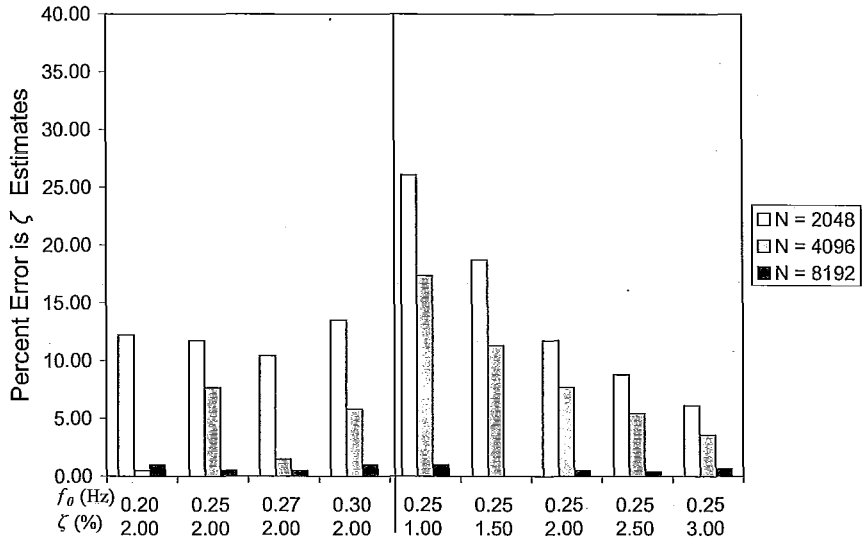

Figure 5.13: Percent Error in ζ Estimates Generated by the LS Program using Time-History Input

is larger than the error in the frequency estimates. This is because the value of the function being minimized changes more rapidly with respect to frequency than it does with respect to damping. This is shown in Figure 5.18. The percent errors in the ζ estimates generated by the LS program are, on average, larger than those generated by the ML program by approximately 2.5 %. The f_0 estimates generated by the LS program are, on average, as accurate as those generated by the ML program.

The errors generated by the ML and LS methods were compared to errors generated by the HPBW method and the random decrement technique (RDT). The RDT was discussed in Section 4.3 and the RDT program used in this test was developed at the Boundary Layer Wind Tunnel at the University of Western Ontario (Morrish, 2009). The maximum $\hat{f}_0$ and $\hat{\zeta}$ errors generated by each program are given in Table 5.2. This table shows the the ML and LS programs are able to estimate both the f_0 value and the ζ value with more accuracy than the HPBW. The RDT produced the most accurate ζ estimates. However, the RDT method cannot accurately analyze 2DOF

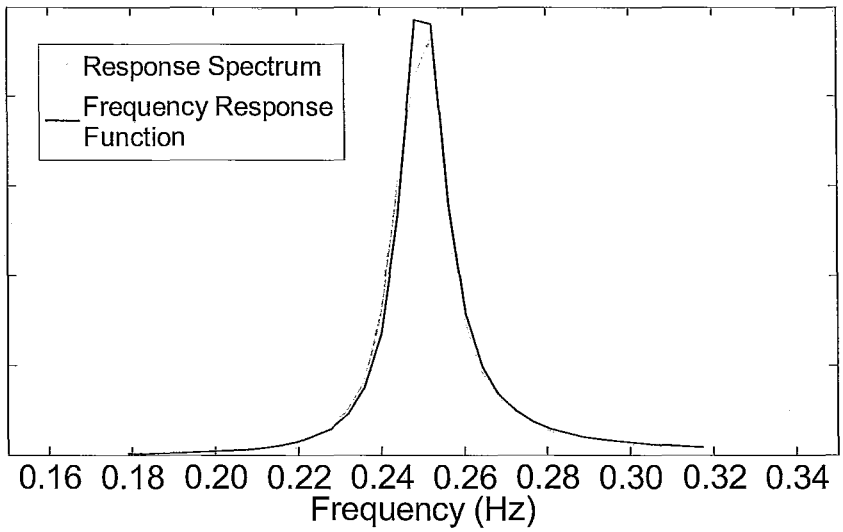

Figure 5.14: Response Spectrum with f_0, ζ, and N Equal to 0.25 Hz, 2.50%, and 2048 Respectively, fit to a Frequency Response Function with f_0 and ζ Equal to 0.25 Hz and 2.50% Respsectively

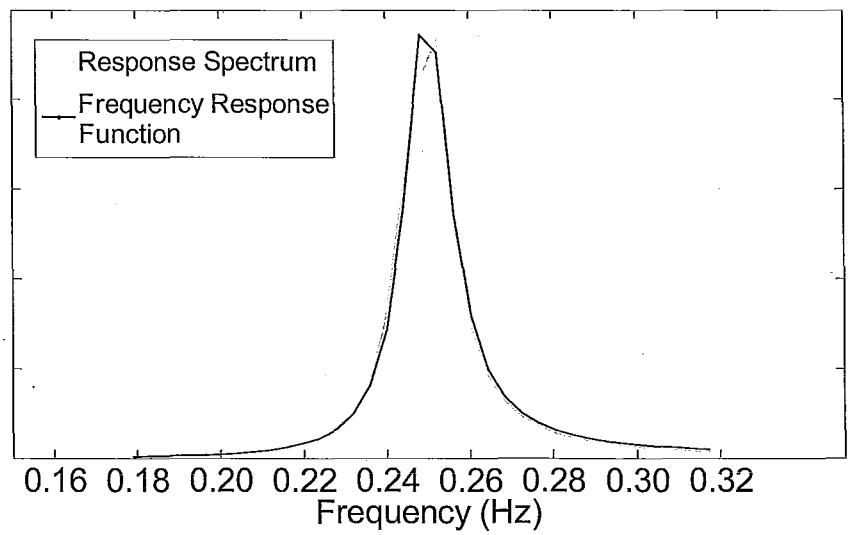

Figure 5.15: Response Spectrum with f_0, ζ, and N Equal to 0.25 Hz, 2.50%, and 2048 Respectively, fit to a Frequency Response Function with Estimated f_0 and ζ Values

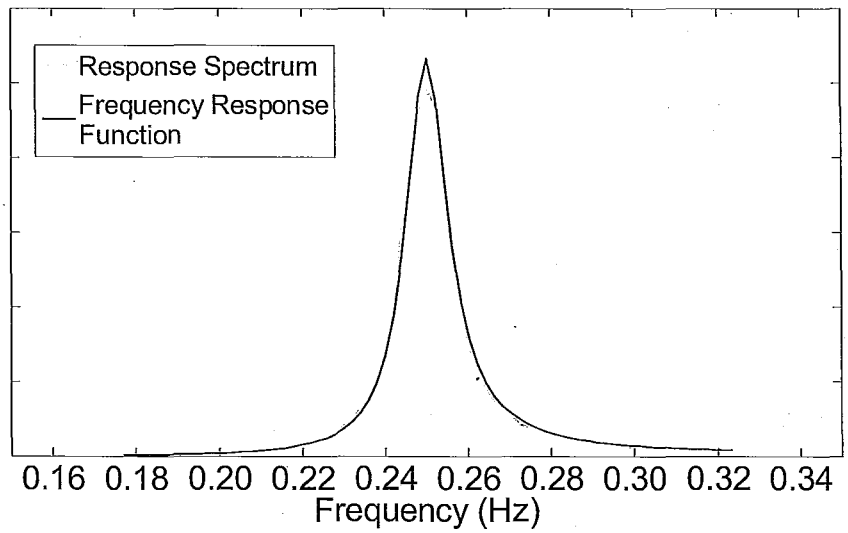

Figure 5.16: Response Spectrum with f_0, ζ, and N Equal to 0.25 Hz, 2.50%, and 4096 Respectively, fit to a Frequency Response Function with f_0 and ζ Equal to 0.25 Hz and 2.50% Respsectively

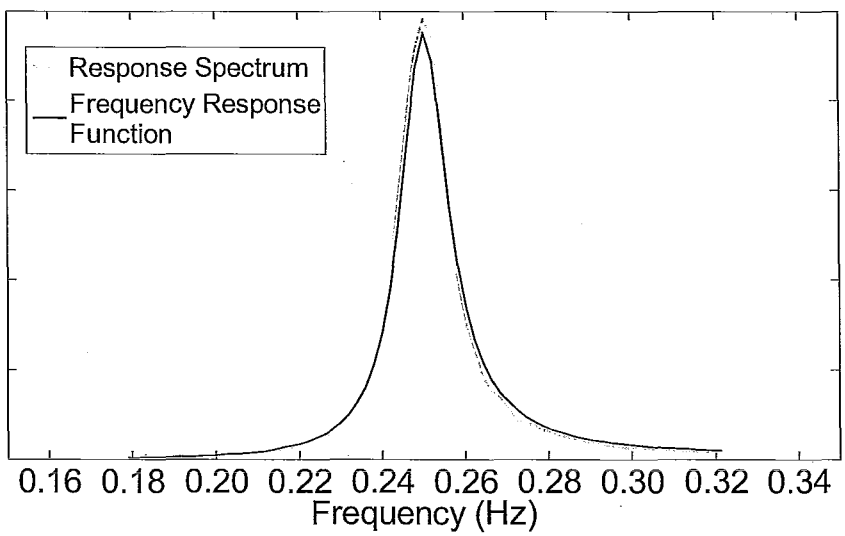

Figure 5.17: Response Spectrum with f_0, ζ, and N Equal to 0.25 Hz, 2.50%, and 4096 Respectively, fit to a Frequency Response Function with Estimated f_0 and ζ Values

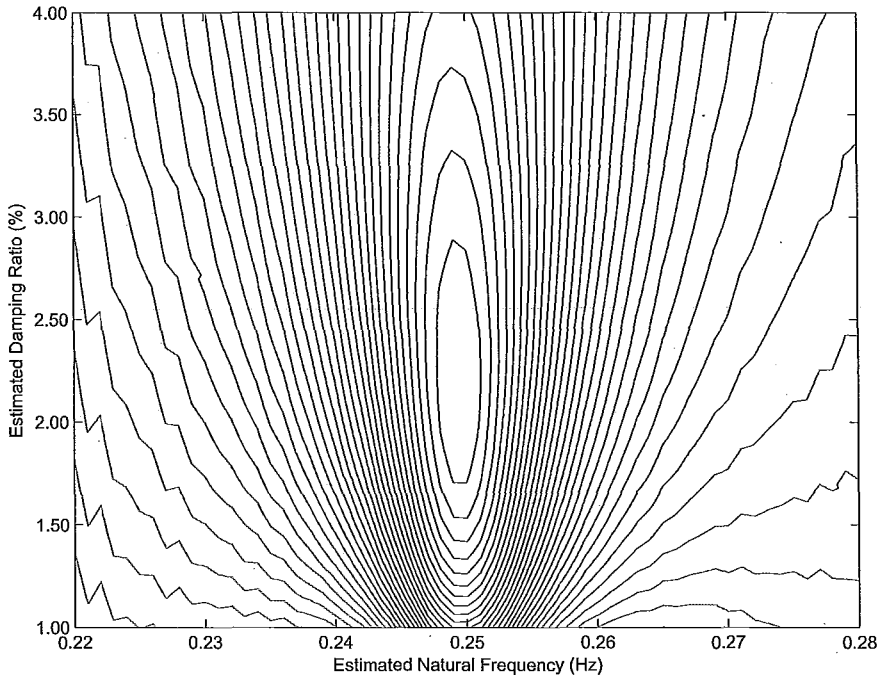

Figure 5.18: Contour Plot of Least Squares Function for True f_0 and ζ values of 0.25 Hz and 2.00% and Various f_0 and ζ Estimates

data as discussed below.

Table 5.2: Maximum Errors in Dynamic Property Estimates generated by Various Methods

Method	$\hat{f}_0$ Error (%)	$\hat{\zeta}$ Error (%)
ML	0.41	32.64
LS	0.30	26.09
HPBW	0.92	68.85
RDT	0.52	13.33

The maximum error generated in the f_0 estimate by either method is 0.41% (generated by the ML program for N is equal to 8192 and true f_0 and ζ values of 0.27 Hz and 2.00% respectively). As discussed in Section 5.3.1 the accuracy of the f_0 estimate is important for the purpose of tuning a structure-absorber system in order to maximize the effective damping. Using the values for an optimally tuned 2DOF

structure-TLD system defined in Table 5.1, a 0.41% error in the estimate of the natural frequency of the structure would result in a relative decrease of 0.05% of the optimal effective damping generated by the TLDs if the estimated natural frequency value was used to tune the TLDs.

The effect of the number of blocks used to estimate the dynamic properties was also examined. Figure 5.19 shows the percent errors in the ζ estimates for various block sizes ranging from 10 to 200. The block size, N, is held constant at 4096 and the estimates are based on a response history with true f_0 and ζ values of 0.2500 Hz and 2.00% respectively. The plot shows that as the number of blocks increases, the accuracy increases. This is the expected result, as increasing the number of blocks decreases the variance error discussed in Section 4.2.2. The f_0 estimates did not exhibit this trend. However, the errors in the f_0 were, in all cases, less than 0.40 %.

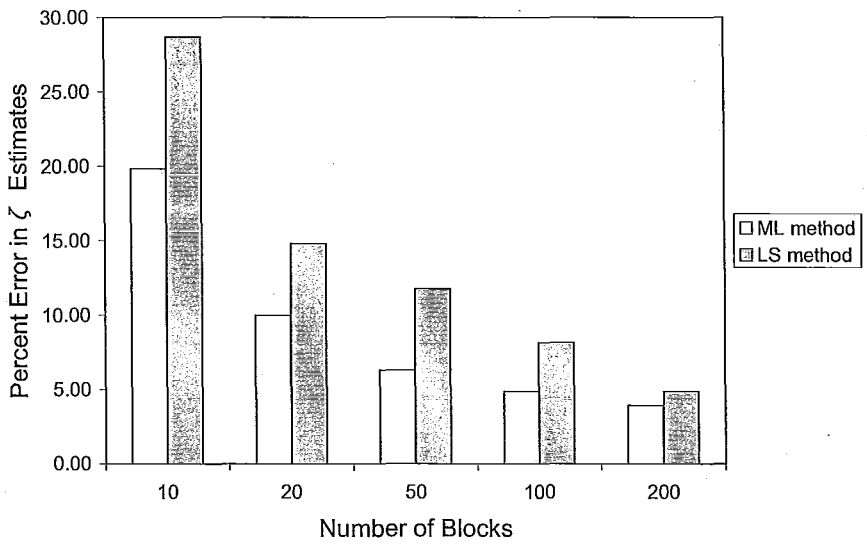

Figure 5.19: Percent Error in ζ Estimates for Various Block Sizes

The 2DOF programs developed in this study were also tested on time history data with known dynamic properties. The time history data was written using Newmark's method for coupled multi-degree-of-freedom systems (Chopra, 2007). In this test the known dynamic property values are set such that the system is optimally tuned. The property values are given in Table 5.1. The white noise force, $p(t)$ is applied to the structure and is shown in Figure 5.8. The time step is set to be 0.12 s, the block size N is set at 4096, and the number of blocks used is set at 100. The accuracies of the estimates generated by the programs are given in Figures 5.20 to 5.23. Figure 5.20 shows the accuracies of the dynamic property estimates generated by the ML program with respect to the accuracies of the initial frequency estimates. In Figure 5.20(a) the initial f_a, ζ_s, and ζ_a estimates are kept constant at the true dynamic property values, while the value of the initial f_s estimate is varied from -20% to 20% of the true f_s value. In Figure 5.20(b) the values of f_s, ζ_a, and ζ_s are kept constant while the value of f_a is varied. Figure 5.21 shows the accuracies of the dynamic property estimates generated by the ML program with respect to the accuracies of the initial damping estimates. In Figure 5.21(a) the initial ζ_s estimate is varied and in Figure 5.21(b) the initial ζ_a estimate is varied. Figures 5.22 and 5.23 show equivalent plots generated by the LS program.

Figures 5.20 and 5.22 show that the f_s, f_a, and ζ_a estimates are within $\pm 0.50\%$ of their true values when the initial frequency estimate being varied is within a certain range of its true value. In Figure 5.20(a) $\hat{f}_s$, $\hat{f}_a$, and $\hat{\zeta}_a$ are within $\pm 0.50\%$ of their true values when the initial f_s estimate is within -4% to 6% of its true value and in Figure 5.20(b) $\hat{f}_s$, $\hat{f}_a$, and $\hat{\zeta}_a$ are within $\pm 0.50\%$ of their true values when the initial f_a estimate is within -9% to 8% of its true value. In the equivalent plots generated by the LS method, Figures 5.22(a) and 5.22(b), $\hat{f}_s$, $\hat{f}_a$, and $\hat{\zeta}_a$ are within $\pm 0.50\%$ of their true values when the inital f_s and f_a estimates are within -8% to 3% and $\pm 4\%$ of their

respective true values. The ζ_s estimates are approximately 18% less than the true ζ_s value when generated by the ML method and approximately 21% less than the true ζ_s value when generated by the LS method over the ranges listed above. The reason the ζ_s estimate is less accurate than the other dynamic property estimates is that its value does not greatly affect the frequncy response function. A 21% decrease in ζ_s increases the variance of the response by only 2.6% and the effect on the shape of the frequency response function is less pronounced than the effect on the variance.

Since the frequency estimates are all within $\pm 0.50\%$ of their true values when the intial estimates are within a given range, the ML and LS programs are well-suited for determining the dynamic properties of a structure-absorber system for the purpose of adjusting the absorber(s) in order to enhance performance. Although the ζ_s estimate is less accurate than the frequency estimates, the impact of the ζ_s estimate on the effective damping is less pronounced than that of the frequency estimates. There are two reasons for this. Firstly, the effective damping changes more rapidly with respect to the tuning ratio than it does with respect to the structural damping. This is illustrated in Figure 5.24 which shows a contour plot of the relative percent change in effective damping generated by a structure-TLD system with respect to changes in the structural frequency and structural damping . Secondly, the structural damping does not impact adjustments made to the absorbers. The process used for the design of absorbers is discussed in Section 5.3.1 and the process of adjusting TLDs to enhance their performance is discussed in Section 3.3. If the f_s estimate used to tune the TLDs in this study was 0.50% less than its true value, this mistuning would result in a relative decrease in the true effective damping would by 0.08%. Conversely, if the $zeta_s$ estimate was inaccurate, it would not affect the true effective damping value because it would not be used to tune the TLDs.

The ML and LS programs are advantageous because they can capture the 2DOF

response of a structure-TLD system. The data generated in these tests was also analyzed using the HPBW method and the RDT in order to show the advantage of the ML and LS methods over the HPBW method and RDT. These methods are not designed to be used on 2DOF data and thus were only able to produce one estimate of natural frequency and one estimate of damping. The HPBW method produced f_0 and ζ estimates of 0.2543 Hz and 11.97% respectively. The f_0 estimate generated by the HPBW method is an estimate of the frequncy that corresponds to the higher resonant peak (f_a in this case). The natural frequency estimate is 6.10% lower than the true f_a. The ζ estimate generated by the HPBW method is, in this case, larger than both the ζ_a and ζ_s values and the effective damping ratio because both resonant peaks are included in the estimate. The damping ratio estimate is 26.82% higher than the true ζ_a value, 146.20% higher than the true ζ_s value, and 76.44% higher than the effective damping ratio value. The RDT produced f_0 and ζ estimates of 0.2533 Hz and 4.66% respectively. The f_0 estimate produced by the RDT is an estimate of the natural frequency associated with the higher resonant peak. The natural frequency estimate is 6.49% lower than the true f_a value. The ζ estimate generated by the RDT is between the ζ_a and ζ_s values since it is based on the decay curve of both resonant responses. The damping ratio estimate is 13.79% lower than the effective damping ratio value. Since the HPBW method and RDT are not able to generate estimates for both resonant peaks the ML and LS programs are clearly more useful in estimating the dynamic properties of a 2DOF system.

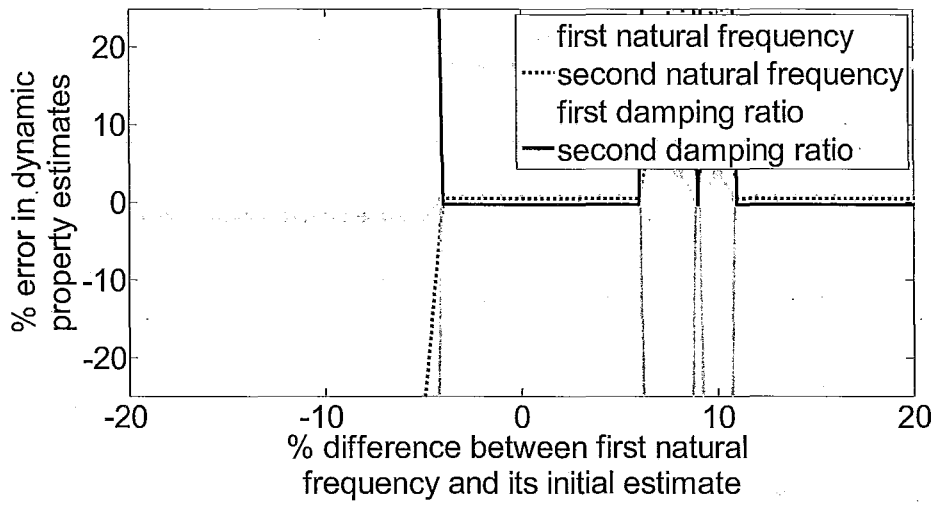

(a) Various Initial $\hat{f}_s$

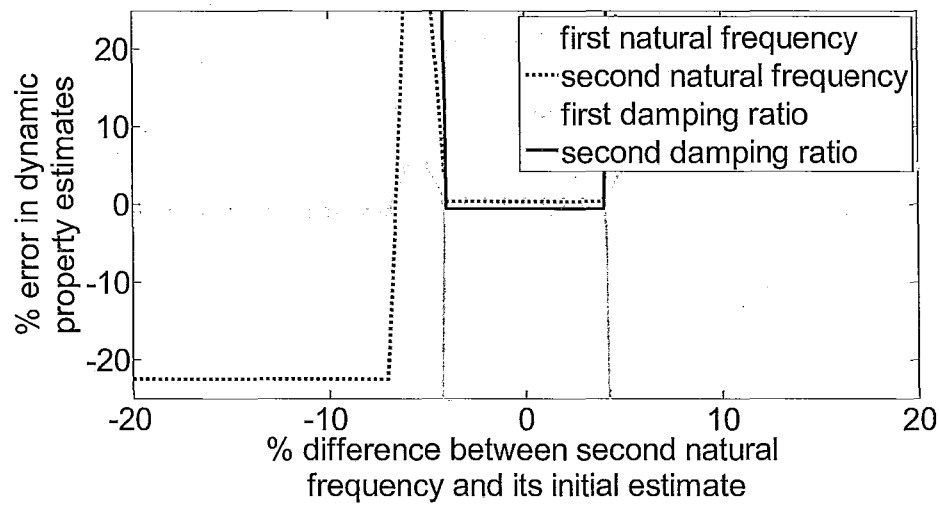

(b) Various Initial $\hat{f}_a$

Figure 5.20: Accuracy of Dynamic Property Estimates for Various Initial Frequency Estimates Generated by the ML Method

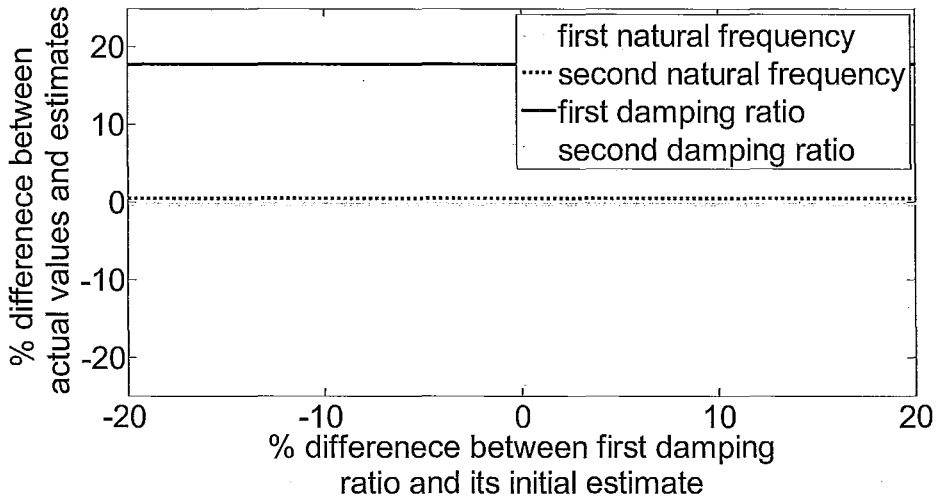

(a) Various Initial $\hat{\zeta}_s$

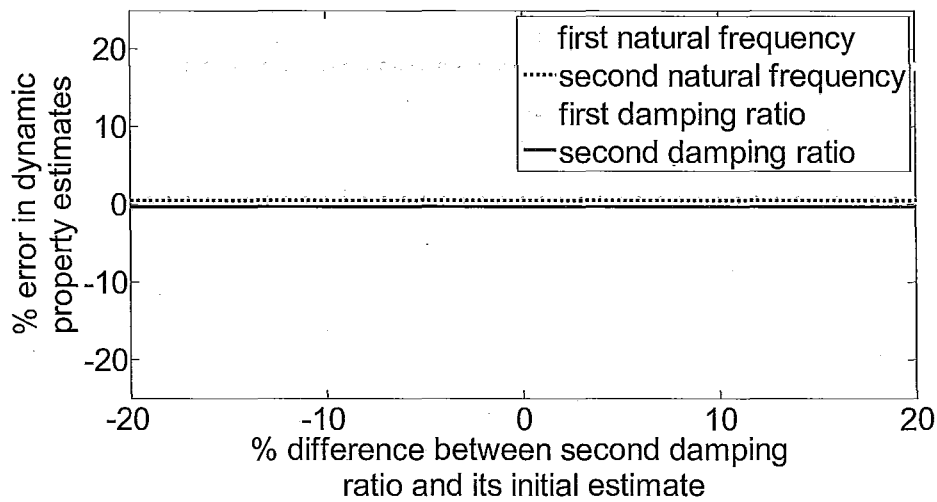

(b) Various Initial $\hat{\zeta}_a$

Figure 5.21: Accuracy of Dynamic Property Estimates for Various Initial Damping Estimates Generated by the ML Method

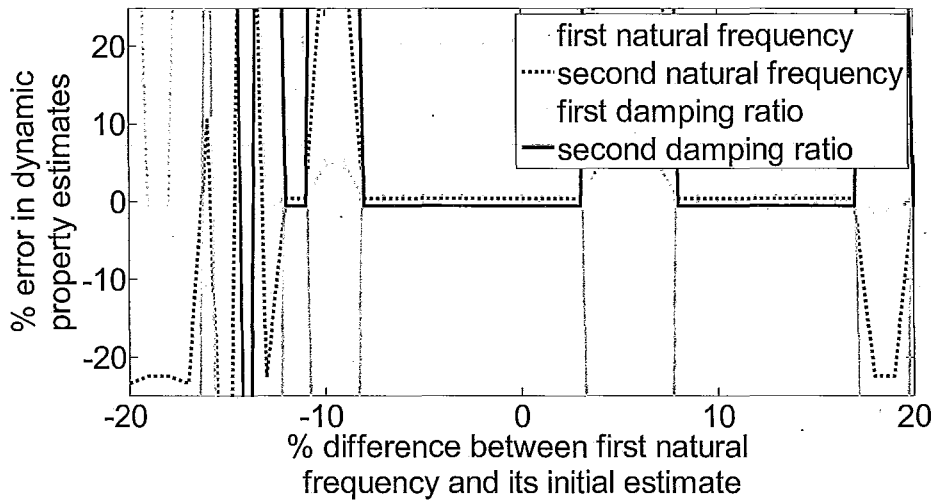

(a) Various Initial $\hat{f}_s$

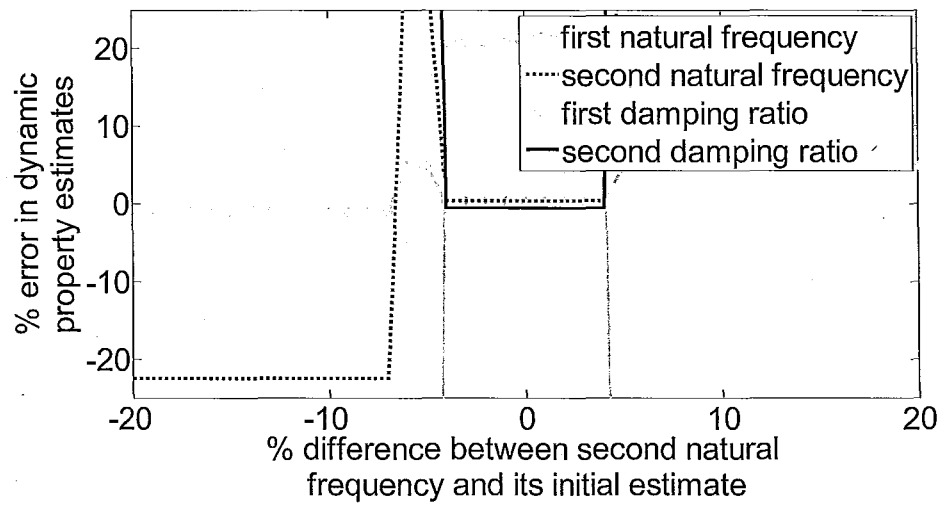

(b) Various Initial $\hat{f}_a$

Figure 5.22: Accuracy of Dynamic Property Estimates for Various Initial Frequency Estimates Generated by the LS Method

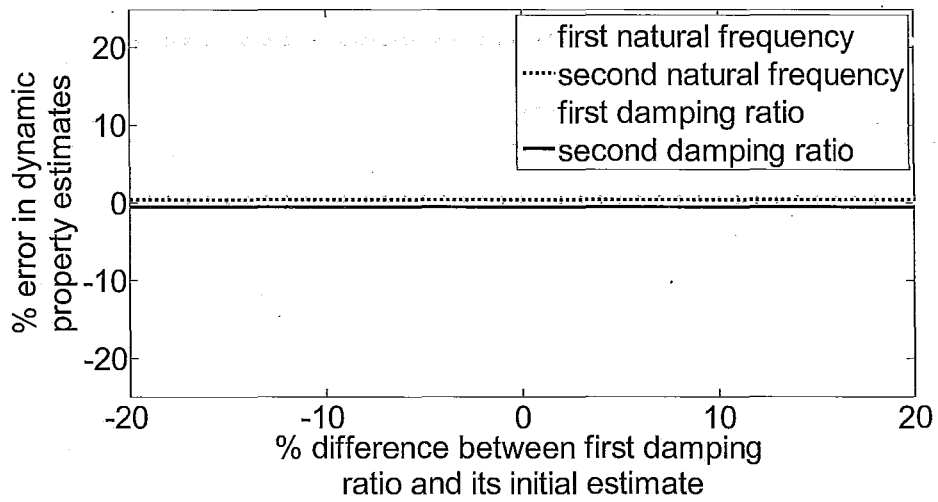

(a) Various Initial $\hat{\zeta}_s$

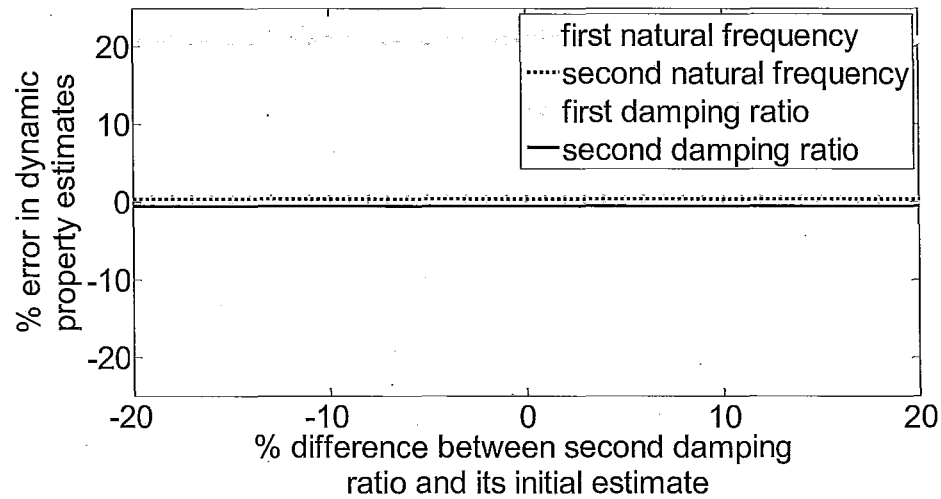

(b) Various Initial $\hat{\zeta}_a$

Figure 5.23: Accuracy of Dynamic Property Estimates for Various Initial Damping Estimates Generated by the LS Method

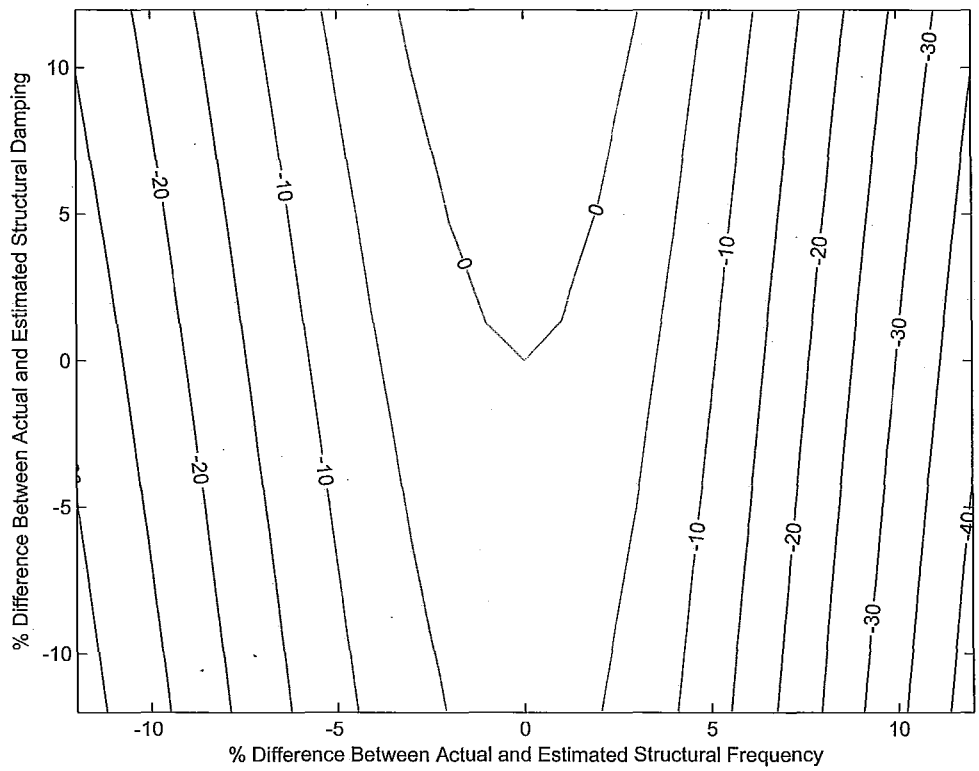

Figure 5.24: Contour Plot of Relative Percent Change in Effective Damping for Various f_s and ζ_s Estimates

5.4 Discussion of Tested Methods

In Section 5.3 the ML and LS programs were tested on spectral data and time-history data with no noise. The results generated by the ML and LS programs were compared to those generated by the HPBW and RDT programs. For spectral SDOF data, it was found that the ML and LS programs had lower maximum errors than the HPBW method. The HPBW method generated maximum errors of 0.72% and 57.14% for the natural frequency and damping ratio estimates respectively. The errors in the estimates generated by the ML program were only 0.19% and 20.63% for the natural frequency and damping ratio respectively. The LS program generated perfectly accurate estimates of the dynamic properties for all SDOF spectral input cases. For the spectral 2DOF

data, the ML and LS programs again generated better estimates than the HPBW program. The ML and LS programs estimated the correct dynamic property values within $\pm 1\%$ when the initial estimates were close to the true dynamic property values. The ranges of initial estimates that cause the dynamic property value estimates to be within $\pm 1\%$ are discussed in Section 5.3.1. The HPBW method generated errors of 6.10% and 30.5% for the absorber natural frequency and damping ratio respectively. The HPBW method is also only able to generate one estimate for natural frequency and one estimate for damping ratio since it is not suited to estimating the dynamic properties of a 2DOF system. Thus the ML and LS programs are clearly superior to the HPBW method for 2DOF systems as they are able to generate estimated dynamic property values for both masses of a 2DOF system. For the SDOF time history data with no noise the LS method generated the smallest maximum error for the natural frequency estimate for all tested cases. The ML had the second-smallest error for the natural frequency estimate followed by the RDT and the HPBW method (see Table 5.2). The RDT had the smallest error for the damping ratio estimate followed by the LS method, the ML method and finally the HPBW method. Although the RDT was able to estimate the damping ratio with more accuracy than the ML and LS method for a SDOF system, the RDT can not be used to estimate the dynamic properties of a 2DOF system. For the 2DOF time history data with no noise the ML and LS programs were able to estimate the f_s, f_a, and ζ_a values within $\pm 0.50\%$ of their true values when the initial estimates were within the ranges discussed in Section 5.3.2. The ζ_s estimates were approximately 18% less and 21% less than the true ζ_s value when generated by the ML and LS programs respectively. Although these error may seem large, the ζ_s estimate is not used in the adjustment of the absorbers to enhance their performance so these errors will have a negligible effect on the efficacy of the absorbers. This was discussed further in Sections 5.3.1 and 5.3.2. The errors generated by the HPBW

method were 6.10% and 26.82% for the absorber natural frequency and damping ratio respectively. The errors generated by the RDT were 6.49% and 13.79% for the absorber natural frequency and effective damping ratio respectively. Thus the errors generated by the ML and LS programs are smaller than those generated by the HPBW method and RDT for most cases. The only exception is that the RDT generates a smaller error for the effective damping estimate than the ML and LS programs generate for the structural damping estimate (the RDT is not able to generate an estimate of the structural damping for a more direct comparison). The ML and LS programs main advantage is that they are able to capture the 2DOF behaviour which the HPBW method and RDT are not.

The results show that the ML and LS programs are well-suited for determining the dynamic properties of a 2DOF structure-absorber system so that adjustments can be made to the absorbers in order to enhance their performance. Tuning of absorbers to a structure's natural frequency is important if the effective damping is to be maximized. This is shown in Figure 5.24. The ML and LS programs were able to accurately estimate the natural frequencies of the structure and TLDs within 0.50% of their true values when the initial f_s estimates were between -4% and 6% and -8 and 3% of their true values for the ML and LS programs respectively and when the initial f_a estimates were between -9% and 8% and $\pm$ 4% of their true values for the ML and LS programs respectively. If frequency estimates within 0.50% of their true values are used to tune the TLDs the effective damping will be within 0.08% of its optimal value.

Chapter 6

Full-Scale Monitoring of a 187 m Building

In this chapter the results from the full-scale monitoring of Building X are presented. Section 6.1 discusses how the data was separated and the method employed to select the block lengths and number of blocks. Section 6.2 presents the results from the initial analysis of Building X and Section 6.3 presents the results obtained from Building X after the TLDs were adjusted to enhance their performance.

6.1 Methods Used to Sort Full-Scale Data

The full-scale data was collected in segments of 16384 data points or approximately 32 minutes and 46 seconds. Each of these segments is a time history of consecutive data points and is identified by the date and time at which it was collected. In order to create time-histories that represent stationary data, the standard deviation of each segment of data was determined and the data segments were ordered according to their standard deviation. The data, ordered according to standard deviation, was then separated into segments each containing 409600 data points. This was done so that each segment of

data could contain 100 blocks of length $N = 4096$. This ensures that the bias error is less than or equal to 2% (see Section 4.2.1) and the variance error is equal to 10% (see Section 4.2.2). Only segments that agreed with Equation 4.18 were used in order to ensure that the data could be treated as stationary.

6.2 Results from Initial Analysis of Acceleration Data

Prior to the adjustment of the TLDs, Building X was acting as a SDOF system as discussed in Section 3.5. The acceleration data obtained from Building X before the TLDs were adjusted was separated as outlined in Section 6.1 and analyzed using SDOF methods. The f_0 estimates, normalized by the predicted natural frequency, f_p, and generated for various time-history segments are presented in Table 6.1. The normalized variance for each time-history is also reported. The variances are normalized by the maximum variance. Table 6.2 presents the ζ estimates, normalized by the predicted damping ratio, ζ_p.

Table 6.1: Normalized f_0 Estimates from Initial Analysis of Acceleration Data

Normalized Variance of Segment	f_0 Estimate, Normalized by f_p			
	ML	LS	HPBW	RDT
0.2636	1.0019	1.0122	1.0096	1.0119
0.3482	1.0296	1.0289	1.0300	1.0289
0.6518	1.0148	1.0133	1.0170	1.0119
1.0000	1.0100	1.0089	1.0096	1.0119

Table 6.1 shows that there is very little variability within the natural frequency estimates both between methods and between data sets.

Table 6.2 shows a tendency for the damping estimates to increase with increasing variance for the ML, HPBW, and RDT methods. The linear regression R^2 values for

Table 6.2: Normalized ζ Estimates from Initial Analysis of Acceleration Data

Normalized Variance of Segment	ζ Estimate, Normalized by ζ_p			
	ML	LS	HPBW	RDT
0.2636	1.42	1.08	1.09	0.75
0.3482	1.55	0.89	1.10	0.70
0.6518	0.90	1.09	1.28	0.95
1.0000	1.22	1.22	1.64	1.03

these methods are 0.4672, 0.9650, and 0.8959, respectively. It is expected that damping should increase with increased variance as discussed in Section 3.2. This trend may not be evident in the estimates produced by the LS method because of the limited number of data sets available. The RDT generated the lowest damping estimates. This was an expected result because the spectral methods have a tendency to overestimate the damping estimates as discussed in Section 4.2.1.

6.3 Results from Analysis of Acceleration Data after Adjustment of TLDs

In order to enhance the performance of the TLDs water was added to the tanks to increase their natural frequency. This increase in water depth was expected to increase the effective damping; however, the increase in damping was not expected to be great enough to cause the response spectra to exhibit the distinctive coupled-2DOF response of an optimally tuned system. Instead the added damping was expected to appear as an increase in the effective damping of a SDOF response. Thus the data was analyzed using the SDOF LS and ML programs. The data was also analyzed using the HPBW method and RDT for comparison.

The data was sorted using the methods outlined in Section 6.1. Due to setbacks involving the acquisition of full-scale data, a limited amount of data was obtained from

the system after the adjustments of the TLDs. Thus Equation 4.18 was not able to be satisfied for the majority of the data. Nevertheless, the result from the data are presented below in order that a comparison of the data before and after the adjustment of the TLDs can be made. The f_0 estimates, normalized by f_p, and generated for various time-history segments are presented in Table 6.3. The variance for each time-history is also reported. The variances are normalized by the same maximum variance used for Tables 6.1 and 6.2.

Table 6.3: Normalized f_0 Estimates from Analysis of Acceleration Data after Adjustment of TLDs

Normalized Variance	f_0 Estimate, Normalized by f_p			
of Segment	ML	LS	HPBW	RDT
0.1609	1.0315	1.0315	1.0322	1.0330
0.1752	1.0281	1.0278	1.0248	1.0289
0.4630	1.0222	1.0219	1.0248	1.0289
0.7553	1.0248	1.0252	1.0248	1.0289

The average natural frequency estimate over all methods and all data sets is approximately 1% higher than the natural frequency estimate obtained before the adjustment of the TLDs. This difference is statistically significant as the two-sided p-value is 0.76%. The difference may be due to the fact that adding water to the TLDs increased their natural frequency which may have a tendancy to shift the natural frequency of the overall system slightly up.

Table 6.4: Normalized ζ Estimates from Analysis of Acceleration Data after Adjustment of TLDs

Normalized Variance	ζ Estimate, Normalized by ζ_p			
of Segment	ML	LS	HPBW	RDT
0.1609	1.58	1.15	0.88	0.58
0.1752	1.25	0.91	1.16	0.63
0.4630	0.89	0.91	0.97	0.72
0.7553	0.95	1.02	1.36	0.67

The average damping ratio estimate over all methods and data sets is 0.14%

lower than that obtained before the adjustment of the TLDs. However this result is not statistically significant as the two-sided p-value is 20.60%. It is expected that the damping ratio for the system has actually increase due to the adjustment of the TLDs. More data is required to see if this has occured.

The results obtained from the ML and LS programs show good agreement with the results obtained from the HPBW and RDT programs. The damping ratio estimated from the RDT is lower than that estimated from the other methods. This is the expected result as the spectral methods have a tendency to overestimate the damping as discussed in Section 4.2.1.

Chapter 7

Conclusions

7.1 Maximum Likelihood and Least Squares Methods

Two MATLAB (2009) programs were developed in order to estimate the dynamic properties of a structural system using the maximum likelihood and least squares methods. Versions of these programs were developed to be used on both SDOF and coupled-2DOF systems. The programs were designed to isolate the resonant peak(s) of a system so that the noise along the rest of the spectrum would not erode the accuracy of the estimates. The SDOF programs determine the initial estimates needed for the optimization problem automatically using the half-power bandwidth method. The 2DOF programs require user input for the initial estimates; however the user is aided in estimating the natural frequencies of the system by a plot of the response spectrum generated automatically by the programs.

The programs were verified using several different methods. First, the programs were tested using spectral data with known dynamic properties. Second, the programs were tested using time-history data. As expected the results generated by the programs

analyzing spectral data were more accurate than those generated by programs analyzing time-history data. The programs were also tested using different spectral block sizes and number of blocks. As expected, the accuracy of the estimates tended to increase with increased number and size of blocks.

The results generated by the ML and LS programs were compared to those generated by the HPBW method and RDT to further validate their accuracy. The results showed that the ML and LS programs produced quite good results when compared to the HPBW method and RDT. The errors produced by the ML and LS programs were smaller than the errors produced by the HPBW method and RDT in most cases tested. The exception to this is that the RDT produced smaller errors for the damping estimates than the ML and LS programs for time-history data. However, the largest advantage of the ML and LS methods is that they can be used to determine dynamic property values for two distinct masses in a 2DOF system which the HPBW method and RDT can not.

This study was limited in that only sample data with certain dynamic property values was tested. In the case of the SDOF data, data sets with four distinct natural frequencies, and five distinct damping ratios were tested. The natural frequencies ranged from 0.20 Hz to 0.30 Hz and the damping ratios ranged from 1.00% to 3.00%. For the 2DOF data only one set of dynamic properties was tested. These dynamic properties represent an optimally tuned structure-TLD system and are given in Table 5.1. The data was tested using block sizes of 2048, 4096, and 8192 and number of blocks of 10, 20, 50, 100, and 200. A number of assumptions were made in the development of the MATLAB (2009) programs and these are discussed in Section 7.3.

7.2 Results of Full-Scale Analysis

The data obtained from the full-scale monitoring of a structure equipped with TLDs (known as Building X) was analyzed using the ML and LS programs developed in this study as well as the HPBW method and RDT. The results suggest that the normalized natural frequency and normalized damping ratio of Building X were originally 1.0163 and 1.1200 respectively. The TLDs of the tested building were then adjusted in order to enhance their performce. After the adjustment of the TLDs the analysis suggests that the normalized natural frequency and normalized damping ratio of Building X are 1.0275 and 0.9800 respectively. Full results from the analysis are presented in Chapter 6. The results show good agreement between the estimates generated by the different methods.

The ML and LS programs were developed for the purpose of analyzing the coupled-2DOF behaviour of a structure-TLD system. However, because the TLDs were not optimally tuned the actual data obtained from Building X did not display 2DOF behaviour, but instead was similar to the data that would be obtained from a SDOF system. As a result, the 2DOF ML and LS programs that were developed in this study were not able to be tested on full-scale data. However, the 2DOF programs were verified and could be used on 2DOF systems in the future.

The behaviour of a structure-TLD system is nonlinear, yet the methods developed in this study are based on a linear system. In order to justify analyzing the nonlinear system as a linear system, it is important that the analyzed data is stationary. The analyzed data was manipulated using selective ensemble averaging in order to force stationarity. The selective ensemble averaging used is discussed in Section 4.2.3 and Chapter 6.

7.3 Recommendations for Future Work

Several assumptions were made in the development of the MATLAB (2009) programs regarding the most accurate way of estimating the dynamic properties of a system. The validity of these assumptions should be tested by performing a sensitivity analysis on several factors. These factors include:

1. The frequency limits used to define the resonant peak(s). For the SDOF programs the lower frequency limit of the resonant peak was defined to begin at the frequency value corresponding to the first discrete frequency response function value that was greater than one. The frequency response function was assumed to be symmetric so that the upper frequency response function could be estimated according to Equation 5.10. These values for the upper and lower frequency limits were based on the recommendations made by Montpellier (1997). The resonant peak could also be defined so that a certain percentage of the total area under the response spectrum was contained between the upper and lower frequency limits. This was the method chosen for the 2DOF programs. The effect of altering the method for determining the lower and upper frequency limits should be examined.

2. The MATLAB (2009) solver method used to solve the minimization problem. The MATLAB (2009) programs use the interior-point algorithm to solve the minimization problems in both the maximum likelihood and least squares methods. MATLAB (2009) has other solver methods available such as the active-set method. The effect of altering the solver method should be examined.

3. The SDOF programs use the HPBW method to determine the initial estimates of the dynamic properties. Other methods to determine these initial estimates could also be employed such as the method developed by Thompson and Tree (1980). The effect of altering the method used to determine the initial estimates

of the dynamic properties should be examined.

4. The MATLAB (2009) programs transform data from the time domain to the frequency domain using Fast Fourier transforms windowed by the Hamming window. The effect of using another window in the transformation could be examined.

In this study the natural frequency of the tested building (Building X) was originally found to be greater than the predicted natural frequency. Since the TLDs had been tuned to the building's predicted natural frequency they were not operating at their optimal level. In order to improve their performance, water was added to the TLDs. However, after water was added to the TLDs it was found that there was no statistically significant change in the estimated effective damping. More data is required to determine the effect of the adjustment to the TLDs.

Bibliography

Bendat, J. and Piersol, A. (2000). *Random Data Analysis and Measurement Procedures. 3rd ed.* John Wiley & Sons, Toronto, Canada.

Chopra, A. (2007). *Dynamics of Structures. 3rd ed.* Prentic-Hall, Inc., Upper Saddle River, USA.

Cole, H. J. (1973). On-Line Failure Detection and Damping Measurement of Aerospace Structures by Random Decrement Signature. *NASA Contract Rep CR-2205.*

Crandall, S. and Mark, W. (1963). *Random Vibration in Mechanical Systems.* Academic Press, New York, USA.

Crandall, S., Dyer, I., Mains, R., McClintock, F., Metzgar, K., Pian, T., Poritsky, H., Powell, A., Priest, D., Rona, T., and Siebert, W. (1958). *Random Vibration.* M.I.T. Press, Cambridge, USA.

Den Hartog, J. (1956). *Mechanical Vibrations.* McGraw-Hill, New York, USA.

Hayter, A. (2002). *Probability and Statistics for Engineers and Scientists. 2nd ed.* Thompson Learning, Pacific Grove, USA.

Ignizio, J. and Cavalier, T. (1994). *Linear Programming.* Prentic-Hall, Inc., Englewood Cliffs, USA.

Isyumov, N. (1995). Motion Perception, Tolerance and Mitigation. In *Proc. 5th World Congress of the Council on Tall Buildings and Urban Habitat*, Amsterdam, The Netherlands.

Isyumov, N. (1999). Overview of Wind Action on Tall Buildings and Structures. In *Proc. ICWE 10*, Copenhagen, Denmark.

Isyumov, N., Case, P., Hasan, A., Tait, M., Morrish, D., Farquhar, S., and Mara, T. (2010). Monitoring of Tall Buildings to Assist the Design of Supplementary Damping Systems. In *Proc. of the 2010 Structures Congress*, Orlando, USA.

Jacquot, R. and Foster, J. (1977). Optimal Cantilever Dynamic Vibration Absorbers. *Journal of Engineering for Industry*, **99 Ser B**(1), 138–141.

Jeary, A. (1986). Damping in Tall Buildings – A Mechanism and a Predictor. *Earthquake Engineering and Structural Dynamcis*, **14**(5), 733–750.

Kareem, A. and Gurley, K. (1996). Damping in Structures: Its Evaluation and Treatment of Uncertainty. *Journal of Wind Engineering*, **59**(2–3), 131–157.

Kareem, A. and Kijewski, T. (1999). Mitigation of Motions of Tall Buildings with Specific Examples of Recent Applications. *Wind and Structures*, **2**(3), 201–251.

Kijewski-Correa, T. Kilpatrick, J., Kareem, A., Kwon, D., Bashor, R., Kockly, M., Young, B., Abdelraxaq, A., Galsworthy, J., Isyumov, N., Morrish, D., Sinn, R., and Baker, W. (2006). Validating Wind-Induced Response of Tall Buildings: Synopsis of the Chicago Full-Scale Monitoring Program. *Journal of Structural Engineering*, **132**(10), 1509–1523.

Kijewski-Correa, T. (2003). *Full-Scale Measurement and System Identification: A*

Time-Frequency Perspective. Ph.D. thesis, The University of Notre Dame, Notre Dame, USA.

Lamb, H. (1945). *Hydrodynamics.* Dover Publications, New York, USA.

Li, Q., Fang, J., Jeary, A., and Wong, C. (1998). Full Scale Measurements of Wind Effects on Tall Buildings. *Journal of Wind Engineering and Industrial Aerodynamics*, **74–76**, 741–750.

Li, Q., Yang, K., Zhang, N., Wong, C., and Jeary, A. (2002). Field Measurements of Amplitude-Dependent Damping in a 79-Storey Tall Building and its Effects on the Structural Dynamic Responses. *Structural Design of Tall Buildings*, **11**(2), 129–153.

Li, Q., Xiao, Y., Wong, C., and Jeary, A. (2004). Field Measurements of Typhoon Effects on a Super Tall Building. *Engineering Structures*, **26**(2), 233–244.

Littler, J. (1995). Assessment of Some of the Different Methods for Estimating Damping from Full-Scale Testing. *Journal of Wind Engineering and Industrial Aerodynamics*, **57**(2–3), 179–189.

MATLAB (2009). *MATLAB & SIMULINK Student Version R2009a (Version 7.8.0.347).* The MathWorks, Inc., Natick, USA.

McNamara, R. (1977). Tuned Mass Dampers for Buildings. *Journal of the Structural Division, Proceedings of the American Society of Civil Engineering*, **103**(ST9), 1785–1798.

Montpellier, P. (1997). *The Maximum Likelihood Method of Estimating Dynamic Properties of Structures.* Master's thesis, The University of Western Ontario, London, Canada.

Morrish, D. (2009). rand_dec_demo.m. BLWT UWO.

Newland, D. (2005). *An Introduction to Random Vibration, Spectral & Wavelet Analysis.* Dover Publications, Mineola, USA.

Roos, C., Terlaky, T., and Vial, J. (2006). *Interior Point Methods for Linear Optimization. 2nd ed.* Springer Science+Business Media, Inc., New York, USA.

Satake, N., Suda, K., Arakawa, T., Sasaki, A., and Tamura, Y. (2003). Damping Evalutation Using Full-Scale Data of Buildings in Japan. *Journal of Structural Engineering*, **2**(3), 470–477.

Schmidt, H. (1985). Resolution Bias Errors in Spectral Density, Frequency Response and Coherence Function Measurements, III: Application to Second-Order Systems (White Noise Excitation). *Journal of Sound and Vibration*, **101**(3), 377–404.

Soong, T. and Dargush, G. (1997). *Passive Energy Dissipation Systems in Structural Engineering.* Wiley & Sons, Chichester, England.

Tait, M. (2004). *The Performance of 1-D and 2-D Tuned Liquid Dampers.* Ph.D. thesis, The University of Western Ontario, London, Canada.

Tait, M. (2008). Modelling and preliminary design of a structure-TLD system. *Engineering Structures*, **30**(10), 2644–2655.

Tait, M., El Damatty, A., Isyumov, N., and Siddique, M. (2005). Numerical Flow Models to Simulate Tuned Liquid Dampers (TLD) with Slat Screens. *Journal of Fluids and Structures*, **20**(8), 1007–1023.

Tamura, Y., Fujii, K., Ohtsuki, T., Wakahara, T., and Ryuichi, K. (1995). Effectiveness of tuned liquid damper under wind excitations. *Engineering Structures*, **132**(9), 609–621.

Tedesco, J., McDougal, W., and Ross, C. (1999). *Structural Dynamics Theory and Applications.* Addison Wesley Longman, Inc., Menlo Park, USA.

Thompson, J. and Tree, D. (1980). Leakage Error in Fast Fourier Analysis. *Journal of Sound and Vibration*, **71**(4), 531–544.

Vandiver, J. and Mitome, S. (1979). Effect of Liquid Storage Tanks on the Dynamic Response of Offshore Platforms. *Journal of Petroleum Technology*, **31**(10), 1231–1240.

Warburton, G. (1982). Optimal Absorber Parameters for Various Combinations of Response and Excitation Parameters. *Earthquake Engineering and Structural Dynamics*, **10**(3), 381–401.

Warnitchai, P. and Pinkaew, T. (1998). Modelling of liquid sloshing in rectangular tanks with flow-dampening devices. *Engineering Structures*, **20**(7), 593–600.

Ye, Y. (1997). *Interior Point Algorithms Theory and Analysis.* John Wiley & Sons, Inc., New York, USA.